
In-vitro Studies on Aptamer - Induced FRET Between λ_{N22} Tagged Fluorescent Protein Variants

Amrita Kuthiala



München 2010

In-vitro Studies on Aptamer - Induced FRET Between λ_{N22} Tagged Fluorescent Protein Variants

Amrita Kuthiala

Dissertation
an der Fakultät für Biologie
der Ludwig-Maximilians-Universität
München

Angefertigt am Max-Planck-Institut für Neurobiologie

vorgelegt von
Amrita Kuthiala

München, September 2010

Erstgutachter:	Prof. Dr. Alexander Borst
Zweitgutachter:	Prof. Dr. Rainer Uhl
Tag der mündlichen Prüfung:	08.12.2010

Contents

1	Introduction	9
1.1	The central dogma of molecular biology	9
1.1.1	The RNA world	10
1.1.1.1	miRNA (micro-RNA)	10
1.1.1.2	snRNA (small nuclear RNA) /snoRNA (small nucleolar RNA)	10
1.1.1.3	piRNA (PIWI-interacting RNA)	11
1.1.1.4	rRNA(ribosomal RNA)	11
1.1.1.5	tRNA (transfer RNA)	11
1.1.1.6	mRNA(messenger RNA)	12
1.1.2	Regulatory conformational changes in RNA	12
1.2	RNA localization and trafficking	13
1.2.1	Advantages of mRNA localization	15
1.2.2	mRNA localization in different organisms	15
1.3	mRNA transport in neurons	17
1.4	Methods to detect RNA in cells	18
1.5	Use of bacteriophage RNA binding peptides for mRNA tagging	21
1.5.1	Binding of the λ_N peptide to boxB	23
1.6	Tn5 transposon system	28
1.7	Fluorescence	28
1.8	FÖRSTER resonance energy transfer (FRET)	30
1.8.1	Principle of FRET	30

1.8.2	Measurement of FRET	33
1.8.2.1	Only donor is fluorescent	33
1.8.2.2	Donor and acceptor are fluorescent	33
1.8.2.3	Design rules of fluorescent proteins for FRET	34
1.9	Fluorescent proteins	34
1.9.1	History	34
1.9.2	Structure and properties	35
1.9.3	GFP derivatives	35
1.9.4	Applications	38
1.10	Aim of the thesis	39
2	Materials and methods	41
2.1	Molecular biology	41
2.1.1	DNA restriction digestion	41
2.1.2	Ligation of DNA fragments	42
2.1.3	Polymerase chain reaction (PCR)	42
2.1.4	λ_{N22} insertions in mKO2 using transposon Tn5	44
2.1.5	Transformation of chemically-competent <i>E. coli</i>	44
2.1.6	Preparation of chemically-competent <i>E. coli</i>	45
2.1.7	<i>In-vitro</i> mRNA transcription	46
2.1.8	RNA isolation	47
2.1.9	cDNA synthesis	47
2.1.10	Agarose gel	48
2.2	Protein biochemistry	49
2.2.1	Protein expression using the <i>E. coli</i> BL21 strain	49
2.2.2	Purification of His-tag proteins via affinity chromatography	49
2.2.3	Spectrophotometer measurements of the fluorescent proteins for calculating extinction coefficient and quantum yield	52
2.2.4	Gel electrophoresis: denaturing SDS-PAGE	53

2.2.5	BCA assay for protein concentration	54
2.2.6	In-vitro FRET measurements to study aptamer induced FRET upon binding of the λ N tagged fluorescent proteins	55
2.3	Cell culture	55
2.3.1	Preparation of HeLa cells culture	55
2.3.2	Transfection of HeLa cells culture using lipofectamine	56
2.3.3	Confocal imaging of transfected HeLa cells	56
2.4	Materials	57
2.4.1	Primers list	57
2.4.2	Instruments	61
2.4.3	Consumables	62
2.4.4	Buffers, solutions and media	62
2.4.5	Chemicals	63
3	Results	65
3.1	Generation of mKO2 variants with λ_{N22} insertions	65
3.2	Comparing the fluorescent properties of the mKO2- λ_{N22} variants	69
3.3	Generation of FRET donors proteins tagged with λ_{N22}	72
3.4	Studying aptamer induced FRET	74
4	Discussion	83
A	Experiment Results	93
A.1	Result graphs	93
A.2	Discussion graphs	107
B	Various tolerant insertion sites in mKO2	111
	Bibliography	125

Abbreviations

APS	Ammonium Persulfate	MOPS	3-(N-morpholino)propanesulfonic acid
bp	Base pair	mTFP	monomeric Teal Fluorescent Protein
BSA	Bovine Serum Albumine	MW	Molecular weight
CMV	cytomegalovirus	N	Lambda-N protein
Da	Dalton	NLS	Nuclear localization signal
DMEM	Dulbecco's Modified Eagle Medium	NTA	nitrioloacetic acid
DMSO	Dimethylsulfoxid	OD _x	Optical density at x nm
DNA	Deoxyribonucleic Acid	PAGE	Polyacrylamide Gel Electrophoresis
dNTP	Deoxyribonucleotid-triphosphate	PBS	Phosphate Buffered Saline
EDTA	Ethylenediaminetetraacetic acid	PCR	Polymerase Chain Reaction
EGFP	Enhanced green fluorescent protein	pH	reverse logarithmic representation
EGTA	ethylene glycol-bis[β -amino-ethyl ether] N,N,N',N'-tetraacetic Acid		of relative H ⁺ concentration
eppi	EPPENDORF 1.5 / 2 ml vial	PMSF	phenylmethylsulfonylfluoride
FP	fluorescent protein	R	ratio
FRET	fluorescence resonance energy transfer	ΔR	difference of ratio
HBSS	Hanks' balanced salt solution	RBP	RNA Binding Peptide
IPTG	isopropyl- β -D-thiogalactopyranoside	RNA	Ribonucleic acid
L	Lambda-N22 (λ_{N22}) protein	RT	Room Temperature
LB	Lysogeny broth Luria broth or Luria-Bertani broth	SDS	sodium dodecyl sulfat
M	Molar	TAE	tris-acetate-EDTA electrophoresis buffer
mKO2	monomeric Kusabira Orange2	TEMED	N,N,N',N'-Tetramethyl-ethylen-
		WT	wildtype

Abstract

Localization of mRNA in the cell plays a vital role in functioning of the cell, especially in development and neuronal plasticity. The aim of this thesis was to generate a new RNA labeling system using FRET between fluorescent proteins. Short specific RNA sequences, called aptamers, were used to bring the fluorescent proteins in close proximity to observe FRET. To achieve this, the aptamer binding peptide, λ_{N22} , was inserted at various sites in the donor (EGFP and mTFP1) and acceptor (mKO2 and mKO3) fluorescent proteins. This provided the advantage of tethering the λ_{N22} tagged fluorescent proteins at different angles on this specific aptamer, the boxB RNA. The idea was to investigate which FRET pair would offer the best FRET efficiency when the peptides bind to the RNA. Depending on the structural conformation the RNA adopts in solution, different distances and orientation between the donor and acceptors would form, which would help to compare the FRET efficiency of different FRET pairs .

The first step towards this approach was generation of mKO2 acceptor proteins which have the λ_{N22} peptide inserted in different tolerant sites in the middle of mKO2 protein. Using the Tn5 transposon system acceptor proteins were generated offering a range of orientational specificity on binding the boxB RNA. Generation of acceptors tagged with λ_{N22} either at N- or C-terminal was done using a mutant form of mKO2 generated in the lab, termed as mKO3. mKO3 is a modified version of mKO2, generated in the lab, where the C-terminus of mKO2 is mutated to introduce last 9 amino acids from *Aequorea* GFP C-terminus thus making mKO3 more tolerant to C-terminus labelling in comparison to mKO2. When these acceptor proteins were brought in close proximity with the donors (also tagged with λ_{N22}) on binding a 5boxB sequence *in vitro*, a small and unspecific FRET ratio change was observed. Along with FRET change, unspecific quenching of emission intensity also occurred. The mKO2- λ_{N22} / mKO3- λ_{N22} variants show unspecific FRET ratio change with the λ_{N22} tagged EGFP / mTFP1 donor proteins. With increase in the concentration of RNA, there was a change in the $\Delta R/R$ values, but the direction of this change differed for different FRET pairs and not related to aptamer binding. This thesis was able to show a FRET ratio change between λ_{N22} donor and

acceptor fluorescent proteins on binding the aptamer. Depending on the conformational change in the aptamer on binding the λ_{N22} peptide certain orientations of the donors and acceptors might be more suitable for FRET to happen, compared to others. This finding might pave the way for a new RNA tagging method, with more extensive and defined work this could be used to label and monitor mRNA in the cytoplasm and therefore reduce the need of a nuclear localization signal to compartmentalize the unbound fluorescently labeled RNA binding protein in the nucleus.

Chapter 1

Introduction

1.1 The central dogma of molecular biology

Life is said to be a contrast between randomness and determinism. The chaotic interaction of biomolecules gives rise to a precise coordination in a living organism and that always seems to be a wonder [1]. A living organism is composed of cells which are in turn formed by a number of biomolecules. These biomolecules cooperate with each other, at different levels either intra-cellular or inter-cellular, in a very precise manner to give rise to every action, thought, or function performed by that living organism. Lack of, or improper functioning at one of the levels, leads to a disorder or diseased condition. The main biomolecules forming a living organism are *DNA* (deoxy-ribonucleic acids), *RNA* (ribo-nucleic acids), *proteins*, *carbohydrates* and *lipids*. Present in the central compartment of a eukaryotic cell, the nucleus, it is responsible for storing and encoding the genetic information required for normal functioning of the cell and also the response under stress. DNA encodes into the functional and structural players of the cell, proteins. Proteins are the main machinery of the cell, as they function as enzymes, form part of the cytoskeleton, the motor machinery like actin and myosin, the receptors on the extra-cellular surface, the channels that let ions and nutrients diffuse through the cell membrane into the cell.

The DNA is not directly encoded to form the protein. It is first transcribed into a messenger RNA (mRNA). The nucleotide sequence in the mRNA determines the amino acid sequence of a protein. Many functional RNAs are needed to get protein from DNA sequences. Eukaryotes express many non-protein-coding RNAs (ncRNAs) that participate in the processing of other RNAs and also in their regulation. The modern RNA world, as we know it, does not consist of just the RNAs involved

in protein synthesis like mRNA, tRNA, rRNA. And it is not a simple process of transformation of DNA to mRNA to protein, but a network of RNA infrastructure is involved. How they interact and connect spatially and temporally, we are still in the process of discovering. As a result, focus of research has shifted from more protein-centric to more genomics.

1.1.1 The RNA world

Interestingly, only 2.3% of the human genome is encoded into a mRNA [2], although not all the genome is transcribed into protein. Therefore a huge part is non-protein-coding and is sometimes referred to as the *dark matter* of the cell [3]. The dark matter or the non-coding genome of the cells consists of various small non-protein coding RNAs (ncRNAs), which despite their nature and small size widely influence protein induction, translation silencing, transport and various other functions in the cell via cleavage, nucleotide modifications, transcription and destruction. The whole RNA infrastructure of the cell includes: mRNA (messenger RNA), tRNA (transfer RNA), rRNA (ribosomal RNA), miRNA (micro RNA), snRNA (small nuclear RNA), snoRNA (small nucleolar RNA), long ncRNA (Long non-protein coding RNA), piRNA (PIWI-interacting RNA), riboswitches.

1.1.1.1 miRNA (micro-RNA)

MicroRNAs were discovered in 1993 by Victor Ambors, Rosalind Lee and Rhonda Feinbaum during a study of the gene *lin-14* in *C. elegans* development [4]. In 2000 a second RNA was discovered, let-7, that lead to a dramatic change in how gene regulation happens in the cell [5]. Animal miRNAs regulate translation by down-regulation of translation via mRNA cleavage or deadenylation of poly-A tail. Within miRNAs there is another category of regulatory RNAs, the siRNA, which down-regulate expression by degrading the mRNA .

1.1.1.2 snRNA (small nuclear RNA) /snoRNA (small nucleolar RNA)

snRNAs bind to small proteins to form snRNPs which are involved in pre-mRNA splicing. snRNAs undergo the cleavage during mRNA splicing [6]. The splicing of pre-RNA yield snoRNAs which are then involved in rRNA splicing. This is one of the examples of how RNAs interact in the cell and influence the overall function of the cell.

1.1.1.3 piRNA (PIWI-interacting RNA)

piRNAs bind to the Piwi family of proteins (PIWI, Argonaute 3, Aubergine) and were discovered initially in *Drosophila* and mammal germline cells [7]. They are known to be involved in transposon defense in *Drosophila* ovaries.

The above are the RNA regulating RNAs.

The following three RNAs form the core of the RNA infrastructure in the cell:

1.1.1.4 rRNA(ribosomal RNA)

rRNAs form the core of the ribosomes on which the mRNA is translated. rRNAs provide a mechanism of peptidyl transferase activity for mRNA decoding into amino acids by interacting with the tRNAs during protein translation. Then the tRNA brings the correct amino acid corresponding to the mRNA codon. The 18S rRNA in most eukaryotes is in the small ribosomal subunit, and the large subunit contains three rRNA species (the 5S, 5.8S and 28S rRNAs). rRNA is the most conserved gene in all cells [8].

rRNA transcripts 18S, 5.8S and 28S are generated in the nucleolus by RNA Pol I. They are also formed first as pre-rRNA and then undergo processing to form rRNA. They are important for the ribosomal assembly formation for protein translation. The processing of pre-rRNAs is guided by snoRNAs which are found in the introns of mRNA and released on proper splicing of mRNAs [9].

1.1.1.5 tRNA (transfer RNA)

tRNAs are adaptor molecules that recognize and bind the triplet codon on the mRNA on one side and an amino acid on the other side. tRNAs are transcribed in the nucleus and undergo modification and splicing in the nucleus. The codon on the mRNA cannot directly recognize the amino acid they specify by the combination of 3 nucleotides. There is when the tRNAs come into picture. They traverse along the length of the mRNA when it is being translated and transfer the appropriate amino acid as per the codon. There are a number of tRNAs synthesized by the cell and the identification of the correct amino acid for the right tRNA is by the help of aminoacyl-tRNA synthetases. The combined action of synthetases and tRNA leads to the correct association of the amino acid on the mRNA codon for synthesis of polypeptide chain, linking amino acids together [8].

1.1.1.6 mRNA(messenger RNA)

mRNAs are the first known form of RNA. They are encoded from the DNA sequence in the form of pre-mRNA. This pre-mRNA form has the presence of protein coding regions, called exons, and protein non-coding regions, called introns. The pre-mRNA is spliced, introns are removed and depending on the splicing pattern or splice sites on the pre-mRNA, isoforms of the protein can be obtained. The mRNAs are spliced by an exon-junction complex, and a number of other spliceosomes and proteins are involved [10]. Their processing has an important significance on the RNA infrastructure of the cell as the snoRNA are found within the introns of rRNA. After splicing the mature mRNA is transported out of the nucleus via the nucleopores, into the cytoplasm for translation into a protein.

Subsequent chapters will deal in more detail about the importance of mRNA transport on spatial and temporal protein expression in the cell.

1.1.2 Regulatory conformational changes in RNA

After the discovery of the various different classes of RNA, it became evident that RNA is not just a target of post-transcriptional genetic regulation. ncRNAs in prokaryotes and eukaryotes function as trans-acting regulators of gene expression. However, recently a new mode of RNA-mediated regulation of gene expression has been uncovered where the mRNA itself serves as the modulator. The mRNA can regulate its transcription, processing and translation by undergoing a conformational change promoted by direct binding with a cellular metabolite or ligand. Such cis-acting RNA sequences, called Riboswitches, are found abundantly in prokaryotes and in a few eukaryotes. Such riboswitches are mostly found as regulators of a cellular metabolic pathway. It is considered as the simplest mode of regulation of gene translation in bacteria.

Riboswitches are usually found on the 5' UTR of the mRNA. They are part of the feedback mechanism in prokaryotes where binding of a small metabolite, such as cofactors, or temperature can change the tertiary structure of the RNA and either inhibit or up-regulate translation of the mRNA [11]. Later, "RNA thermometers" were found. They have a highly structured 5'UTR that covers the ribosome binding site under normal temperatures. Once it senses the selected temperature, it undergoes a conformational change and exposes the Shine-Dalgarno (SD) sequence, facilitating ribosome bindings and initiating translation. Recently a Mg^{2+} metal sensing riboswitch, called the *M-box*, was also discovered.

Riboswitches are generally formed of two parts: the aptamer, where the metabolite binds; and the

expression-platform which undergoes the conformational change on aptamer binding the ligand (metabolite), and thus regulates the expression of the gene downstream. The conformational change of the riboswitch is usually in the form of an alternative hairpin structure, which leads to occlusion or exposure of ribosome binding sites thereby forming or disrupting transcriptional terminators or anti-terminators. The various metabolites riboflavin-, cyanocobalamine-, thiamine-, bind to their respective riboswitches FMN-box, B₁₂-box, THI-box (translation termination).

Thiamine riboswitch

Thiamine riboswitch (THI-box) is the only riboswitch which is found in all three kingdoms: it has been found in many bacteria, archaea, algae, fungi and in plants. In bacteria, the THI-box causes translation inhibition and premature transcription termination. In fungi and algae, it controls mRNA splicing [12]. In plants it is postulated to be involved in processing or mRNA stability [13]. Since the cellular levels of TPP is low, the cell carefully regulates the TPP production to meet biological need by regulating the gene expression of the enzymes involved in TPP production. THI-box is present in the intron of 5'-UTR in fungi (e.g. *Aspergillus oryzae*, *Neurospora crassa*) and in the 3'-UTR in plants (*Arabidopsis thaliana*).

Structurally THI-box consists of five helices, P1-P5. They are arranged in two parallel helical structures: P2, bulge J3-2, P3, loop L3, form one helical structure; P4, bulge J4-5, P5, loop L5, form a second helical structure. They are both connected to helix P1 and thus the whole structure represents a tuning fork [14]. Helix P2/J3-2/P3/L3 bind the pyrimidine moiety and helix P4/J4-5/P5/L5 bind the phosphate group of TPP. When TPP is bound it is completely buried in the RNA, sitting perpendicular to the two helices. In presence of Mg²⁺ (1 mM physiological concentration) the affinity of THI-box for TPP is shown to increase by 50 fold [15]. The *E. coli* THI box, called thiM, forms the helices P4 and P5 only on binding to the TPP as they base pair with parts of the expression domain to form a long helix. This leads to the anti-SD sequence becoming unpaired and binding to the SD sequence which then leads to the inhibition of translation [16].

1.2 RNA localization and trafficking

Since the discovery of ncRNAs, there is a need to understand how these players of the same family interact with each other to achieve the proper functioning of the cell. RNA processing is strongly

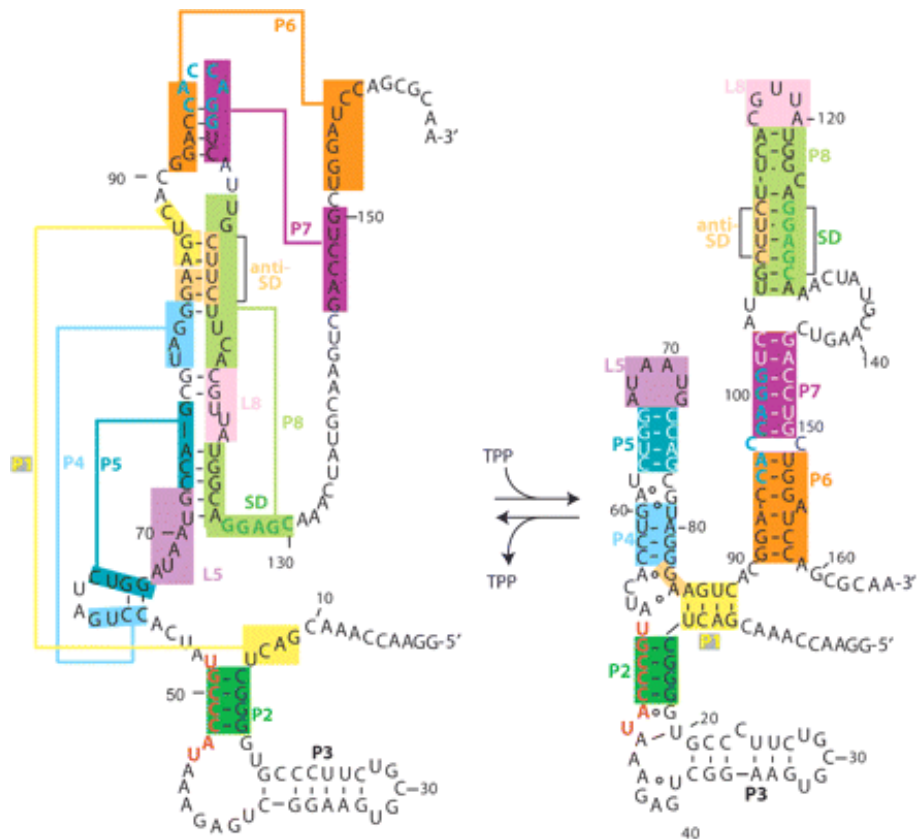


Figure 1.1: thiM riboswitch structure model in the absence (left) and presence (right) of TPP. Nucleotides that form stem structures or loops in the TPP-bound state are color-coded. The nucleotides representing the SD region are depicted in green and the anti-SD region is colored in light orange [16].

interconnected, especially how the different components move through the cell during maturation and RNA processing. As seen from the chapter above, RNAs are processed and regulated by other RNA molecules and a network of interactions exist between different RNA classes. A good example of that is the gene expression, from transcription to translation, a process which involves processing of 3 major RNAs, the rRNA, tRNA and mRNA. rRNA is processed by RNaseMRP and snoRNAs, the tRNA by RNaseP and the pre-mRNA by snRNA which are present in the spliceosomes. Another good example is the regulation of mRNA by miRNA or siRNA so that translation happens only when the correct stimulus is received by the cell, which is a very important feature for neuronal cells. To understand how RNA processing works, i.e. transcription, translation, splicing, silencing, it is needed to have a mechanistic view of how RNA moves in the cell during each process, to gain an integrated view of eukaryotic cellular biology [9] RNA tagging and detection *in vivo* is important to understand how mRNAs are transported to specific sites in the cell and also how different RNAs interact with each other.

Observed in *Ascidian* eggs almost 20 years ago, RNA localization is now considered to be a very essential cellular process governing gene expression in eukaryotic cells. Intracellular mRNA localization is a common mechanism to achieve asymmetric distribution of proteins [17].

1.2.1 Advantages of mRNA localization

mRNA localization is a very important mechanism for the cell and has many advantages. Firstly it allows gene expression to be spatially restricted in the cytoplasm. Secondly, it gives high temporal resolution to protein expression as a local stimuli can initiate on-site translation of the mRNA. Thirdly, the cell saves energy and resources as it does not have to translate mRNA at one site and transport each protein individually to each site. With mRNA transport, localized mRNAs can be translated multiple times to generate many copies of the protein at the required site itself. Lastly, the local translation of proteins protects the cell from some toxic or deleterious proteins, as they are translated only at the site of action and maybe excised out of the cell.

1.2.2 mRNA localization in different organisms

Almost 70% of the mRNA in *Drosophila* embryo has been observed to have asymmetrical distribution [18]. The cellular distribution of maternal mRNAs plays an important role in patterning and

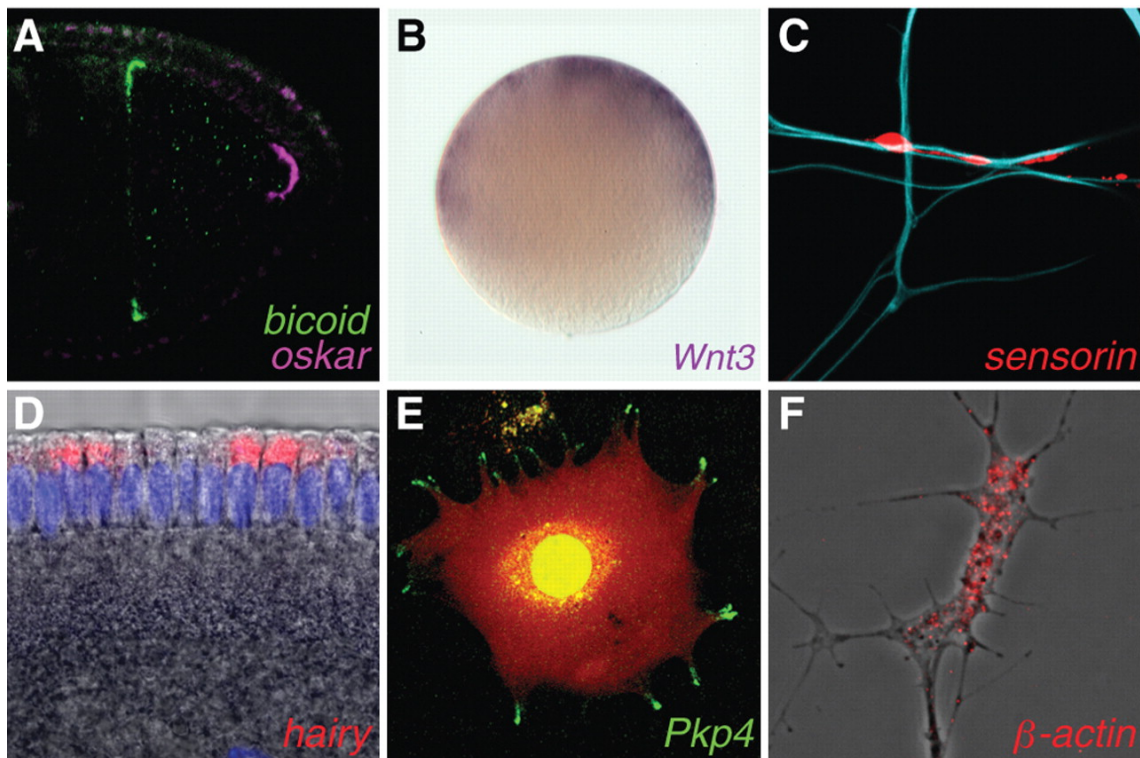


Figure 1.2: Examples of asymmetrically localized mRNA, (A) *Drosophila* oocytes, (B) Egg of a cindarian, *Clytia*, (C) *Aplysia* sensory neuron, (D) *Drosophila* embryo, (E) Cultured mammalian fibroblasts, (F) *Xenopus* axonal growth cone.
Christine E .Holt *et al.* *Science*, Vol.326 #1212, 2009

establishing of dorso-ventral and antero-posterior body axes in *Drosophila* [19]. In *Xenopus* they are found to be important for germline development and patterning of the mesoderm and endoderm [20]. In yeast, *Saccharomyces cerevisiae*, actomyosin-dependent mRNA trafficking participates in polar growth, asymmetric cell division, targeting of membrane proteins and import of mitochondrial proteins [21]. The best example is transport of *ASH1* mRNA to the bud tip of a dividing cell. This ensures that the mRNA is delivered only in the nucleus of the daughter cell. This was also the system in which for the first time, in 1998, Bertrand *et al.* [22] reported the first glimpse of live cell mRNA trafficking. They inserted MS2phage binding sites in the *ASH1* mRNA and labeled the MS2 coat protein with GFP and described *ASH1* movement in the cell (mechanism described in subsequent chapters). This was the launch pad for *in vivo* detection of mRNA monitoring in a number of organisms. Recently, Zipor *et al.* have reported the use of the MS2 phage system to study the localization of peroxisomal protein encoding mRNAs in *Saccharomyces* [23]. mRNA trafficking has also been observed in

Candida albicans and *Ustilago maydis*, and seems to be universally important for polar growth of fungi.

RNA targeting is also shown to be an essential process for plant growth and development. mRNA transport and localization is emerging as an important mechanism to control protein targeting, determining cell fate and polar cell growth as well as RNA silencing in plants [24].

1.3 mRNA transport in neurons

One of the most remarkable functions of mRNA transport appears to be in the neuronal cells. Neuronal process often extends great distances from the soma. For rapid local response to stimuli and for undergoing change in synaptic strength and structure it is necessary that the protein is translated then and there at the site of stimulation or at the growth cone of the axons in developing brains where the β -actin mRNA has been seen in abundance for stimulant changes in growth in streeing [25]. Activity dependent synaptic changes are required for memory formation and storage in the brain [26], and the models for that are LTP (long-term potentiation) and LTD (long-term depression) [27]. It has now become evident that protein translation is required for the late phase of LTP and intermediate stages of LTD are dependent on new protein translation which is independent of transcription. RNA-binding proteins target specific mRNAs to the synapse. Depending on the stimulus received at the synapse only the right kind of protein is translated and used, proteins that are not used are present in a repressed phase of translation. In hippocampal neurons, strong synaptic activation is accompanied by rapid transcription and transport of *Arc* mRNA to the activated synapse [28]. The *Arc* protein is implicated in the endocytosis of AMPA receptors to maintain synaptic homeostatis [29]. This has been a very important mRNA for studying the rapid induction and transport to the activated synapse for monitoring mRNA transport in the neurons. Guwoski *etal.* conducted enrichment learning experiments on mice followed by a catFISH assay to study how different neurons are stimulated by different stimuli based on this unique feature of *Arc*. Study of *sensorin* mRNA in *Aplysia* shows that not only mRNA localization to the synapse is important, but also newly synthesized Sensorin protein affects synaptic properties, depicting that newly synthesized protein could have different properties from older protein copies. One of the common functional protein mRNAs that localize to the cellular processes in the neurons is CREB (cAMP response element-binding) protein. It can be translated locally in the axons in response to nerve growth factor and undergoes retrograde transport to the nucleus where it activates transcription of target genes [20]. Defective transport of mRNA to the synaptic sites has been

shown to cause a number of disease like conditions, e.g. Fragile X Mental Retardation, which is due to improper binding and transport of mRNA by FMRP (fragile X mental retardation protein).

For dendritic targeting of mRNAs, the sequence carrying their destination address is usually encoded in the 3'-UTR. Shortly after transcription and splicing, the newly formed mRNA is bound by RNA-binding proteins at its 3'-UTR before it comes out of the nucleus. It is also attached by hnRNPs (heterologous nuclear ribonucleoproteins) in the nucleus, which have been shown to shuttle out with the RNA and then shuttle back in the nucleus once their cargo has been delivered. As soon as the RNA comes out of the cytoplasm it is bound by other RNA binding proteins, ribosomes, RNA helicases, protein translation machinery (e.g eIF4), motor proteins and small ncRNAs that keep the mRNA translation repressed or stalled till the mRNA reaches its target site, or receives the correct stimulus for translation as in some dendritic proteins. Thus the mRNA does not travel unattended, but accompanied by a whole set of proteins and this whole complex is called a Ribonucleoprotein particle (RNP). The RNPs travel rapidly, at a rate of $0.1 \mu\text{m/s}$, bidirectionally and with support of the microtubules or kinesin. Once the RNPs reach the target destination, and receive the right stimulus, the translation machinery is activated, the hnRNPs are sent back to the nucleus and the mRNA is translated into a protein.

Understanding the dynamics of mRNA transport, the specificity of its localization, the spatial and temporal aspects of transport are vital. For this, visualizing the mRNA in live cells is important.

1.4 Methods to detect RNA in cells

Sensitivity and precision in RNA detection and tagging methods is very important for determining the functioning of a cell and understanding the diseased states. There are a number of diseases linked to defects in expression or functioning of the RNA [30, 31], also miRNA's function has been implicated in cancer biology, fragile X syndrome, schizophrenia, which makes it important for us to detect RNA expression and study its transport and functioning in the cell. Also, in the recent years studying the transport of mRNA has been a very interesting and exciting subject. The finding that IEGs (Immediate Early Genes) e.g. *c-fos*, *Arc*; are rapidly expressed in the neurons on stimulation and some of them are transported to the sites of synaptic plasticity as a ribonucleoparticle (RNP) to be translated. This has necessitated the study about which IEGs are expressed by which neurons on what stimulus and the sites of stimulation to where the RNP translocates.

The initial methods to study RNA expression in a given population on cells was done by cell disrupt-

tion, extraction on total cellular RNA and its analysis *in vitro* to quantify RNA, like semi-quantitative PCR. The other methods are Northern Blotting, separating cellular RNA by size, microarray, and serial analysis of gene expression for high throughput detection of many RNAs at once. The major disadvantage of the above mentioned methods is that these involve extraction of RNA from the cell and subsequent analysis. Therefore, it is not possible to determine when the RNA is transcribed and how, and where it transports into the cell. But this information is important in order to understand malfunction in the cells due to latency in gene expression or due to non-directed transport of the RNP e.g. defects of oocyte development if the RNA is not transported to the polar region. To overcome these problems, newer methods were designed to understand the temporal and spatial behavior of RNA in the cell. These methods include fluorescence *in situ* hybridization (FISH) where exogenous short oligonucleotide probes carrying a fluorophore tag are used to bind to a specific sequence on the targeted cellular RNA. A modification of this method is the catFISH [32]. catFISH allows temporal and spatial quantification of a neuronal population which have been activated by two distinct stimuli, thereby a separate set of animals for quantification by each stimuli is not required. The above methods though label the RNA in the cells, do cause disruption of the cell membranes because of the chemicals used to introduce the oligoprobes and secondary labels inside the cells; the cells must be fixed and excessive washing is required to wash off the unlabeled probes which otherwise leads to false signal. Other methods include 'Quenched probes', Molecular beacons, dual FRET probes, and quantum dots to label the endogenous RNA and track its localization or study RNA dynamics. A cartoon representation of various methods to study RNA localization is given in figure 1.3. The disadvantage here is that these methods also involve disruption of the cell membrane to introduce the probes in the cell [33]. Other methods include selection of RNA aptamers which bind a fluorescent dye and this binding causes increase in the fluorescence signal of the dye, called 'light up' method, and such aptamer-fluorophore complex is sometimes called 'light-up pairs'. A number of such light up probes for RNA detection have been developed like Malachite green (shown in 1.4), nonspecific dye thiazole orange (TO) which binds to small molecules such as GMP and AMP. But the drawback of this dye is that it binds to endogenous GMP and AMP. To work with this method, generation of an RNA aptamer that binds specifically to the dye is necessary. That aptamer should then be fused to the gene of interest. The aptamer size is also quite small and is advantageous. A number of groups are working on dyes like Sulforhodamine B, Dimethyl Indole Red (DIR), but work needs to be done to make them work *in vivo* so that the dyes are not toxic to the cell and can penetrate the cell without disrupting the membrane, plus increasing the number of dyes with which we can monitor more than one RNA at a time or RNA-RNA interactions [33].

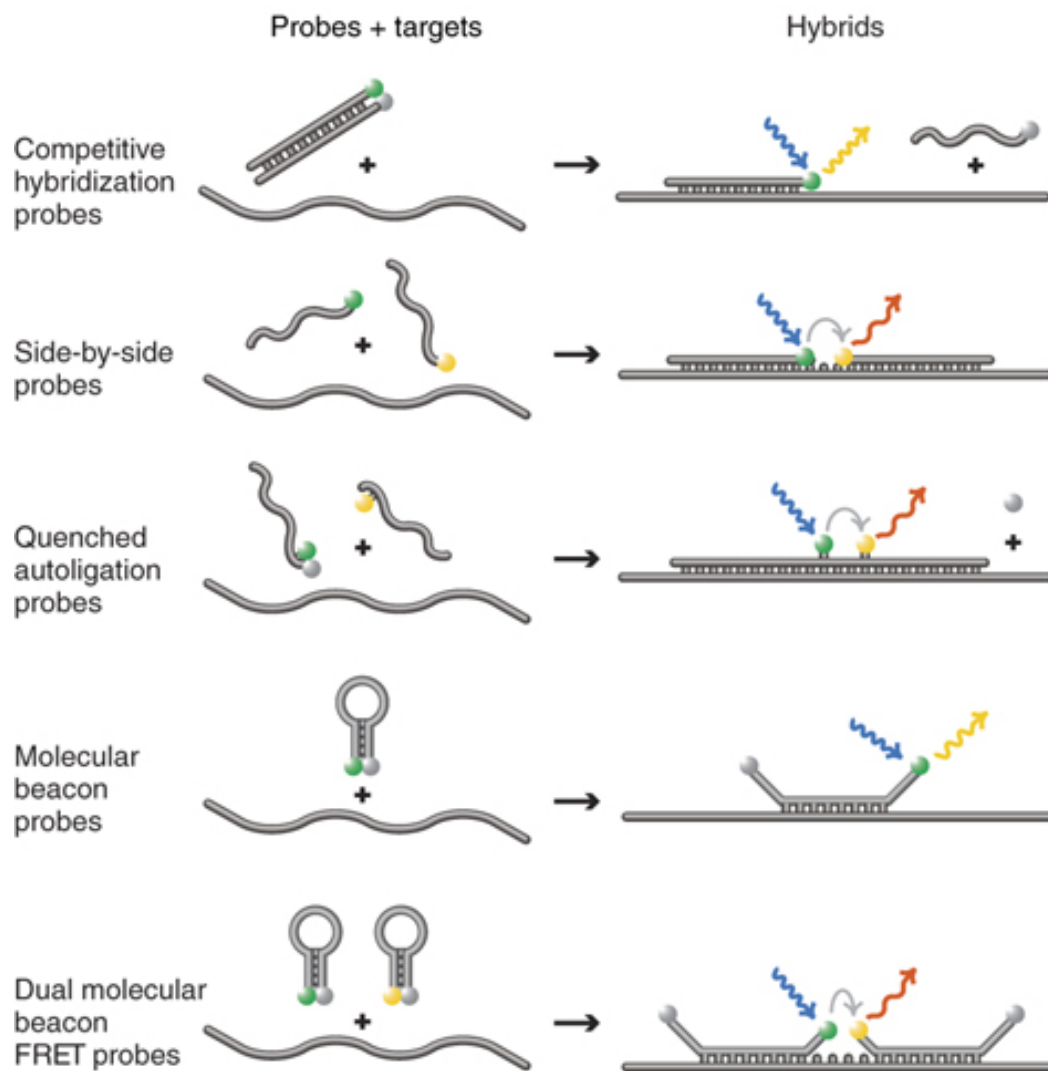


Figure 1.3: Schematic representation of different fluorogenic probes for detection of mRNAs. Donor (green), quencher (gray) and acceptor (yellow) dyes are attached to the probes and interact as indicated.

Sanjay Tyagi, Nature Methods, Vol.6 #5, May 2009

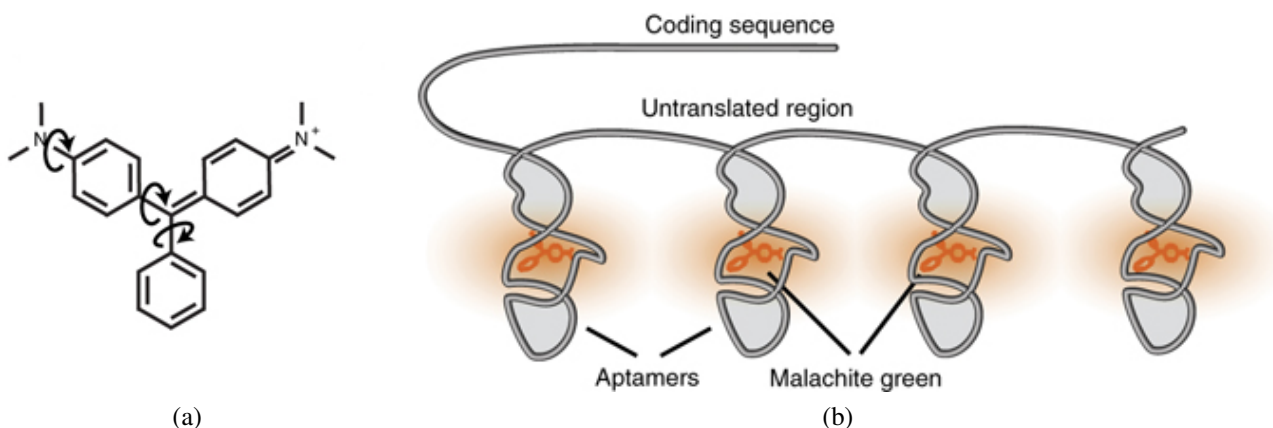


Figure 1.4: Malachite green binds to mRNA and makes it fluorescent. (a) Chemical Structure of Malachite Green, it is non fluorescent because of the phenyl rings that rotate like a propeller and dissipate the energy that the dye absorbs from light. (b) Schematic representation of an mRNA with aptamer motifs bound to Malachite green in the UTR.

Sanjay Tyagi, *Nature Methods*, Vol.6 #5, May 2009

1.5 Use of bacteriophage RNA binding peptides for mRNA tagging

Monitoring RNA transport and kinetics in live cells would be much easier if fluorescent RNA tags existed that could be directly cloned into the RNA of interest. But the lack of such fluorescent RNA tags necessitated the development and use of a different approach to study RNA transport *in vivo*. This approach involved the use of two recombinant molecules. First one is a hybrid RNA where the mRNA of interest is fused to a RNA binding sequence specific to an RNA-binding protein (RBP) and the second is the RNA-binding protein fused in-frame to an easily readable protein (mostly a fluorescent protein). When these two constructs are co-expressed in a cell, the fluorescently tagged RBP should be tethered to the exogenous mRNA via the cognate RNA sequence. This tethering approach allows to monitor the RNA in live cells since a functional read-out protein is fused with the RBP. In some cases this approach is used to study the functional domains of a RBP. An ideal RBP should bind with great affinity and specificity to its cognate RNA (among the many other RNA sequences in the cell) and should not be naturally found in the cells used for RNA imaging. Since the success of using GFP based fluorophores for protein detection *in vivo*, their use has been adapted for RNA detection *in vivo* [34]. To achieve the purpose of imaging RNA, multiple copies of the phage hair-pin motif

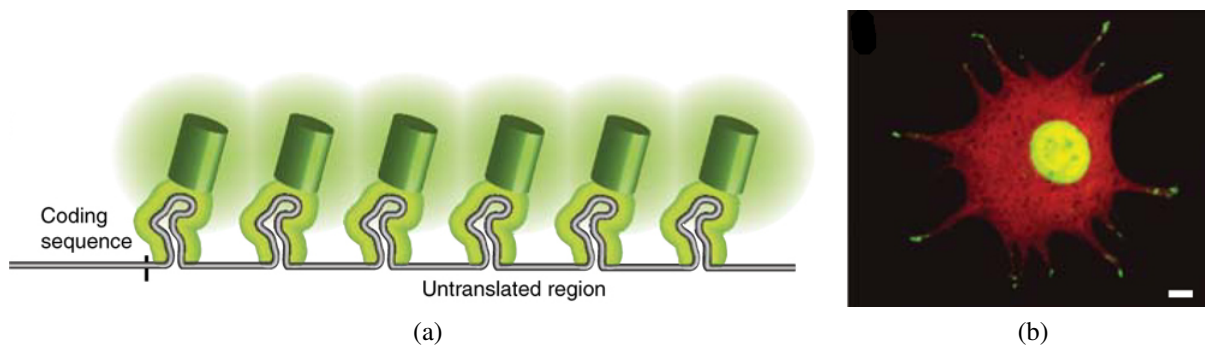


Figure 1.5: mRNA imaging with GFP tagged RBPs. (a) Schematic representation of MS2 phage coat protein-GFP based tagging. A number of MS2 coat proteins bind to cognate RNA sequence which is introduced in the 3'UTR of the target mRNA. Since each MS2 coat protein carries a GFP tag, it makes the mRNA more fluorescent than the surrounding. (b) Fluorescence image of a fibroblast expressing MS2 coat protein-GFP and an mRNA containing a RAB13 UTR, and 24 copies of MS2 phage hairpin.

Sanjay Tyagi, Nature Methods, Vol.6 #5, May 2009

are cloned in the UTR of the mRNA under study. And this mRNA, along with the RBP fused with a fluorescent protein reporter, are co-expressed in the cell. Upon binding of the fluorescently tagged RBP on the RNA motif, the mRNA is rendered fluorescent and thus can be imaged in the live cell. Since GFP tagged RBP is always fluorescent, GFP bound to mRNA needs to be differentiated from unbound GFP. This was achieved by introducing a nuclear localization signal to the GFP-fused RBP, so that the unbound RBP-GFP resided in the nucleus and only on being bound to the mRNA it comes out in the cytoplasm to be imaged. The advantages offered by this method are that it allows kinetic studies of RNA turnover, transport and interactions as two different RBPs can be used at the same time to label two different RNAs and there is no need to perturb the cellular membrane to introduce the probe in the cell. This approach is used in many laboratories for studying mRNA localization in live cells and two most widely used proteins are of bacteriophage origin: MS2 phage coat protein and 1-22 peptide of Lambda N protein. A cartoon representation of RNA tagging and monitoring using bacteriophage system is shown in figure 1.5 .

In 1998 Bertran *et al.* used MS2 phage coat protein for studying *ASH1* mRNA localization in yeast cells. MS2 coat protein binds to a unique RNA hair pin structure towards which it has a strong affinity. The MS2 phage coat protein is 129 amino acids and it binds as a dimer to a 19 nucleotide long stem-loop structure. At higher concentrations, the MS2 coat protein dimerises. It was also observed that on increasing the number of binding sites for the MS2 coat protein, the binding affinity is not increased

but causes a decrease in the steady state level of the reporter mRNA. The MS2 phage is not affected by the nucleotides in the stem region of the RNA. The reasons for more number of studied using MS2 phage coat protein for tethering over the λ_{N22} peptide can therefore be purely historical [35].

The λ_N system was recently discovered as an alternative to the MS2 phage system. It binds with tight affinity and specificity to its cognate RNA sequence boxB. The development of λ phage in *E.coli* depends on the positive control of genes transcribed by promoters pR and pL, which in turn are regulated by two operon specific antiterminator proteins *cro* and *N*, respectively. The *N* antiterminator activates the early operons and the *cro* antiterminator activates the late operon. These proteins function by binding to RNA polymerase (RNAP) during early phase of transcription and block its response downstream. The *N* protein is an RNA binding protein that requires a specific RNA sequence in the transcribed RNA for binding.

The *N* protein requires a *nut* site for its action. The *nut* site functions in the form of an RNA, it binds *N* protein, then undergoes RNA looping and delivers *N* protein to RNAP thus facilitating interaction between *N* protein and RNAP. The interesting discovery here is that the *nut* site contains two important domains: boxA and boxB. boxA is 8-12 bp, and 5-10 bp downstream of it is the 15 bp boxB domain. boxB is an interrupted palindrome which can fold into a hairpin (stem-loop) structure. boxA is a conserved sequence and is recognized by *N* proteins of related ‘lambdoid’ phages. But boxB’s sequence varies from phage to phage and is recognized only by its cognate *N* antiterminator protein and binds to it [36].

1.5.1 Binding of the λ_N peptide to boxB

The λ_N peptide interacts with boxB site via its arginine-rich domain. Studies on a number of RNA-binding proteins like ribosomal proteins, the coat protein from RNA viruses, the human immunodeficiency virus (HIV) Tat and Rev proteins and the bovine immunodeficiency virus Tat protein show that they have a similar RNA binding structure. It consists of one arginine rich motif, as short as approximately 8-20 amino acids in length. Tan and Frankel, in 1995, showed via extensive mutagenesis and CD spectroscopy that the λ_N (1 – 22 amino acids) peptide consists of an arginine rich domain and displays 35 % α -helical conformation. The isolated peptide largely displays a random coil structure, but the bound peptide shows an α -helical content of 80 %. Mutations like Glu Pro, at position 9 eliminated the α -helical conformation and bound their cognate RNA with very poor affinity [37].

Binding of the protein to the RNA is accompanied by structural rearrangement of the RNA structure, like nonstandard base pairing and stacking plus changes in groove dimensions. The λ_N peptide

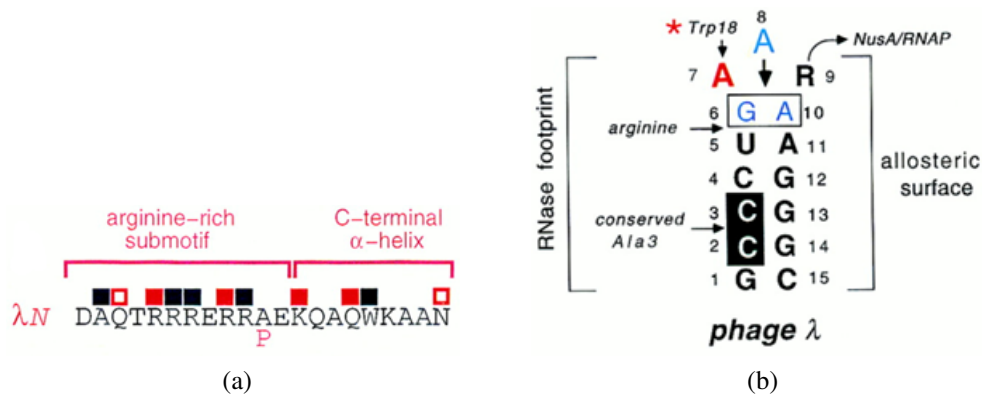


Figure 1.6: Alignment of arginine-rich N sequences in phages λ (Franklin 1985b; Chattopadhyay *et al.* 1995b (a) Consensus boxB hairpin in phage λ showing specific pattern of base-pairing and base-flipping (purines 7 and 9) (b). Three sites of peptide-base contact (Su *et al.* 1997) are as indicated. The open box indicates a sheared GA base pair; the black box highlights the position of contact with Ala-3 in the major groove. The RNase footprint of the N protein (Chattopadhyay *et al.* 1995a) is shown at left; the proposed allosteric surface involved in binding to the core antitermination complex is shown at right. (R) The proposed interaction of the flipped base (R9) with NusA in an antitermination complex is indicated.

Su L *et al. Genes Dev.* 1997; 11:2214-2226

recognizes both the stem and loop region nucleotides for effective binding. The boxB of λ phage is 15 nucleotides long, a palindrome hairpin structure which contains a purine rich pentaloop. As discussed above that the N protein binding to the *nut* site of the RNA leads to RNA looping and forms a functional bridge between the N protein and the RNAP (as shown in figure 1.6). Su *et al.* in 1997, showed that the asymmetrical binding of the arginine rich domain of the λ_N peptide to one side of the RNA leads to the re-structuring of the other via base-pairing, stacking and flipping. This structural change is strongly required for its biological activity, as boxB binds NusA only once it is bound to N protein and its conformation changes. The unbound boxB consists of a stem and a flexible loop with stable base pairing and base-stacking. Once the λ_N peptide binds to the boxB, the 5'-G and the 3'-A form a sheared base pair. Over this are stacked purine and pyrimidine bases (or displaced), leading to the formation of a GNRA tetraloop. This tetraloop structure requires the indole-base stacking which is provided by the Trp-18 of the λ_N peptide. Trp-18 forms a direct stacking with the A7 purine of the RNA and this stabilizes the tetraloop, which stabilizes the G-A sheared base thereby leading to the looped conformation that is needed for the N-protein RNAP interaction, as shown in figure 1.7. Change of base from A to U decrease the stacking with the TRp-18[38].

Austin, *et al.* in 2002 showed that the λ_{N22} peptide binds with picomolar affinity to their cognate

Overview of λ N regulatory system.

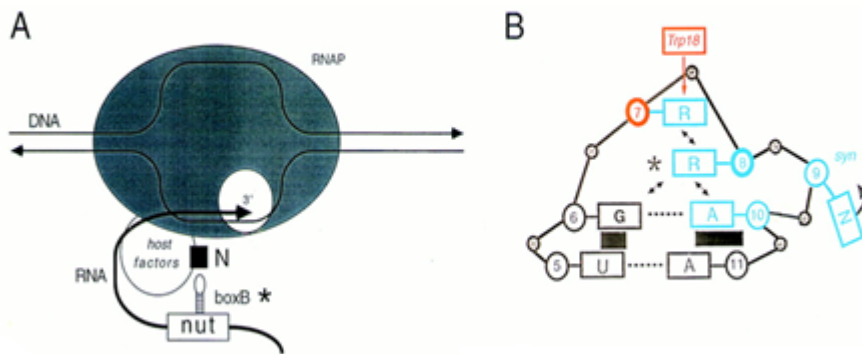


Figure 1.7: (A) The N protein binds to an RNA enhancer element in the nascent message (nut site; asterisk indicates boxB RNA hairpin) and to host factors and RNAP to direct formation of a processive antitermination complex. (B) Closing base pair (U5 and A11) and purine-rich pentaloop (bases 6–10; underlined) of 15-basenuL boxB (5′-GCCUCGAAGAAGGGC-3′), with numbering scheme as shown. Red-outlined box (Trp-18) and nucleoside position (7) indicate site of indole–adenine stacking; blue nucleosides (7–10) exhibit a specific pattern of base-pairing (A10), -stacking (asterisk), and flipping (G9). Black rectangles indicate stacking between closing base pair (UA) and GA sheared base pair. Bidirectional arrows indicate NOEs between purines; base 9 is “flipped out.” Peptide–RNA contacts (such as A7–Trp-18) were identified by isotope-filtered NMR experiments designed to resolve NOEs between ^{13}C - or ^{15}N -attached protons in a labeled peptide and ^{12}C - or ^{14}N -attached protons in the unlabeled RNA .

Su L et al. Genes Dev. 1997; 11:2214-2226

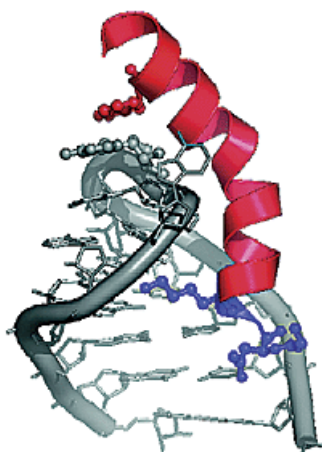


Figure 1.8: Structural model of λ_{N22} - λ_{boxB} . The second base in λ_{boxB} (in Grey) loop stacks with Trp18 of λ_{N22} (in red) in the cognate complexes.

Ryan J. Austin, *et al.* JACS, 124, 10966-10967, 2002

RNA hairpin at physiological salt concentrations [39]. The structural model of λ_{N22} - λ_{boxB} binding is shown in figure 1.8.

These studies lead to the use of λ_{N22} peptide as an RNA tethering protein to study RNA-protein interactions and mRNA transport. Initially the λ_N peptide was used by De Gregorio *et al.*, in 1999, with just 1 λ_{boxB} site; later 5 λ_{boxB} sites were used for effective binding and tethering by Nathalie Daigle and Jan Ellenberg to study mRNA transport via β -actin zip code. The λ_{boxB} insertion sites also varied from the 5'-UTR to the inter-cistronic region, the 3'-UTR, to just before the stop codon, with 3'-UTR region being the most common RNA insertion site. λ_N peptide's RNA binding property has been used to analyze protein function for Agronulate 1 & 2 in HeLa cells [40, 41]; for studying mRNA transport via β -actin zip code in NRK cells [42]; for studying the translation in *Xenopus* oocytes by injecting the oocytes with the *in vitro* transcribed mRNA [43].

The recent advantage is that with the development and use of λ_{N22} , it has provided an opportunity to image two mRNA species simultaneously, e.g. monitoring of ASH1 mRNA by λ_{N22} , and IST2 mRNA by MS2 phage done in yeast by S. Lange *et al.* [17].

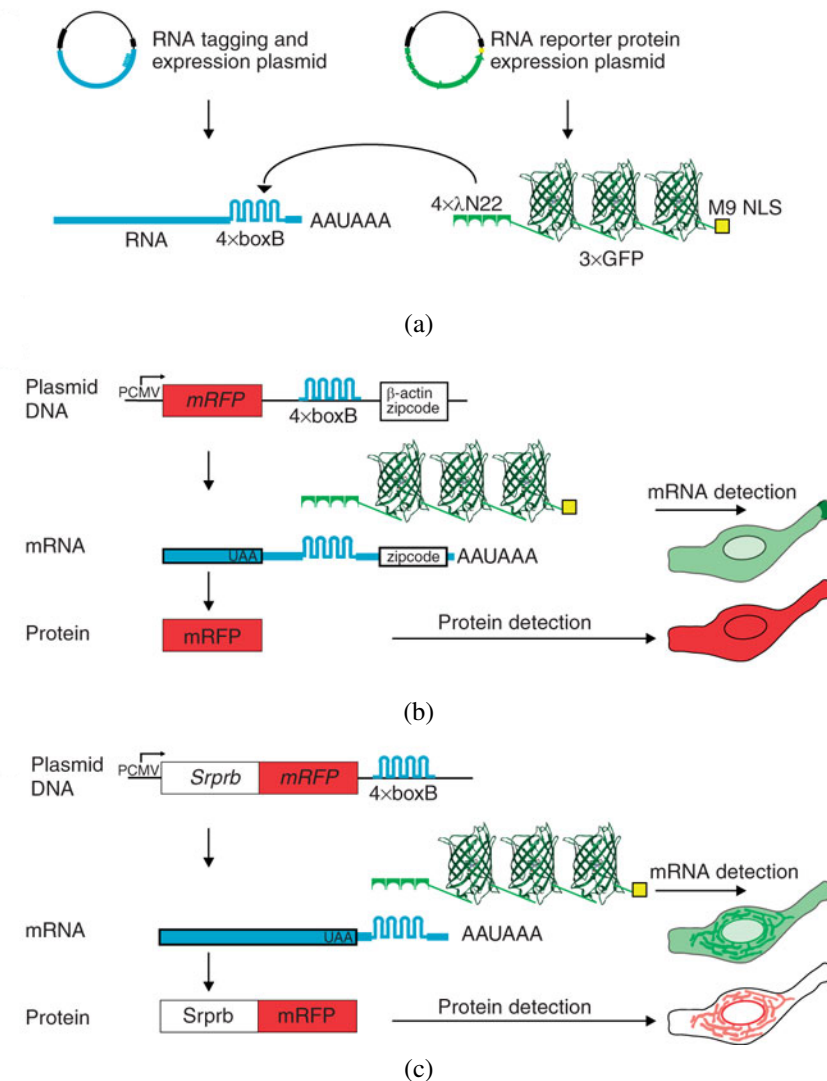


Figure 1.9: Schematic representation of the GFP-based tagging with λ_{N22} . (a) Expression plasmids encoding RNA fused to 4XboxB (left), and the RNA reporter protein, a fusion of 4X λ_{N22} , 3XmEGFP and M9 nuclear localization sequence (NLS). Arrow shows binding of λ_{N22} peptide to the RNA hairpin. (b,c) Test plasmid, RNA product and cartoon representation of expected sub-cellular localization of mRNA and encoded protein for an mRNA exported from the nucleus and localized to the cell leading edge (b) and targeted to the ER (c). Expression driven by pCMV promoter. *Daigel & Ellenberg, Nature Methods, Vol.4, No.8, 2007*

1.6 Tn5 transposon system

Transposons are mobile DNA sequence found in prokaryotic and eukaryotic genomes. Transposons have long been used for randomly distributing primer binding sites, creating knockouts, and introduction of genetic tag into long DNA sequences. One of the most commonly used transposon systems is Tn5 which was isolated from gram negative bacteria.

Tn5 consists of two inverted, almost identical sequences called IS50L and IS50R that encompass genes coding for resistance for kanamycin, bleomycin and streptomycin. Tn5 transposition mechanism occurs through 'cut and paste' method. The transposon is excised from its site on the donor DNA and inserted into target DNA sequence. This activity is executed by enzyme Transposase (Tnp) which is encoded by IS50R. No host proteins are required for this action. Tnp first identifies and binds to the ES (End Sequences) within a compacted DNA polymer. The ES are inverted 19 bp DNA sequences at the termini of IS50 in order to catalyze transposition. The Tnp forms a complex with the two ES-bound Tnps thus forming a scaffold for enzymatic catalysis. The DNA cleavage occurs that releases the ES sequence at each end of the donor DNA. The cleaved Tnp-ES DNA complex is then bound to the target DNA as the DNA cleavage from the donor results in displacement of donor DNA. Tnp then catalyses the insertion of ES DNA into the target DNA via nucleophilic attacks by two 3'OH groups on either side of a 9 bp target DNA. In the end, the Tnp complexes with ES and target DNA are released and the 9 base pair gaps on either side of the inserted Tn5 sequence are filled by the host cell machinery.

The transposon Tn5 has been modified for commercial use and has 1000 fold higher transposition efficiency than a wild type Tn5 system.

1.7 Fluorescence

Fluorescence is known to be a process of luminescence describing an electronic system that is excited by absorbing light of a certain wavelength and relaxed by releasing light with a higher wavelength. Molecules having the ability to undergo fluorescence are called fluorophores, those that only absorb light without being able to emit light are named chromophores.

A fluorophore can absorb one photon of a certain energy or several photons with equivalent summed energy (time slot for several photons: 10^{-15} s), leading to the transition of an electron from ground state to an excited singlet state. Precondition for absorption is parallelism of transition dipole moment

of the molecule with the photon's electric field component oscillation plane.

Fluorescence lifetime

The average time a fluorophore stays in its excited state is called fluorescence lifetime τ . It is typically in the range of some nanoseconds and shows a single exponential decay for most fluorescent molecules:

$$I(t) = I_0 e^{-\frac{t}{\tau}}$$

Every fluorophore has a characteristic fluorescence lifetime that is dependent on environment conditions and can be quenched by oxygen or nearby fluorophores. Thus it can be measured to estimate energy transfer (FRET) that is described in the next section.

Stokes shift

After absorbing a photon, some of the gained energy will be internally converted to heat. Thus, the emitted photon will have a longer wavelength (shifted to red spectrum) - the offset of emitted wavelength to excitation wavelength is called Stokes shift. It is as well as the fluorescence lifetime characteristic for each fluorophore and also shows a dependence on environment conditions.

Quantum yield

Another important characteristic of fluorophores is the quantum yield, also called quantum efficiency, describing the chance of emitting a photon from the excited state:

$$QY = \frac{N_{emitted}}{N_{absorbed}}$$

where $N_{emitted}$ is the number of emitted photons and $N_{absorbed}$ is the number of absorbed photons. A quantum yield of 1.0 (equals 100 %) implies that all excited molecules release a photon when relaxing to the ground state. There is no dependence of the quantum yield on the wavelength of a fluorophore.

Extinction coefficient

Based on the Beer-Lambert law, absorbance of electromagnetic radiation passing through a substance of molar concentration and 1 cm thickness is defined by the molar extinction coefficient ε :

$$\varepsilon = \frac{E}{c \cdot d}; E = \log_{10} \frac{I_0}{I}$$

where E is the extinction (decrease of initial intensity), c is the concentration and d is the film thickness in a cuvette. ε is dependent on temperature and wavelength and can easily be determined by a photometer with the common unit of measurement $l \text{ mol}^{-1} \text{ cm}^{-1}$.

Intrinsic brightness

As a measure for comparison of optical properties among different fluorophores, the intrinsic brightness is introduced as the product of quantum yield and extinction coefficient. The unit of measurement is $l \text{ mol}^{-1} \text{ cm}^{-1}$.

1.8 FÖRSTER resonance energy transfer (FRET)

1.8.1 Principle of FRET

FÖRSTER resonance energy transfer, named after Theodor Förster, is the physical process of radiationless energy transfer from a *donor* molecule to an *acceptor* molecule. In relation to fluorescence measurement methods the donor or both, donor (D) and acceptor (A) must be fluorophores.

This powerful technique can be applied as a sensor method on molecular level to monitor amongst others (see figure 1.10 on the facing page):

- cleavage
- interactions of molecules
- proteolysis
- protein modifications

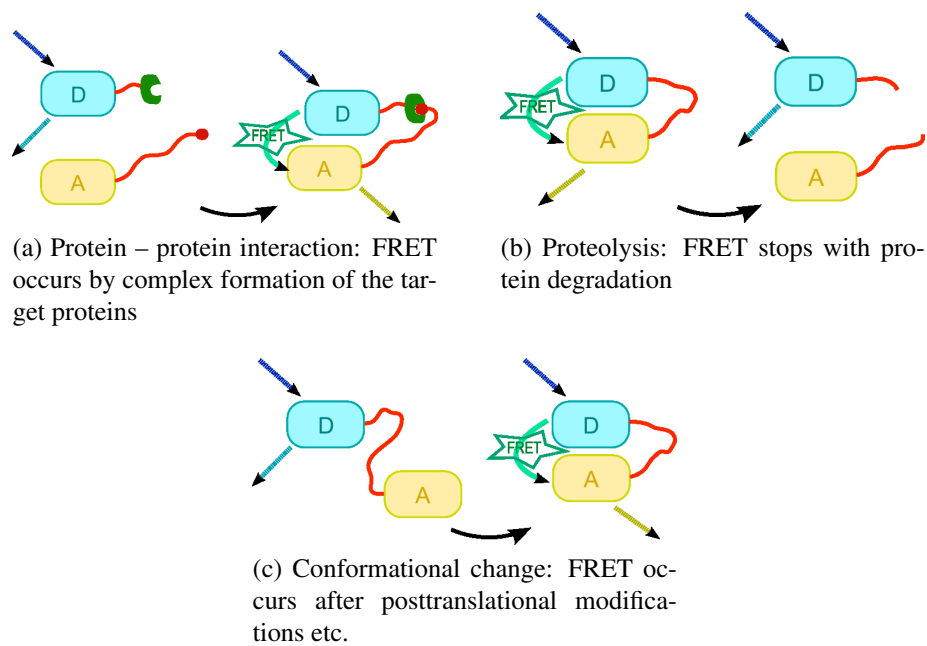


Figure 1.10: Typical applications of FÖRSTER resonance energy transfer (FRET) with fused fluorescent proteins. *D* and *A* refer to the donor and acceptor, respectively
Kees Jalink, Netherlands Cancer Institute (NKI-AVL)

- conformational changes

The ratio of the number of energy transfers to the number of donor excitations is defined as FRET efficiency *E*:

$$E = \frac{N_{energy\ transfers}}{N_{donor\ excitations}}$$

It also reflects the resonance energy transfer rate in a ratio to the sum of the donor emission rate, energy transfer rate and the radiationless decay rate:

$$E = \frac{k_{ET}}{k_f + k_{ET} + \sum k_i}$$

Three major preconditions must be fulfilled in order to achieve a high rate of radiationless energy transfers:

1. Spectral overlap:

The donor emission spectrum must overlap with the acceptor excitation spectrum (see figure 1.11)

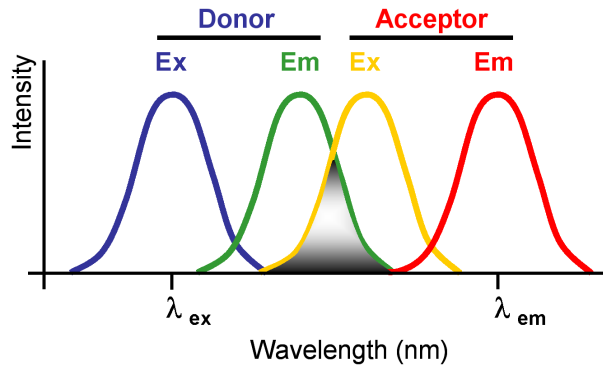


Figure 1.11: Spectral overlap of donor emission and acceptor absorption: emitted photons from the donor are within the wavelength range of the acceptor. Nevertheless, the energy from donor to acceptor is transferred radiationless.

Author: Maurel Damien

2. Distance of donor and acceptor:

At a certain distance between donor and acceptor, called FÖRSTER radius R_0 , the FRET efficiency reaches 50%. It is of utmost importance to control the distance r , which is in the range of 1 – 10 nm, as it affects the FRET efficiency by the sixth power:

$$E_{FRET} = \frac{R_0^6}{R_0^6 + r^6}$$

where r is the distance of the FRET pair.

3. Orientation:

Donor and Acceptor should have parallel or close to parallel oscillation planes. The energy transfer rate and the 6th power of FÖRSTER-Distance R_0 are proportional to κ^2 :

$$k_{ET}, R_0 \sim \kappa^2$$

Values of κ^2 are in the range of 0 to 4, where 0 describes orthogonality of donor and acceptor,

whereas 4 indicates parallel and collinear orientation. For measurement of FRET with freely diffusing donor and acceptor molecules, e.g. in a fluorescence spectrometer cuvette, κ^2 equals $2/3$. If two fluorescent proteins that are suitable for FRET are fused intra-molecular, controlling the orientation of both is especially important. Thus, changes in FRET efficiency can originate from conformational or orientation variations.

1.8.2 Measurement of FRET

1.8.2.1 Only donor is fluorescent

Energy transfer from donor to acceptor can be measured with a fluorescence spectrometer or a fluorescence microscope using different methods:

- measurement of donor emission

Resonance energy transfer leads to a decreased intensity of donor emission. Thus, measurement of donor emission in presence (I_{DA}) and absence (I_D) of the acceptor can give quantitative results for FRET efficiency:

$$E_{FRET} = 1 - \frac{I_{DA}}{I_D}$$

- measurement of fluorescence lifetime

The characteristic fluorescence lifetime of the donor fluorophore can be quenched by energy transfer or local environment:

$$E_{FRET} = 1 - \frac{\tau_{DA}}{\tau_D}$$

Measurement approaches are time domain or frequency domain based.

1.8.2.2 Donor and acceptor are fluorescent

The ratio of donor intensity to acceptor intensity can provide a measure for energy transfer, but due to the strong dependence on intensity and fluorophore concentrations, this approach requires complex data acquisition and processing.

1.8.2.3 Design rules of fluorescent proteins for FRET

Design and improvement of FPs for FRET experiments should focus on maximizing the FRET efficiency E and the intensity ratio of donor and acceptor ($R=I_A/I_D$). Additionally, a good FRET pair reveals conformational changes or bindings by providing an adequate change in FRET efficiency (ΔE) and accordingly a robust change in $\Delta R/R_{min}$.

1.9 Fluorescent proteins

Fluorescent proteins (FPs) are proteins that emit fluorescence light of a certain wavelength range in the visible spectrum when exposed to light with shorter wavelength. They are of invaluable relevance for modern cell biology as they can be fused to other proteins of interest to function as markers or biosensors, as they are less toxic than chemical dyes when excited by fluorescence light. Another major advantage over synthetic dyes, that need to be manually introduced in the cells, FPs can be expressed by intracellular transcriptional and translational machinery and do not require external cofactors except oxygen to find the final conformation [44]. Due to the fluorescence of FPs it is possible to record time and space distribution of the fused protein in living cells, organs and whole organisms. Most of engineered FPs to be used in biology labs are based on the discovery of the *green fluorescent protein*.

1.9.1 History

In the 1960s and 1970s Osamu Shimomura [45] first purified the *green fluorescent protein* (GFP) from the jellyfish *Aequorea victoria*. It took then another two decades until Douglas Prasher achieved cloning and sequencing of wtGFP in 1992 [46]. The lab of Martin Chalfie published expression of wtGFP in *E. coli* and *C. elegans* in 1994 [47] with some minor changes in the sequence. The experiments showed, that this near-wtGFP folded and was fluorescent at room temperature, without the need for exogenous cofactors specific to the jellyfish. But wtGFP had several drawbacks, including dual peaked excitation spectra, pH sensitivity, chloride sensitivity, poor fluorescence quantum yield, poor photostability and poor folding at 37°C.

The crystal structure of GFP was first reported independently in 1996 by the Remington group [48] and the Phillips group [49]. Solving the crystal structure was important for understanding the chromophore formation and interactions of neighboring residues.

1.9.2 Structure and properties

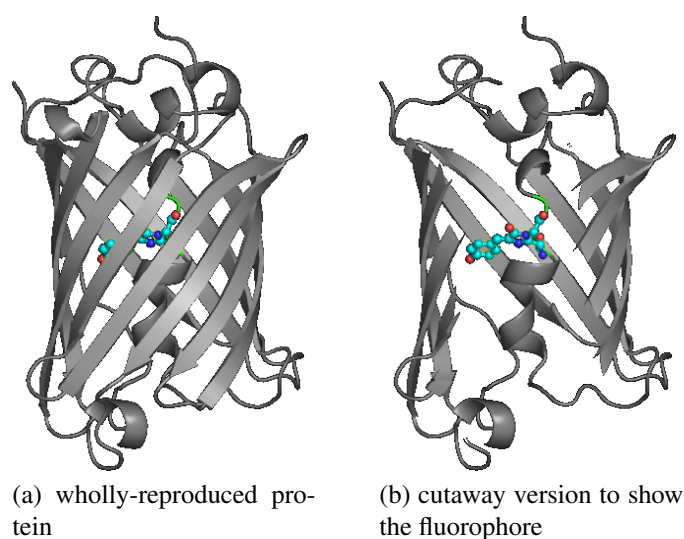


Figure 1.12: Green Fluorescent Protein drawn in cartoon style with fluorophore highlighted as ball-and-stick

A fluorescent protein consists of a few amino acids forming a small chromophore which is encased in a 11-stranded β -barrel structure of ~ 27 kDa [46, 50] (figure 1.12). The GFP from *A. victoria* has a major excitation peak at a wavelength of 395 nm and a minor one at 470 nm. Its emission peak is at 509 nm which is in the lower green portion of the visible spectrum [51]. Its physical and chemical properties are dependent on environment conditions (pH value, temperature) and on the composition of amino acids. The emission of wild-type GFP for example is quenched by acidic pH values with an apparent pKa near 4.5, whereas excitation efficiency is slightly shifted from the main excitation peak at 395 nm to the subsidiary peak at 470 nm [50]. Oxygen is only required for maturation of GFP and does not seem to effect the fluorescence properties. High GFP concentrations amplify excitation peak at 395 nm at the expense of the peak at 470 nm [51]. Table 1.1 shows fluorescence properties of the commonly used enhanced GFP (EGFP) from CLONTECH. Changes in the sequence can emerge the development of dedicated FPs for specific applications, e.g FRET (see 1.8).

1.9.3 GFP derivatives

The wide range of applications (see 1.9.4) as well as the negative properties of wtGFP (see 1.9.1) triggered the development of derivatives with improved spectral characteristics, like fluorescence in-

tensity, photostability, and excitation and emission wavelengths matching those of common filter sets. The lab of Ole Thastrup [52] discovered enhanced GFP (EGFP), a point mutation leading to an increased folding efficiency at 37 °C, opening GFP to applications in mammalian cells.

Many color mutants have been designed, including blue fluorescent protein (EBFP, Azurite etc.), cyan fluorescent protein (ECFP, Cerulean, CyPet), yellow fluorescent protein (YFP, Citrine, Venus, YPet), orange fluorescent protein (mOrange, mKO, mKO2) and red fluorescent protein (mCherry, tdTomato), see figure 1.13. Derivatives of CFP and YFP are often employed for FRET experiments (see 1.8). Inserting peptides at specific sites in FPs and employing circular permutation FP variants have lead to empirically improved response of FRET-based sensor constructs, leading to increased intensity ratio of donor and acceptor or optimization of orientation between donor and acceptor chromophores. Especially FRET based Ca^{2+} indicators benefit from optimization, resulting in increased dynamic range upon binding of Ca^{2+} , maximized FRET efficiency E intensity ratio of donor and acceptor ($R=I_A/I_D$). They are chimeric proteins composed of a short-wavelength variant of GFP, calmodulin (CaM), a glycylglycine linker, the CaM-binding peptide of myosin light-chain kinase (M13), and a long-wavelength variant of GFP [53].

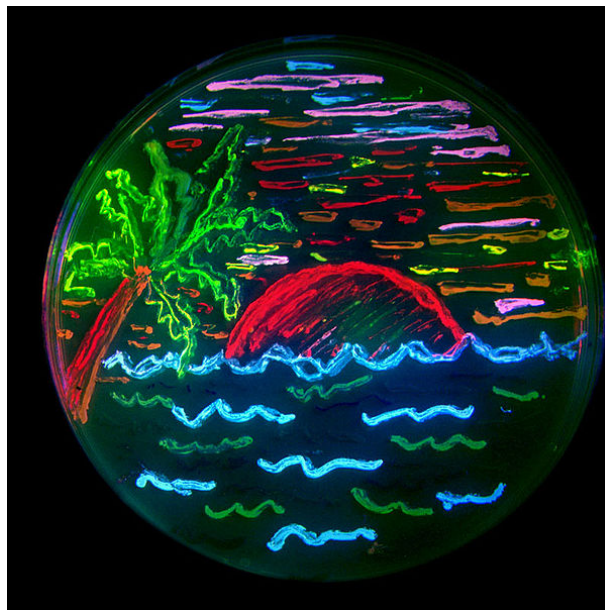


Figure 1.13: A San Diego beach scene drawn with an eight color palette of bacterial colonies expressing fluorescent proteins derived from GFP and the red-fluorescent coral protein dsRed. The colors include BFP, mTFP1, Emerald, Citrine, mOrange, mApple, mCherry and mGrape. *Artwork by Nathan Shaner; photography by Paul Steinbach, created in the lab of Roger Tsien in 2006*

mKO2 and mTFP1

The mKO is derived from CoralHue Kusabira-Orange (KO), which was cloned from the stony coral, whose Japanese name is Kusabira-ishi. Wild-type CoralHue KO forms a brightly fluorescent dimer and has been carefully engineered to form mKO that maintains the brilliance and pH stability of the parent protein. Recently, a fast-folding mutant of mKO named monomeric Kusabira orange 2 (mKO2) was introduced [54]. The monomeric Kusabira orange 2 mKO2 construct was provided by Atsushi Mikawaki (Brain Science Institute RIKEN, Japan). It shows an absorption maximum at 551 nm, a maximum emission at 565 nm and is very photostable.

The plasmid encoding the monomeric teal fluorescent protein (mTFP), was provided by Robert E. Campbell (University of Alberta, Edmonton, Canada). A study [55] showed that mTFP has many advantages, such as a high quantum yield and improved brightness and photostability. The peak excitation of mTFP is at 462 nm and peak emission is at 492 nm. mTFP is already known to be a good FRET donor for mKO2 as both mTFP and mKO2 are very photostable. mKO2 emission spectral overlap with mTFP emission spectrum is less than the overlap of yellow FPs with mTFP, and the excitation percentage of mKO2 at 458 nm (excitation wavelength of mTFP) is just 4.3% which helps to reduce acceptor spectral bleedthrough thus making them an excellent pair for detecting varying separation distances by measuring FRET efficiencies [55] (figure 1.14). Table 1.1 shows spectral properties of mTFP and mKO2.

FP	Peak excitation	Peak emission	Quantum yield	Extinction coefficient ($\times 10^{-3} M^{-1} cm^{-1}$)	Intrinsic brightness (see 1.7)
mTFP1	462	492	0.85	64	54
mKO2	551	565	0.62	63.8	53
EGFP (CLONTECH)	488	507	0.60	55	34

Table 1.1: The characteristics of mTFP and mKO2

Yuansheng Sun and Cynthia F. Booker and Sangeeta Kumari and Richard N. Day and Mike Davidson and Ammasi Periasamy, Characterization of an orange acceptor fluorescent protein for sensitized spectral fluorescence resonance energy transfer microscopy using a white-light laser, Journal of Biomedical Optics (2009), S. 054009

EGFP is used as a FRET donor the excitation of mKO2 is at 550 nm and should perform well as FRET acceptors when paired with EGFP. In my work I used a directed evolution of mTFP, called mTFP1,

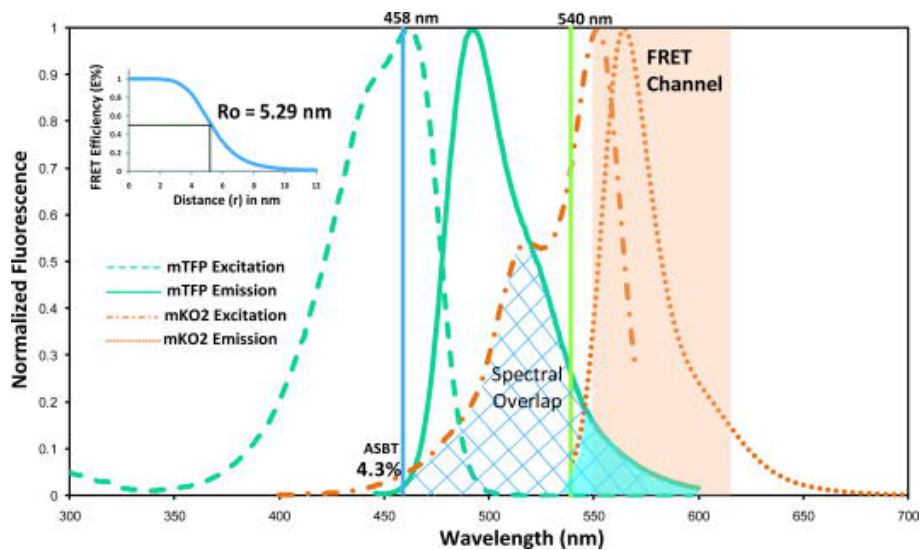


Figure 1.14: Excitation and emission spectra of mTFP and mKO2

Yuansheng Sun and Cynthia F. Booker and Sangeeta Kumari and Richard N. Day and Mike Davidson and Ammasi Periasamy, *Characterization of an orange acceptor fluorescent protein for sensitized spectral fluorescence resonance energy transfer microscopy using a white-light laser*, *Journal of Biomedical Optics* (2009), S. 054009

which has the same spectral properties but slightly higher photostability than mTFP [56].

1.9.4 Applications

The easy expression of FPs in cells together with being not or much less phototoxic compared to chemical dyes has initiated a revolution of fluorescence microscopy and thus has changed the use of this technique in different biological fields. Long-term experiments with highly automated microscopes enable the study of growth of cells, signaling and transport events to the point of observing development of whole embryos of small specimens like *Caenorhabditis elegans* or *Drosophila melanogaster*. FP based biosensors can act as passive fluorophores, showing insensitivity to environmental changes. Active FP biosensors are designed to change fluorescence properties (e.g. emission wavelength or intensity) dependent on environment conditions. Thus, they can act as sensors for Ca^{2+} and FRET sensors (section 1.8) [57]. Last but not least, photokinetic experiments like fluorescence recovery after photobleaching (FRAP) and photoactivation are group of important applications for FPs. Both approaches reveal mobility properties of FP-tagged proteins by either bleaching (FRAP) the fused FP or activating its fluorescence from the dark state (photoactivation) and recording the

recovering signal or intensity distribution, respectively. The latter one is also used for localization microscopy (PALM [58], STORM [59]) to produce superresolution images.

1.10 Aim of the thesis

The aim of this study was to generate a method of labeling and detecting mRNA transport in cells using FRET. In eukaryotic cells there has been increased interest in the recent years to study mRNA movement as targeted mRNA transport leads to localized translation of specific proteins involved in embryonic development, synaptic plasticity in neurons, yeast budding; and also faculty mRNA transport has been implicated in diseases like Fragile X Syndrome. The tagging and monitoring of mRNA has, therefore, been a field of great interest. Monitoring transport of RNA in live cells is a challenge undertaken by many labs. Most recently the method used to achieve this using a phage system like MS2 or λ_{N22} , where a fluorescent reporter is tagged to a RNA binding protein and the cognate binding site for the RBP is inserted in the RNA of interest under study. But there have been many drawbacks to using these strategies. The first system designed for this purpose was the MS2 system and was developed in the yeast cell system and there are some difficulties in optimizing it for the mammalian cells. Also, the use of MS2 or λ_{N22} system involves that the RBP-fluorescent reporter is confined in the nuclear compartment till the RNA is expressed and carries the RBP-fluorescent reporter tethered to it into the cytoplasm and eventually the site of RNA localization. But if the nuclear localization signal (NLS) on the RBP is not compatible to the cell system or not very stringent, then the RBP-fluorescent reporter might diffuse out of the nucleus leading to false signals. Or the expression patterns of the RNA and the RBP are not synchronous leading to the degradation of the RNA even before the expression of RBP. Since this varies for the system from cell type to cell type, it employs a lot of effort to optimize the system for a specific cell type. A similar situation we observed while trying to study the riboswitch action of thiM using FRET, we had no fluorescent signal out of the nucleus in co-transfected cells, implying the need for a better, more uniform system of labeling RNA. Therefore, we wanted to design a method of monitoring mRNA transport by circumventing the problems of leaky NLS sequences, by using FRET.

This should notify the binding of the RBP-fluorescent proteins on the RNA and thus the RNA transport can be monitored. Also, once the RNA is discharged or degraded the FRET should be reversed. The first step to achieve the above was to see FRET change in a cell free system, *in vitro*, as a proof of the binding of the RBP-fluorescent proteins on the RNA sequence and thereby to confirm the functionality

of the system.

Chapter 2

Materials and methods

2.1 Molecular biology

2.1.1 DNA restriction digestion

The restriction sites on vectors consist of a short sequence that usually comes along in a palindromic manner and have a length of 6/8 bp. These sites can be recognized by a specialized restriction endonuclease that breaks the double strand and often leaves a single stranded (sticky) end. Restriction of DNA was used to prepare the vector backbone/PCR fragment for subsequent cloning or to analyze a given DNA for the correct introduction of a desired DNA-fragment after ligation. Control digests for checking the successful incorporation of a DNA stretch was done with 1 - 2 μ l (100–200 ng) of DNA.

After incubation for one hour at 37 °C, the digestion samples were then run on an Agarose gel at 75 V for one hour for the bands to separate and check for DNA fragments of various sizes.

Preparative digests for subsequent cloning were performed as follows:

2 - 10 μl DNA (2-10 μg)	
BSA (bovine serum albumin 100 x, NEB)	0.5 μl
Restriction buffer for restriction enzyme (10 x, NEB)	5 μl
Restriction enzyme (10 U)	1 - 3 μl
H2O	To make total volume upto 50 μl

Incubate for 3 h–16 h at 37 °C (dependent on the restriction enzymes that were used and on the manufacturer’s advice [NEB]).

2.1.2 Ligation of DNA fragments

To introduce a new stretch of DNA into a vector backbone it is necessary to place different restriction sites at each end of the desired DNA. Treatment of the vector backbone and the DNA of choice with the same set of restriction enzymes enables the directed introduction of the desired fragment into the vector backbone. The molar ratio of vector to insert should be 1 : 3 to 1 : 5. Amount of DNA to be used was determined by a NANODROP spectrophotometer (NANODROP TECHNOLOGIES) to measure DNA amount.

Vector DNA (50 ng)	0.5 - 1 μl
Insert (dependent of the size and concentration)	1 - 3 μl
T4 ligase buffer (10 x)	1.5 μl
T4 DNA ligase (300 U)	1 μl
H2O	To make total volume to 20 μl

After incubation for one hour at room temperature, the samples were transformed with 2 μ l *E. coli* XL blue chemically competent cells.

2.1.3 Polymerase chain reaction (PCR)

Originally developed by Kary Mullis, this method allows the amplification of a distinct strand of DNA. For that purpose one makes use of a thermal-stable variant of DNA polymerase. This can be Taq (*Thermus aquaticus*), Vent (*Thermococcus litoralis*) or Pfu (*Pyrococcus furiosus*). The different enzymes vary in speed and accuracy of amplifying DNA. Pfu polymerase is known to have a high proof-reading capacity and is the choice for subsequent cloning.

PCR-reaction mix	50 μl (final volume)
DNA template	0.5- 1μl (depending on DNA concentration)
Forward primer	0.5 μl (50 μM)
Reverse primer	0.5 μl (50 μM)
Herculase Polymerase buffer (10X)	10 μl
dNTP solution	1 μl (12.5 mM)
H2O	36 μl
Pfu Polymerase	0.8 μl (2 U)

Addition of DMSO to the reaction mix often enhances the yield of DNA obtained by the PCR especially when the reaction initially produces too little DNA.

Reaction cycle for 1 λ_{N22} :

- 1. 95°C – 5 min**
 - 2. 95°C – 30 seconds**
 - 3. 57°C – 30 seconds**
 - 4. 72°C – 30sec**
 - 5. Repeat steps 2 X 30 Cycles**
 - 6. 72°C – 5min**
 - 7. incubate at 4°C**
-

Reaction cycle for mTFP1/EGFP/mKO3:

- 1. 95°C – 5 min**
 - 2. 95°C – 30 seconds**
 - 3. 57°C – 1 min**
 - 4. 72°C – 1min**
 - 5. Repeat steps 2X 30Cycles**
 - 6. 72°C – 5min**
 - 7. incubate at 4°C**
-

Reaction cycle for T75boxBSp6:

- 1. 95°C – 2 min**
 - 2. 95°C – 20 seconds**
 - 3. 55°C – 2 seconds**
 - 4. 72°C – 30sec**
 - 5. Repeat steps 2X 29 Cycles**
 - 6. 72°C – 3min**
 - 7. incubate at 4°C**
-

PCR-reaction mix was prepared in an ice block and put into thermal-cycler which was pre-heated to a temperature of 95 °C.

2.1.4 λ_{N22} insertions in mKO2 using transposon Tn5

To achieve the idea of different orientations of mKO2, FRET pair acceptor, when bound on the RNA I needed to obtain mKO2 variants with λ_{N22} insertion at different sites in mKO2. For this purpose transposons were used. The transposon Tn5 has been modified for commercial use and has 1000 fold higher transposition efficiency than a wild type Tn5 system. Any sequence contained between the 19 bp ES sequence will be transposed into the target DNA sequence. This feature is made use of by the EZ-Tn5™ In-Frame Linker Insertion kit from EPICENTRE.

By using this Tn5 system NotI restriction enzyme sites were introduced into mKO2 target sequence contained in pRSETB plasmid by Anselm Geiger in the lab. After the insertion reactions the clones were selected on kanamycin-containing plates to identify and screen the transposed clones. After the determination of insertion of the transposon site by PCR and restriction digestion, the clones were digested by NotI restriction enzyme and the linearized segments were purified and re-ligated. The re-ligation gave a single NotI site and 57 nucleotide insertion in the target mKO2, 9 of these nucleotides are the 9 bp sequence duplication on either side of the transposon site. The colonies were selected on ampicilin-containing plates

2.1.5 Transformation of chemically-competent *E. coli*

Chemically competent cells (50 μ l aliquots, storage -80 °C) were thawed on ice and transformed with desired DNA. Cells were kept on ice for 20 *min* and heat-shocked for 1 *min* in a water bath (42 °C).

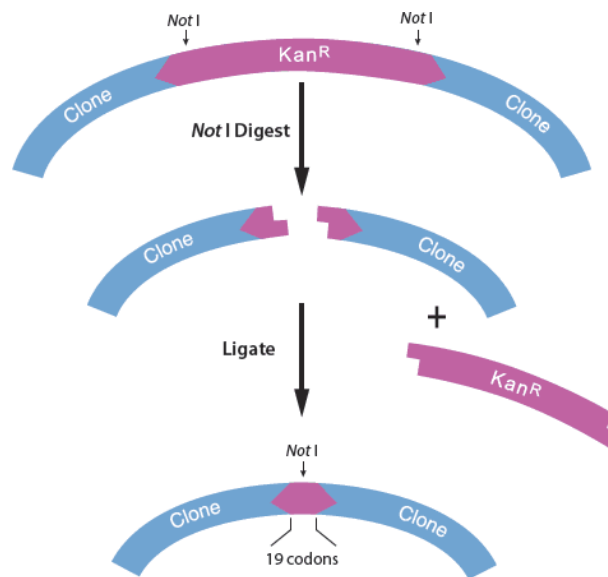


Figure 2.1: NotI Digestion and Religation of the EZ-Tn5<NotI/KAN-3> Transposon *EZ-Tn5TM In-Frame Linker Insertion Kit, EPICENTRE*

Before striking out on LB-agar plates cells were additionally stored on ice for 2 min. When working with ampicillin resistance bacteria were immediately plated, for other resistance transformed bacteria were added with 150 μ l of LB-medium and let grow

without antibiotics for 1 h at 37 °C in a shaker before plating onto LB-agar plates with the appropriate antibiotic.

2.1.6 Preparation of chemically-competent *E. coli*

4 ml LB medium were inoculated with the desired strain of *E. coli* and grown overnight without supplementing with antibiotics. The next day culture was transferred into 300 ml LB medium and grown to an OD600 of 0.6. Next the suspension was placed on ice for 20 min followed by harvesting the cells by centrifugation at 2500 g for 20 min (4 °C). Supernatant was discarded and the cells were resuspended with 60–80 ml of cooled Inoue transformation buffer. Again cells were harvested by centrifugation at 2500 g for 15 min (4 °C). Once more cells were resuspended with cooled Inoue transformation buffer but this time with 20 ml supplemented with 1.5 ml DMSO. Suspension was incubated on ice for 10 min. Cells were aliquoted (50 μ l) and stored at -80 °C until usage.

2.1.7 *In-vitro* mRNA transcription

The *in-vitro* RNA transcription was performed as per the T7 RIBOMAX™ Express Large Scale RNA Production System Kit. Accordingly, the DNA to be converted to RNA was cloned in pcDNA3 between T7 and Sp6. The DNA was then PCR amplified to yield good amount of the DNA product. The PCR product is then purified and the concentration measured. For the next step of RNA *in-vitro* transcription 1 – 1.5 μg of DNA was used and accordingly the T7 Express 2X buffer was adjusted. The following was the protocol followed for *in-vitro* transcription:

Reaction mix	30 μl (final volume)
DNA template	13 μl
RiboMAX™ Express T7 2X Buffer	15 μl
Enzyme Mix, T7 Express	2 μl

The reaction was incubated at 37 °C for 45 *min*, after which the entire reaction sample was subject to DNase treatment to get rid of the template DNA, according to the following protocol:

Reaction mix	75 μl (final volume)
RNA reaction sample	30 μl
10X DNaseI Buffer	7.5 μl
RNase free DNaseI	3.75 μl
Nuclease Free H₂O	33.75 μl

After incubating the reaction tube for 15 *min* at 37 °C, the reaction sample was purified to obtain clean RNA. The purification was done using RNeasy kit from QIAGEN™ with the following steps: To the 75 μl of sample, 2 μl Nuclease free H₂O was added. To this 350 μl of RLT buffer was added and mixed properly. Next 250 μl of 95 % Ethanol was added, mixed properly and all was added in an RNeasy Spin column. The column was spun for 30 *s* at 10,000 *rpm*. The flow-through was discarded, and 500 μl of RPE buffer was added to the column, spun for 30 *s* at 10,000 *rpm* and the flow-through was discarded. Again 500 μl of RPE buffer were added to the column, the column was spun for 2 *min* at 10,000 *rpm*, the flow-through discarded and the column was put in a clean eppi. The empty column was spun for 2 *min* at 10,000 *rpm*. Next, the column was put in a clean autoclaved elution tube, 30 μl of pre-heated Nuclease Free H₂O was added (pre-heated to 50 °C), the tube left to stand for 30 *s* and then spun for 1 *min* at 10,000 *rpm*. The RNA was eluted out in the tube. The amount of RNA was measured and the value used to calculate the concentration of the RNA obtained.

2.1.8 RNA isolation

HeLa cells were grown on a 10 *cm* petri dish. Once the cells are 60 % confluent, they were transfected with DNA. They were incubated overnight at 37 °C and 5 % CO₂. After that the cells were lysed directly in the culture dish by adding 1 *ml* of TRIzol Reagent and pipetted up and down multiple times to break the cells. The homogenized cells were then incubated for 5 *min* at RT (to cause complete dissociation of the nucleoprotein complexes). 0.2 *ml* of Chloroform per 1 *ml* of TRIzol reagent was added to the dish. The dish was shaken for roughly 15 *s*, by hand, and then incubated further for 2–3 *min*. The cells were then transferred to an eppi and centrifuged at 12,000 *g* (2000 *rpm*) for 15 *min* at 4 °C. After the centrifugation the mixture in the tube is separated into a lower red, Phenol-Chloroform phase (as interphase), and a colorless upper aqueous phase. The RNA remains exclusively in the the aqueous phase.

The aqueous phase containing the RNA was transferred to a fresh eppi and 0.5 *ml* of Isopropanol per 1 *ml* of TRIzol used for initial homogenization was added to precipitate the RNA. The samples were incubated for 10 *min* at RT and rotated for 10 *min* at RT. The RNA precipitate formed a gel-like pellet on the side and bottom of the tube. Carefully the supernatant was pipetted out. The RNA pellet was washed once with 75 % ethanol and 1 *ml* of 75 % ethanol (per 1 *ml* of TRIzol added for initial homogenization) was added to this pellet. The sample was then vortexed for 5 *min* at 7000 *g*. Finally, the RNA pellet was dried briefly (air-dried) for 5–10 *min*, but not completely. Then the RNA pellet was dissolved in RNase-free water and incubated for 10 *min* at 55 °C–60 °C. The re-dissolved RNA can be stored at -80 °C. 1 μ *l* from the sample was taken for cDNA synthesis to get sample for Q-PCR.

2.1.9 cDNA synthesis

The RNA sample obtained by RNA isolation is treated with DNases to remove DNA contamination.

Mix for cDNA Synthesis	
RNA Sample	20μ<i>l</i>
10X DNaseI Buffer	3μ<i>l</i>
RNase-Free DNaseI	1μ<i>l</i>
RNase Free Water	10μ<i>l</i>

The above reaction mix was incubated it for 30 *min* at 37 °C. Next 200 μ *l* of RNA binding buffer (100 μ *l*) + Ethanol 95–100 % (100 μ *l*) was added and it was mixed well. The mixture was transferred

to a ZYMO-SPIN™ IC column in a collection tube and centrifuged at 12000 x g for 1 *min*. The flow through was discarded. 800 μ l of RNA wash buffer was added to the column and centrifuged again at 12000 x g for 30 s. The flow through was discarded and the wash step was repeated with 400 μ l of RNA Wash Buffer. The flow through was discarded and the ZYMO-SPIN™ column was centrifuged at 12000 x g in an empty collection tube for 2 *min*. The ZYMO-SPIN™ column was removed from the collection tube and transferred into an RNase free eppi. 6 μ l of DNase / RNase-Free Water was added directly onto the column matrix and the column was allowed to stand for 1 *min* at RT. The final spin was given at 10000 x g for 30 s. The eluted RNA was then used for cDNA synthesis.

cDNA synthesis was done as per the protocol for "High Capacity cDNA Reverse Transcription" kit from APPLIED BIOSYSTEMS™. RNA concentration was measured, and the ratio for 260/280 and 260/230 was measured to check the purity of the RNA sample. The reaction mix was thus prepared:

RNA sample	2 μg (10μl)
10X RT Buffer	2μl
25X dNTP mic (100mM)	0.8μl
10X RT Random Primers	2μl
MultiScribe Reverse Transcriptase	1μl
RNase Inhibitor	1μl
Nuclease Free H2O	3.2μl

Total volume: 20 μ l

The reaction tube was kept at 25 °C for 10 *min*, then it was subjected to 2 *h* at 37 °C and then 2 *h* at 85 °C. Finally the sample could be used for normal PCR reaction with the respective primers to check for the bands corresponding to the correct DNA strand. The sample could also be stored at -80 °C.

2.1.10 Agarose gel

For a 1 % gel in the small mold (10 x 7 *cm*²), 0.6 g Agarose (SIGMA-ALDRICH, Munich, Germany) was mixed to 60 *ml* of 1 x TAE to it. Agarose was boiled in a microwave oven until being completely dissolved. The mixture was then poured into the small mold and ethidium bromide was added to a final concentration of 0,5 μ g/*ml*. After the gel had cooled down, 30 *min*, the sample was loaded on the gel. The samples for loading on the gel were prepared with Orange G (SIGMA) and distilled water. The gel was usually run at 77 V for 1 *h* for better separation of the different length DNA fragments.

TAE electrophoresis buffer is used, whose composition is described below:

Buffer Tris-Acetate (TAE)

Working solution 1x:	
Tris-Acetate	0.04 M
EDTA	0.001 M

Concentrated Stock (per Liter) 50x:	
Tris base	242 g
Glacial acetic acid	57.1 ml
EDTA (pH 8.0)	100 ml 0.5 M

2.2 Protein biochemistry

2.2.1 Protein expression using the *E. coli* BL21 strain

DNA for the protein of interest was cloned in the pRSETB vector that is optimized for protein expression and carries a 6 x His-tag 5' of the multiple cloning site. The vector containing the DNA of interest was transformed in the *E. coli* strain BL21. It was incubated for 30 *min* and then added to 4 *ml* of LB media, plus 4 μ l of Ampicilin. The culture was grown overnight on a shaker at 37 °C. The next morning the culture was transferred to 800 *ml* of LB, plus 800 μ l of Ampicilin. It was grown on the shaker at 37 °C till the OD of the culture at 600 *nm* is between 0.7 to 0.8, then 100 μ M of IPTG was added to the culture. The culture was grown overnight at 18 °C. The next day the culture was centrifuged at 6000 *rpm* for 10 *min*.

2.2.2 Purification of His-tag proteins via affinity chromatography

Protein Re-suspension & Wash buffer:

Na₂PO₄	20mM
NaCl	300mM
pH	7.8

Elution Buffer:

Na₂HPO₄	20mM
NaCl	300mM
Glycerol	10%
Imidazol	250mM
pH	7.8

Using His-Trap column from GE HEALTHCARE:

The supernatant was thrown out and the pellet was re-suspended in 20 ml protein re-suspension & wash buffer. 20 μ l PMSF (1 M in DMSO), 20 μ l Pepstatin (1 mg/ml in DMSO) and 20 μ l Leupeptin (1 mg/ml in DMSO) were added. The re-suspended cells were frozen at -80 °C for at least 1 hour. Afterwards the cells were thawed, and one spatula head of Chicken Egg White Lysozyme was added, and incubated on ice for 30 min. Then 50 μ l of DNAase (1 mg/ml in 10 % Glycerol) was added, 0.1 % Triton X100, and sonicated with ice for 30 min. The cells were then centrifuged at 13000 rpm for 30 min. The supernatant was taken in a falcon tube and the pellet discarded. The protein sample was then run for affinity chromatography on a His-Trap column (GE HEALTHCARE).

First, 5 ml of dd (double distilled) water was run through the column at the run speed of 0.5 ml per minute. Next 5 ml of protein re-suspension & wash buffer was run through the column. Afterwards the protein sample supernatant was run through the column, followed by 20 ml of protein re-suspension & wash buffer. Next, the elution buffer was run through the column and the fluorescent fraction from the column was collected in an eppi. It was kept overnight at 4 °C.

Using Ni-NTA HisBind Resin:

The supernatant was thrown out and the pellet was re-suspended in 20 ml protein re-suspension & wash buffer. 20 μ l PMSF (1 M in DMSO), 20 μ l pepstatin (1 mg/ml in DMSO) and 20 μ l Leupeptin (1 mg/ml in DMSO) were added. The re-suspended cells were frozen at -80 °C for at least 1 h. After that the cells were thawed, and one spatula head of Chicken Egg White Lysozyme was added, and incubated on ice for 30 minutes. Then 50 μ l of DNAase (1 mg/ml in 10 % Glycerol) was added, 0.1 % Triton X100, and sonicated with ice for 30 min. The cells were then centrifuged at 13000 rpm for 30 min. The supernatant was taken in a falcon tube and 50 % NiNTA resin (600 μ l) was added. It was rotated with a table rotator for 4 h and then the solution was passed through Polypropylene columns (QIAGEN). Once the solution passes through the columns, the NiNTA beads settle at the bottom of the column. It was washed by passing through the column protein re-suspension solution

3 x 5 ml. Then 1.2 ml elution buffer was added in the column, the base of the column was closed. The elution buffer was pipetted up and down 2–3 times to mix well with the NiNTA beads. It was allowed to stand for 20 min and then the protein was eluted out of the column in the elution buffer and collected in an eppi. The protein sample was stored at 4 °C overnight.

The next day the protein sample was run through the ÄKTA column for ion exchange chromatography. The flow through fractions were collected and the ones showing the highest value for the protein concentration and fluorescence (determined via the graph of the sample run via ÄKTA) were pooled together and concentrated to 2 ml of the sample. This was the pure protein sample finally obtained via protein purification.

The purified sample for mKO2 and mKO2-Lambda constructs was then measured via a spectrophotometer to measure its extinction coefficient and run also on an SDS-PAGE to check the purity of the protein sample. To the remaining protein Glycerol was added (10 %) and it was shock frozen in liquid nitrogen and stored at -80 °C.

ÄKTA Buffer:

MOPS	30mM
KCl	100mM
EDTA	100μM
EGTA	100μM
ph	7.2

Stripping Buffer:

MOPS	30mM
KCl	500mM
EDTA	100μM
EGTA	100μM
ph	7.2

Recharging Buffer:

NiSO4	100mM
--------------	--------------

After that the protein sample was run through the ÄKTA column for ion exchange chromatography. The flow through fractions were collected and the ones showing the highest value for the protein concentration and fluorescence (determined via the graph of the sample run via ÄKTA) were pooled together and concentrated to 2 ml of the sample. This was the pure protein sample thus yielded via protein purification.

The purified sample for mKO2 and mKO2-Lambda constructs was then measured via a spectrophotometer to measure its extinction coefficient and run also on an SDS-PAGE to check the purity of the protein sample. To the remaining protein sample Glycerol (final concentration 10 %) was added and it was shock frozen in liquid nitrogen for subsequent storage at -80 °C.

2.2.3 Spectrophotometer measurements of the fluorescent proteins for calculating extinction coefficient and quantum yield

The fluorescent proteins obtained via protein purification were concentrated using Amicon Ultra Centrifugal filter devices (MILLIPORE). Therefore the protein fractions showing the maximum protein and fluorescence peaks values, from the ÄKTA profile of protein purification, were collected in the Amicon Ultra Centrifugal filter devices (MILLIPORE) and the tube was centrifuged at 4000 rpm for 10 min at 4 °C. After concentration of the protein, the protein sample was collected in a 2 ml eppi and the flow through was collected in another 2 ml eppi and used as a buffer blank for the spectra measurements.

Absorption Spectroscopy:

The CARY UV-Spectrophotometer from VARIAN was used to measure the spectra. The wavelength used was between 240–600 nm (to measure both the protein and fluorescence of the protein). 1 ml of blank was added in the cuvette and the baseline was set. Next 5 µl of the protein sample were added to the blank and the measurements were made by subsequently increasing the volume of the protein in the cuvette.

Fluorescence spectroscopy of mKO2 variants:

Emission spectra were excited at 520 nm and measured between 530 nm and 640 nm. After that, spectra were used to calculate ϵ_{520} , ϵ_{550} and the quantum yield compared to mKO2 (see results).

2.2.4 Gel electrophoresis: denaturing SDS-PAGE

The separation of denatured proteins was carried out using sodium dodecyl sulfate (SDS) gel electrophoresis. For separation of proteins in the desired range a 8 % SDS-polyacrylamide gel was used. The acrylamide stock solution was Protogel (mixture 30 % Acrylamide, 0.8 % Bisacrylamide).

SDS Page Separation Gel (10 %):

H2O	2400 μl
1.5M Tris Buffer (pH 8.8)	1250 μl
40% Acrylamide mix^{SIGMA}	1250 μl
10% SDS (pH 7.2)	50 μl
10% Ammonium Persulfate^{SIGMA}	50 μl
TEMED^{SIGMA}	2 μl

SDS Page Stacking Gel (5 %):

H2O	1440 μl
1M Tris Buffer (pH 6.8)	250 μl
40% Acrylamide mix^{SIGMA}	250 μl
10% SDS (pH 7.2)	20 μl
10% Ammonium Persulfate^{SIGMA}	20 μl
TEMED^{SIGMA}	2 μl

Loading-buffer6X, pH 6.8:

Tris HCl	350 mM
SDS (w/v)	10%
Glycerol (v/v)	30%
Bromophenol blue (w/v) (Serva-blue G)	0.1%
β-mercaptoethanol (v/v)	12%
Dithiothreitol (w/v)	9.3%

All solutions were mixed in screw-capped falcon tubes with very gentle rocking. The separation gel polymerised for 30 *min* in the electrophoresis apparatus, with a layer of Isopropanol overlaid, to fasten

the polymerisation by avoiding contact with oxygen. Then, after removing the Isopropanol, the stacking gel was poured and polymerized for 45 *min*. After loading of the samples on the polymerized gels, they migrated at 30 V for around 1 h 30 *min*. For sample preparation, I mixed the 6X loading buffer at a ratio sample/buffer 3 / 1 to maintain an excess of SDS. The samples were heated immediately after adding sample buffer for 10 *min* at 95 °C, and then loaded immediately.

Coomassie-blue staining, modified

Chemicals /	Serva-blue	Acetic Acid	Methanol
Buffers	G-250 (w/v)	(v/v)	(v/v)
Staining Sol	0.25%	10%	5%
De-staining	-	10%	40%

After running the gel, the SDS gel was removed from the electrophoresis apparatus and put into a square plastic chamber (to keep the gel flat and not folded) and stained with staining solution, heated for 1 minute and gently rocked overnight at room temperature. The next day, the stain was removed, de-staining solution was added and heated for 1 minute, and gently rocked for 20 *min*. The de-staining process was repeated until the band became visible. Then some dd H₂O was added and the gel was rocked for a couple of hours before it was imaged.

2.2.5 BCA assay for protein concentration

Protein concentrations were measured before FRET analysis using BCA Protein Assay^{ThermoFisher} kit. In this method, 8 diluted BSA standards were prepared from the range of 2,000 $\mu\text{g}/\text{ml}$ – 25 $\mu\text{g}/\text{ml}$ and there was one blank, using the Elution Buffer used to elute out the proteins as the dilutant. The working reagent was formed with one part of Reagent B + 50 parts of Reagent A. Microplates were used for the measurements, therefore 200 μl of the Working reagent was added to each well of the microplate and 10 μl of the BSA diluted standard, one dilution per well, therefore 9 such wells for the standards. The standards were done in triplicates. For the samples, 10 μl was added to each well, also done in triplicates. The microplate was then shaken for 30 s, covered with an aluminum foil and kept at room temperature for 2 h before the reading was taken on an ELISA plate reader at 550 nm. A graph is formulated from the average-blank values for the standards. The sample values are also average-blank calculated and then from the graph the concentration of the protein is calculated for each sample.

2.2.6 In-vitro FRET measurements to study aptamer induced FRET upon binding of the λ N tagged fluorescent proteins

The measurements were done with a CARY ECLIPSE fluorescence spectrophotometer (VARIAN). In a microcuvette RNA binding buffer was added and $0.1 \mu\text{M}$ of the donor protein, i.e. EGFP or mTFP1 and $0.1 \mu\text{M}$ of m acceptor protein, i.e. mKO2 variants, are added. The EGFP/mKO2(or mKO3) FRET constructs were excited at 460 nm and the emission was recorded from 490 nm to 650 nm . For the mTFP1/mKO2(or mKO3) FRET constructs were excited at 458 nm and the emission was recorded from 480 nm to 650 nm . Then $0.1 \mu\text{M}$ of RNA was added (1 x RNA), mixed properly and the spectra was again measured. Another reading with another $0.1 \mu\text{M}$ of the RNA (2 x RNA) was performed. The final volume in the cuvette was always kept at $100 \mu\text{l}$.

RNA-binding buffer:	
Tris pH 7.8	20 mM
MgCl₂	10 mM
NaCl	300 mM

To calculate the $\Delta R/R$ value on addition of the aptamer the following formula was used:

$$\frac{\Delta R}{R} = \frac{\text{Ratio}_{\text{RNA}} - \text{Ratio}_{\text{zero}}}{\text{Ratio}_{\text{zero}}}$$

where Ratio for EGFP/mKO2(or mKO3) constructs = $\text{Peak}_{m\text{KO}2(3)}/\text{Peak}_{\text{EGFP}}$ ($570 \text{ nm}/508 \text{ nm}$), and Ratio for mTFP1/mKO2(or mKO3) constructs = $\text{Peak}_{m\text{KO}2(3)}/\text{Peak}_{m\text{TFP}}$ ($570 \text{ nm}/490 \text{ nm}$).

2.3 Cell culture

2.3.1 Preparation of HeLa cells culture

The HeLa cells stock, kept in $-80 \text{ }^\circ\text{C}$, was melted in water bath at $37 \text{ }^\circ\text{C}$. The contents from the HeLa cells eppi were added to a falcon tube containing 5 ml of DMEM. Centrifuge the falcon at 1200 rpm for 4 min (rotor number 19777, Centrifuge: SIGMA, 3K30). Discarded the supernatant and re-suspended the pellet in 5 ml DMEM. 4.5 ml of this re-suspended media and cells was added to 10 cm petri dish containing 5 ml DMEM with 10% FCS (Fetal Calf Serum). The media was changed the next day. Check the confluency of the cells, when they are 90% confluent, the DMEM media

was removed. The cells attached to the bottom of the dish were washed with 4 ml of 1XPBS, twice. 2 ml of 0.25 % Trypsin was added, and the cells were incubated with Trypsin for 5 min. Next, the Trypsin was pipetted out and the cells washed once with 1XPBS. 8 ml of fresh DMEM media was added, titrated the cells with pipette and one drop from this was added to glass-bottom dishes (MTek) containing 2 ml of DMEM (with 10 % FCS).

2.3.2 Transfection of HeLa cells culture using lipofectamine

LIPOFECTAMINE™ 2000 *Standard Plasmid Transfection* reagent was used for transfection of HeLa cells. For plasmid transfection, the DNA to Lipofectamine ratio for transfection was 2 : 1 or 3 : 1 respectively. The cells were transfected if they were 60 % confluent. First, 6 μ l lipofectamine were added to 250 μ l OptiMEM for subsequent 5 min of incubation. Next, DNA was added to 250 μ l OptiMEM, depending on the concentration of the plasmid DNA so as to keep the ratio of Lipofectamine : DNA as 1 : 2 or 1 : 3. The DNA and OptiMEM mixture was added to the Lipofectamine tube and given a slight tap, and left to incubate for 20 min at room temperature. After 20 min, 500 μ l of conditioned media was taken out from the dish of cells, to be added later. The DNA+Lipofectamine was added onto the cells, drop-wise, and left to incubate at 37 °C, 5 % CO₂ for 3 h. After 3 h the cells were washed with 2 ml of 1XPBS, twice. Fresh DMEM (10%FCS) and the 500 μ l of conditioned media was added. The cells were left at 37 °C and 5 % CO₂ incubator overnight and imaged the next day.

2.3.3 Confocal imaging of transfected HeLa cells

The images were acquired with a LEICA TCS SP2 confocal laser scanning microscope. The lens used was 40 X oil immersion, 488 nm excitation laser was used for EGFP and for YFP 514 nm excitation laser was used.

2.4 Materials

2.4.1 Primers list

Primers for 1 λ_{N22} peptide

5'Lmbda_mKO2ORF1:

ACATCGGGCGGCCGCAAGCCACCATGGACGCACAAACAC

NotI

3'Lmbda_mKO2ORF1:

ACATCGGGCGGCCGCGGTGGGTTTGCAGCTTTCCATTG

NotI

5'Lmbda_mKO2ORF2:

ACATCGGGCGGCCGCAAGCCACCATGGACGCACAAACAC

NotI

3'Lmbda_mKO2ORF2:

ACATCGGGCGGCCGCGCGGTGGGTTTGCAGCTTTCCATTG

NotI

5'Lmbda_mKO2ORF3:

ACATCGGGCGGCCGCGCCACCATGGACGCACAAACAC

NotI

3'Lmbda_mKO2ORF3:

ACATCGGGCGGCCGCGCGGTGGGTTTGCAGCTTTCCATTG

NotI

mKO3- λ N

5'mKO3 (mKO3-BamHI):

CGGGATCCGAAGCTTGCCACCATGGTGAGTGTGATTAAACCAG

BamHI

3'mKO3 (mKO3-SacI):

ACATCGGGAGCTCGGTACCGCCCTTGACAGCTCGTCCA

SacI

5'Lambda:

ACATCGG**GAGCTC**GCCACCATGGACGCACAAACA

SacI

3'Lambda:

ACATCGG**GAATTC**TTACGGTGGGTTTGCAGCTTTCCATTG

EcoRI

λN-mKO3

5'mKO3 (mKO3-SacI):

CGAGCTCATGGTGAGTGTGATTAACCAG

SacI

3'mKO3 (mKO3-EcoRI):

GGAATTCATCGATTCAGCTATGAGCTACTGCATCTTC

EcoRI

5'Lambda:

ACATCGG**GGATCC**GGCCACCATGGACGCACAAACA

BamHI

3'Lambda:

ACATCGG**GAGCTC**CGGTGGGTTTGCAGCTTTCCATTG

SacI

Primers for donor proteins

mTFP1_Lambda

5'mTFP1:

ACATCGG**GGATCC**GGCCACCATGGTGAGCAAGGGCGAGGAGACCAC

BamHI

3'mTFP1:

ACATCGG**GAGCTC**CCTTGTACAGCTCGTCCATGCCGTC

SacI

5'Lambda:

ACATCGGGAGCTCGCCACCATGGACGCACAAACA

SacI

3' Lambda:

ACATCGGGAATTC TTACGGTGGGTTTGCAGCTTCCATTG

EcoRI

Lambda_mTFP1:

5' Lambda:

ACATCGGGGATCCGGCCACCATGGACGCACAAACA

BamHI

3' Lambda:

ACATCGGGAGCTCCGGTGGGTTTGCAGCTTCCATTG

SacI

5' mTFP1:

ACATCGGGAGCTCATGGTGAGCAAGGGCGAGGAGACCAC

SacI

3' mTFP1:

ACATCGGGAATCTTACTTGTACAGCTCGTCCATGCCGTC

EcoRI

EGFP_Lambda:

5' EGFP:

ACATCGGGGATCCGATGG TGAGCAAGGGCGAGGAGCTG

BamHI

3' EGFP:

ACATCGGGAGCTCCTTGTACAGCTCGTCCATGCCGAG

SacI

5' Lambda:

ACATCGGGAGCTCGCCACCATGGACGCACAAACA

SacI

3' Lambda:

ACATCGGGAATTCCTTACGGTGGGTTTGCAGCTTCCATTG

EcoRI

Lambda_EGFP:

5' Lambda:

ACATCGGGGATCCG GCCACCATGGACGCACAAACA

BamHI

3' Lambda:

ACATCGGGAGCTCCGGTGGGTTTGCAGCTTCCATTG

SacI

5' EGFP:

ACATCGGGAGCTCATGG TGAGCAAGGGCGAGGAGCTG

SacI

3' EGFP:

ACATCGGGAATTCCTTACTTGTACAGCTCGTCCATGCCGAG

EcoRI

Primers for 5boxB DNA

5' _pcDNA3_5boxB:

ACATCGGAAGCTTTACGCCCTGAAAAAGGGCTGTACAGCCCTG

Hind III 5boxB

3' _5boxB_thibox_2 :

ACATCGGGGTACCCGCCCTTTTTCAGGGCG

KpnI 5boxB

Primers for 5boxB PCR for *in vitro* transcription

5' T7 Primer:

TAATACGACTCACTATAGGG

3' _Sp6 Primer :

CATTTAGGTGACACTATAG

Riboswitch

5' _5boxB_thibox_2:

AGTGGATCC GAATTC TACGCCCTGAAAAAGGGCTGTACAGCCCTG

BamHI EcoRI 5boxB

3'_5boxB_thibox_2 :

ATAAGATCTCGCCCTTTTTCAGGGCGTGC

BglIII 5boxB

Fw_MS6_thibox_2:

CGCCCATGGTAATTGCCTAGAAAACATGAGGATC

NcoI MS-BS

Rv_MS6_thibox_2 :0

CAAAGCTTGCGGCCGCTTAGGATCTAATGAACCCGGG

HindIII NotI

thiM_5UTR_2_5':

ATTAGATCTGGAACCAAACGACTCGGGGTGC

BglIII

thiM_5UTR_2_3':

ATACCATGGTTGCGCTGGATCCAGCAGGTCG

NcoI

2.4.2 Instruments

<i>Name</i>	<i>Supplier</i>
Cary 100 Scan UV-Visible Spectrophotometer	VARIAN, Mulgrave (Australia)
Cary Eclipse Fluorescence Spectrophotometer	VARIAN, Mulgrave (Australia)
Dyad DNA Engine Peltier Thermal Cycler	MJ RESEARCH INC., Waltham (USA)
NANODROP spectrophotometer	NANODROP TECHNOLOGIES (USA)
LEICA MICROSYSTEMS TCS SP2 Confocal microscope Heidelberg (Germany)	LEICA MIKROSYSTEME GmbH,

2.4.3 Consumables

<i>Name</i>	<i>Supplier</i>
BCA Protein Assay kit	THERMO FISHER SCIENTIFIC (Germany)
EZ-Tn5 TM In-Frame Linker Insertion kit	EPICENTRE (USA)
Glass Bottom Culture Dishes 35mm, No. P35G-0-14-C	MATTEK CORP., Ashland (USA)
High Capacity cDNA Reverse Transcription Kit	APPLIED BIOSYSTEMS (Germany)
Polypropylene Columns Qiagen	HILDEN (Germany)
PUREYIELD TM Plasmid Miniprep System	PROMEGA (Germany)
QIAQUICK Gel Extraction Kit Qiagen	HILDEN (Germany)
QIAQUICK PCR Purification Kit Qiagen	HILDEN (Germany)
QIAQUICK Spin Miniprep Kit Qiagen	HILDEN (Germany)
T7 RIBOMAX TM Express Large Scale RNA Production System Kit	PROMEGA (Germany)

2.4.4 Buffers, solutions and media

<i>Name</i>	<i>Recipe</i>
DMEM/10 % FCS	500 ml DMEM 50 ml FCS, heat-inactivated
DNA Gel Loading Buffer (10 x)	100 mM Tris/HCl, pH 7.5 10 mM EDTA 50 % Glycerol 1 % Orange G
HBSS for imaging	25 mM HEPES pH 7.4 140 mM NaCl 5 mM KCl 1 mM CaCl ₂ 1 mM MgCl ₂ 1 mM Glucose
0.25% BSA	

LB (Luria-Bertani) medium pH 7,0	20 g/l LB broth base in ddH ₂ O
LB Agar LB Medium	15 g Agar in 1 l ddH ₂ O
PBS (10 x)	100 mM Na ₂ HPO ₄ , pH 7.4
20 mM KH ₂ PO ₄	
1.37 M NaCl	
27 mM KCl	
Poly-L-Lysine Hydrobromide in H ₂ O	0.01 % (w/v) Poly-L-Lysine

2.4.5 Chemicals

<i>Name</i>	<i>Supplier</i>
Agar	SIGMA, St. Louis (USA)
Ampicillin, sodium salt	ROTH, Karlsruhe (Germany)
β -mercaptoethanol;	
Chloroform	MERCK, Darmstadt (Germany)
DMSO (Dimethylsulfoxide)	SIGMA, St. Louis (USA)
Dulbecco's modified Eagle's medium (DMEM) w/o Sodium Pyruvate;	INVITROGEN, Carlsbad (USA)
w/ 4500 mg/ml Glucose;	
w/ Pyridoxine-HCl	SIGMA, St. Louis (USA)
EGTA (Ethylene glycol bis(beta-amino ethyl ether tetra-acetic acid)	
Formaldehyde	MERCK, Darmstadt (Germany)
HEPES free acid	SIGMA, St. Louis (USA)
Imidazole	MERCK, Darmstadt (Germany)
Isopropyl β -D-1-thiogalactopyranoside	SIGMA, St. Louis (USA)
Leupeptin hydrochloride	SIGMA, St. Louis (USA)

Lipofectamine	INVITROGEN, Carlsbad (USA)
Lysozyme	SIGMA, St. Louis (USA)
Ni-NTA Agarose	QIAGEN, Hilden (Germany)
Opti-MEM I	INVITROGEN, Carlsbad (USA)
Pepstatin A	SIGMA, St. Louis (USA)
Phenylmethylsulfonylfluoride (PMSF)	SIGMA, St. Louis (USA)
Poly-L-lysine hydrobromide	SIGMA, St. Louis (USA)
Potassium chloride	MERCK, Darmstadt (Germany)
Sodium bicarbonate	SIGMA, St. Louis (USA)
Sodium chloride	SIGMA, St. Louis (USA)
Sodium dodecyl sulfate Sigma, St. Louis (USA)	
Sodium phosphate monobasic, anhydrous	SIGMA, St. Louis (USA)
T4-Ligase	NEW ENGLAND BIOLABS, Beverly (USA)
Triton-X-100	SIGMA, St. Louis (USA)
Trypsin	SIGMA, St. Louis (USA)

Chapter 3

Results

3.1 Generation of mKO2 variants with λ_{N22} insertions

The mKO2 variants with NotI restriction enzyme sites introduced via EZ-Tn5 transposon used for λ_{N22} ligation were variants number: 49, 51, 53, 88, 90, 92, 162, 186, 188 and 210. These variants were selected as they were tolerant to EZ-Tn5 insertions and yielded fluorescent colonies during screening on agar plates. Numbering of these mKO2 variants is dependent on the position of the amino acid, in the mKO2 protein sequence, where the transposon is inserted. All the cloning work was done in pRSETB vector, the map of which is given in figure 3.1.

The mKO2 variants chosen for the project had NotI restriction enzyme site inserted in one of the following amino acid positions for mKO2: 49, 51, 53, 54, 88, 90, 92, 186, 188 and 210, as shown in figure 3.2.

The λ_{N22} sequence was obtained via PCR using p4LambdaN22-mEGFP3-m9 as template (obtained from Dr. Jan Ellenberg's Lab, EMBL, Heidelberg) with NotI restriction enzyme sites on both ends and was ligated in the modified mKO2 variants, as shown in figure 3.3. Colonies obtained after ligation were fluorescent for all variants except #210. Ten colonies per ligation plate were picked to check for the insertion of λ_{N22} and sequence analysis.

In addition to cloning of mKO2 variants with λ_{N22} inserted in different positions, I also generated variants tagged with λ_{N22} either at the N- or the C-terminus of mKO3 as shown in figure 3.4. For this, I used a modified mKO2 version where the C-terminus has been mutated to introduce the last 9 amino acids of the *Aequorea* GFP C-terminus. Thus, the mKO2 has a GFP C-terminus and is tolerant

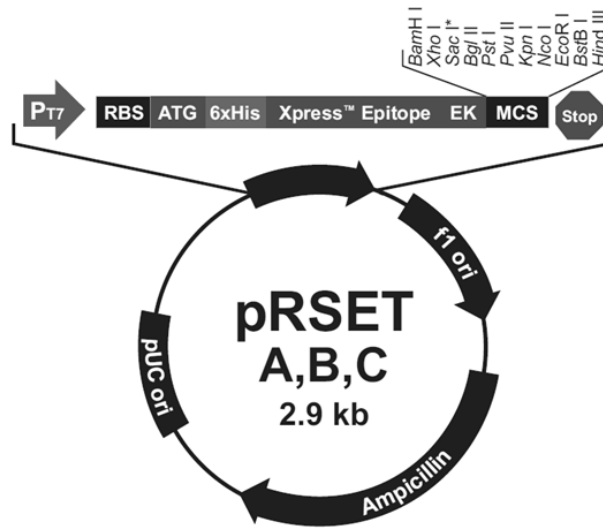


Figure 3.1: pRSETB Vector map

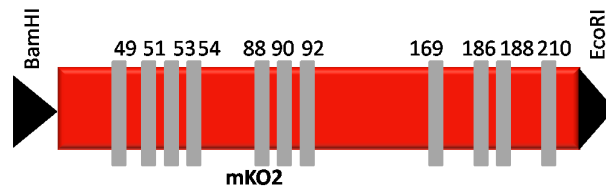


Figure 3.2: Amino acid positions in mKO2 where the NotI site is inserted via EZ-Tn5 transposon element is inserted

to C-terminus tagging. This mutated mKO2 as been termed as mKO3, for ease of differentiation from mKO2. All colonies obtained after λ_{N22} ligation with mKO3 were fluorescent and 8 colonies per ligation plate were cultured and control digested to check for the insertion of the λ_{N22} fragments and sequenced to check the orientation of λ_{N22} .

The clones showing the correct insertion of λ_{N22} were set for protein purification and the purified proteins were run on an SDS gel to check for the purity of proteins as shown in figure 3.5.



Figure 3.3: Schematic representation of λ_{N22} insertion in mKO2 containing transposon introduced NotI site

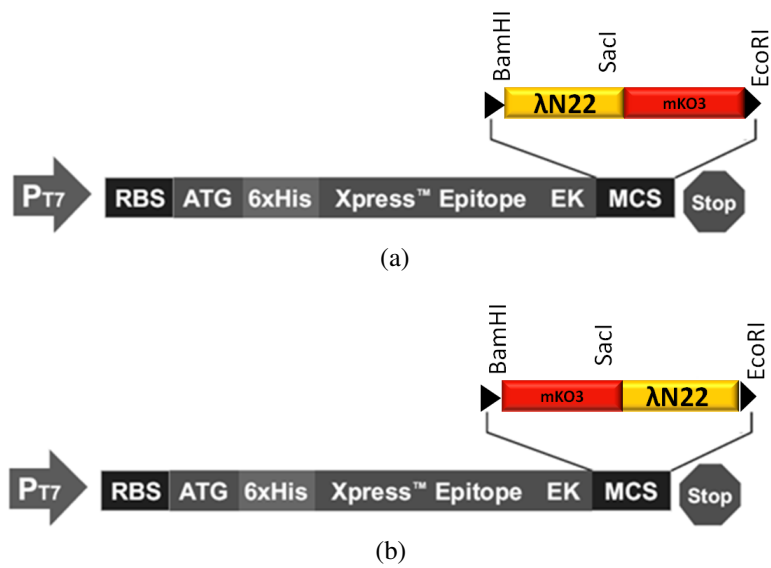
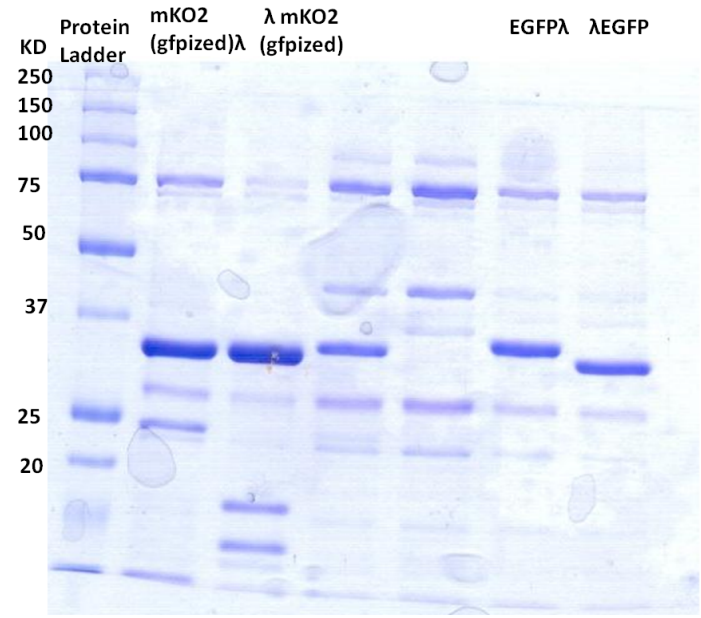
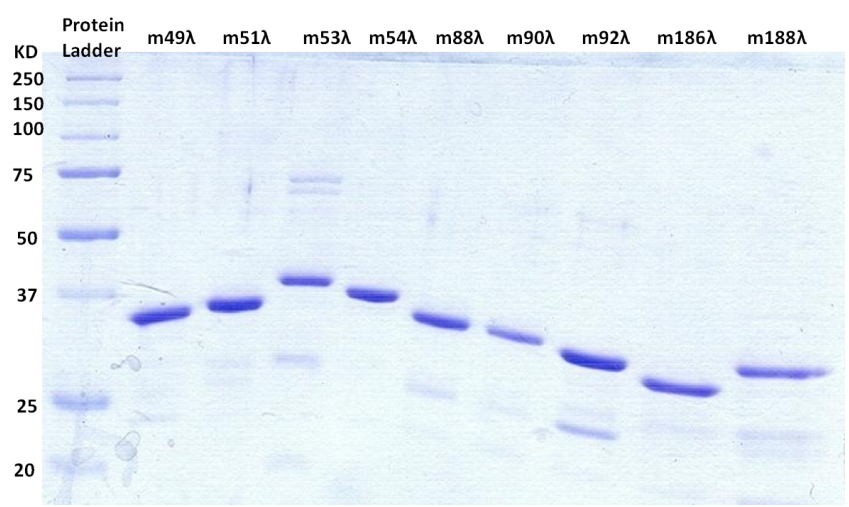


Figure 3.4: Schematic representation of mKO3 tagged at (a) N-terminus and (b) C-terminus with λ_{N22}



(a) ÄKTA purified mKO2- λ_{N22} variants and purified EGFP- λ_{N22} variants



(b) ÄKTA purified mKO2- λ_{N22} variants

Figure 3.5: SDS PAGE run for purified λ_{N22} variants

3.2 Comparing the fluorescent properties of the mKO2- λ_{N22} variants

The λ_{N22} inserted mKO2 variants were characterized for their fluorescent properties i.e. quantum yield and extinction coefficient.

Figure 3.6 shows the absorption spectra of mKO2- λ_{N22} variants compared to that of mKO2 (WT) (wild type). The spectra of the mKO2- λ_{N22} variants have been adjusted to the absorbance at 280 nm.

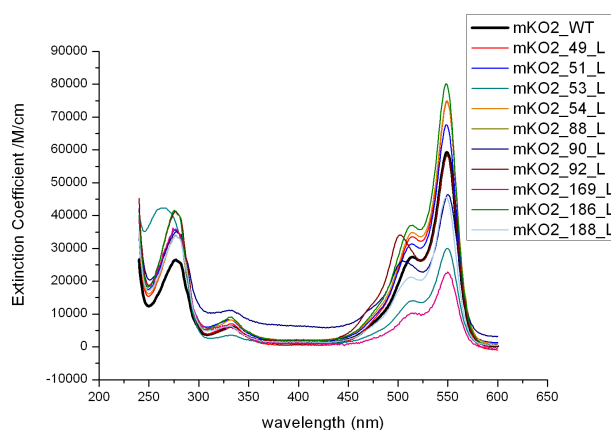


Figure 3.6: Absorption spectra of the mKO2- λ_{N22} variants in comparison to mKO2 (WT)

The concentrations of proteins in solutions were calculated from the absorption at 280 nm using the calculated extinction coefficient obtained using the program: www.expasy.ch/tools/protparam.html. To calculate the extinction coefficient, the amino acids forming the chromophore were excluded. The fluorescence emission of the proteins was measured. For that the concentrations of all the proteins measured were diluted to have the same final concentration in the cuvette. Figure 3.7 shows the emission spectra of the different mKO2- λ_{N22} variants in comparison to the mKO2 (WT).

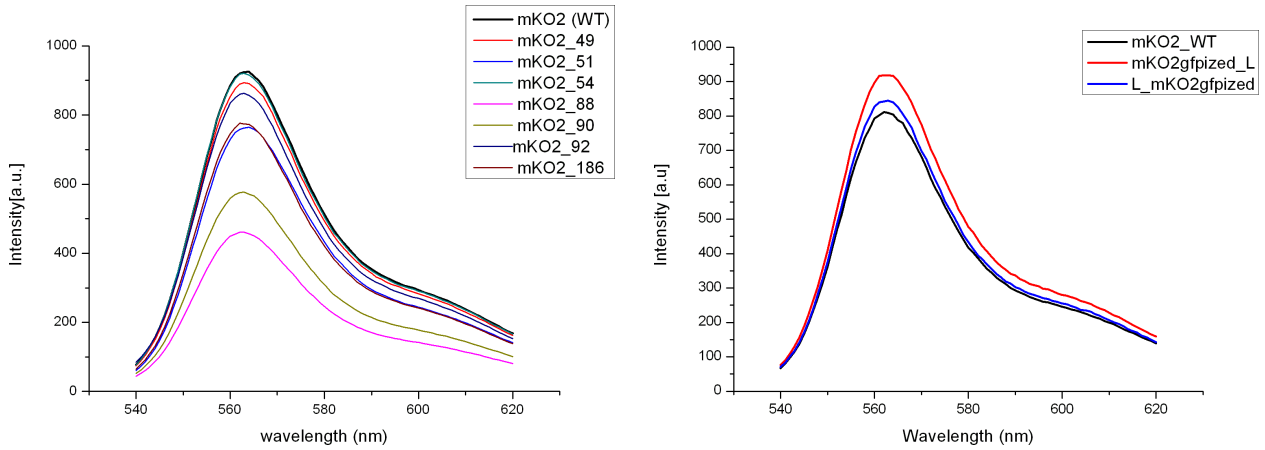
The quantity of absorbed photons at 520 nm is given through the ratio of extinction coefficients at 520 nm via the equation:

$$F_1 = \frac{\varepsilon_{520, mKO2}}{\varepsilon_{520, variant}};$$

where

$\varepsilon_{520, mKO2}$ is the extinction coefficient of mKO2 at 520 nm, and

$\varepsilon_{520, variant}$ is the extinction coefficient of mKO2- λ_{N22} inserted variant at 520 nm.



(a) mKO2- λ_{N22} variants in comparison to mKO2 (WT) (b) mKO3- λ_{N22} and λ_{N22} -mKO3 in comparison to mKO2 (WT)

Figure 3.7: Fluorescence emission spectra of various mKO2- λ_{N22} (a) and mKO3- λ_{N22} (b) variants in comparison to mKO2 (WT)

Emitted photons were quantified by calculating the ratio of emission at 563 nm (emission maximum) via the following equation:

$$F_2 = \frac{\varepsilon_{563,mKO2}}{\varepsilon_{563,variant}};$$

where

$\varepsilon_{563,mKO2}$ is the extinction coefficient of mKO2 at 563 nm, and

$\varepsilon_{563,variant}$ is the extinction coefficient of mKO2- λ_{N22} inserted variant at 563 nm.

After calculating these factors, the quantum yield (QY) of mKO2- λ_{N22} and mKO3- λ_{N22} variants was calculated from the QY of mKO2 (WT) as shown in the following equation:

$$QY_{variant} = \frac{QY_{mKO2} F_1}{F_2}$$

where

$QY_{variant}$ depicts the quantum yield of the mKO2- λ_{N22} inserted variant, and

QY_{mKO2} is the quantum yield of mKO2 = 0.57 (45).

Table 3.1 shows an overview of the spectral properties of mKO2- λ_{N22} and mKO3- λ_{N22} variants in comparison to mKO2 (WT) with

The ε_{549} was calculated as given in the following equations:

Sample	Extinction coefficient 280 nm ($M^{-1}cm^{-1}$)	Extinction coefficient at 549 nm ($M^{-1}cm^{-1}$)	Quantum Yield	Result Conc. [μ M]
mKO2_λ #49	33140	74498.72	0.52	31
mKO2_λ #51	34630	67286.09	0.47	21
mKO2_λ #53	34630	13796.6	—	9
mKO2_λ #54	33140	73637.08	0.51	45
mKO2_λ #88	34630	46092.53	0.37	14
mKO2_λ #90	34630	51910.37	0.44	9
mKO2_λ #92	40130	57385.9	0.62	16
mKO2_λ #169	34630	9706.8	—	1.41
mKO2_λ #186	40130	79537.66	0.41	9
mKO2_λ #188	33140	45302.38	—	5
mKO3_λ	32890	74660	0.56	43.25
λ_mKO3	33015	75934.5	0.53	41
mKO2 (WT)	25900	67892	0.57	113

Table 3.1: Overview of spectral properties of generate mKO2- λ_{N22} & mKO3- λ_{N22} variants

$$\varepsilon_{549} = \frac{\varepsilon_{280} Abs_{549}}{Abs_{280}};$$

where Abs_{549} is the absorbance at 549 nm and Abs_{280} is the absorbance at 280 nm.

After evaluating the fluorescent properties of the mKO2- λ_{N22} and mKO3- λ_{N22} variants, I selected the following for the aptamer induced FRET experiments: mKO2- λ_{N22} variants #49, 51, 54, 92, 186, mKO3- λ_{N22} and λ_{N22} -mKO3. For FRET experiments, the rate of energy transfer is influenced by the quantum yields of both the donor and acceptor; and the lifetimes of the fluorescent proteins, which can be evaluated from the absorption spectra, extinction coefficient and the emission spectra. The constructs mKO2- λ_{N22} #49, 51, 54, 92, 186, mKO3- λ_{N22} and mKO3- λ_{N22} exhibited high values for quantum yield, extinction coefficient at 549 nm and higher absorption spectra than mKO2 (WT). The remaining constructs #53,88,90,169 and 188 had very poor absorption spectra and low values for extinction coefficient at 549 nm. Therefore, the mKO2- λ_{N22} variants # 49, 51, 54, 92, 186, mKO3- λ_{N22} and λ_{N22} -mKO3 were selected for FRET experiments.

3.3 Generation of FRET donors proteins tagged with λ_{N22}

The donor proteins used for the experiment were EGFP and mTFP1. λ_{N22} PCR product was ligated with EGFP and mTFP in a pRSETB vector as shown in figure 3.8

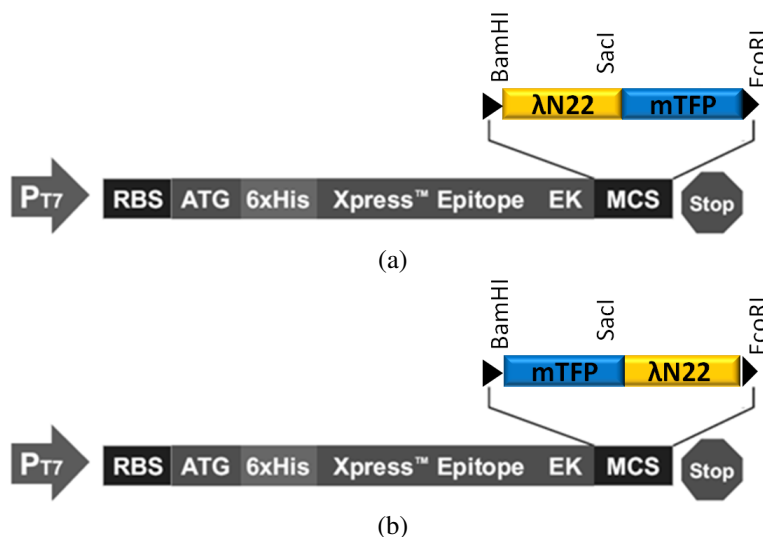


Figure 3.8: Schematic representation of mTFP1 tagged at (a) N-terminus and (b) C-terminus with λ_{N22}

and figure 3.9. . The donor proteins were tagged with λ_{N22} either at the N-or C-terminus. All colonies obtained on the ligation plates were fluorescent. Eight colonies per ligation plate were picked for harvesting the culture and later screened to verify the correct sequence. The clones with the correct DNA sequence were set for protein purification and purity checked by running the protein sample on a SDS gel. BCA assay was performed to obtain the concentration of the proteins.

SDS-gels ran for the purified proteins as depicted in the figures 3.10a, 3.10b and 3.5a.

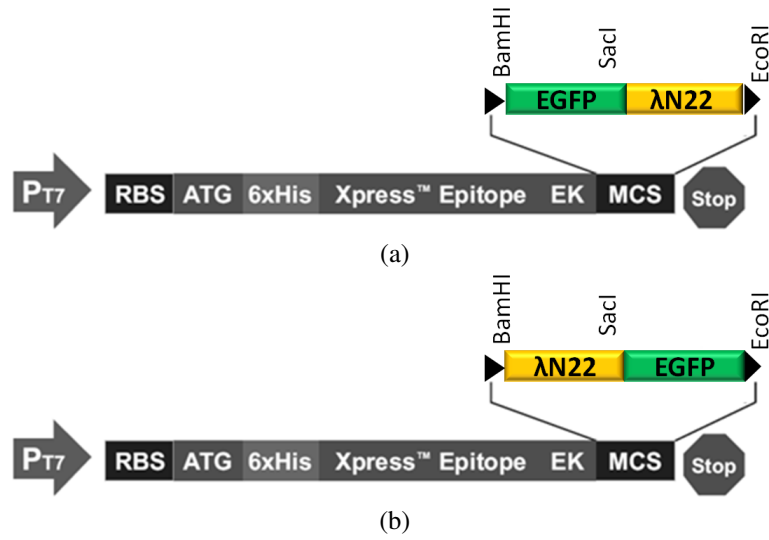


Figure 3.9: Schematic representation of EGFP tagged at (a) C-terminus and (b) N-terminus with λ_{N22}

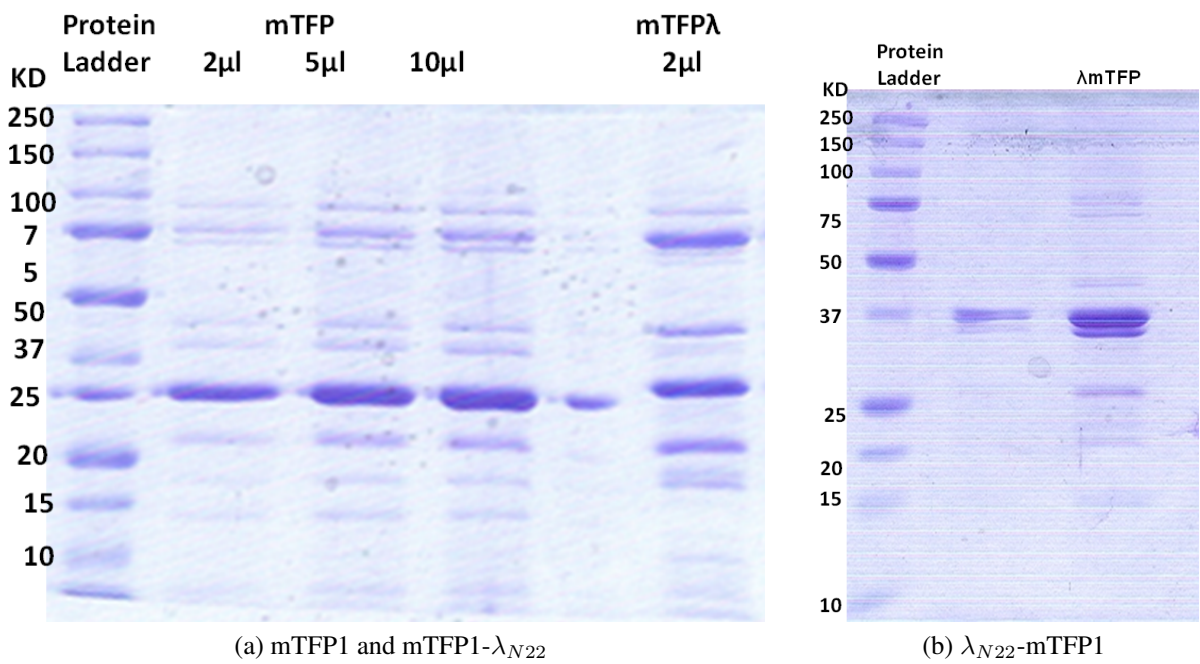


Figure 3.10: SDS PAGE for purified proteins

3.4 Studying aptamer induced FRET

To study aptamer induced FRET upon binding of λ_{N22} tagged fluorescent proteins, *in-vitro* experiments were conducted in a cuvette and FRET was measured via a photometer. The acceptor proteins were the λ_{N22} inserted mKO2 variants, #s 49, 51, 54, 92, 186; and mKO3 tagged N- and C-terminally with λ_{N22} . The donor proteins were EGFP and mTFP1 tagged with λ_{N22} at the N- and C-terminus. The cognate sequence for binding is the boxB RNA. For *in vitro* FRET experiments 5boxB RNA sequence was transcribed *in vitro* using T7 and Sp6 primers from a pcDNA3-5boxB. This construct was generated using a 5boxB PCR fragment and inserted in pcDNA3 as shown in figure 3.11.

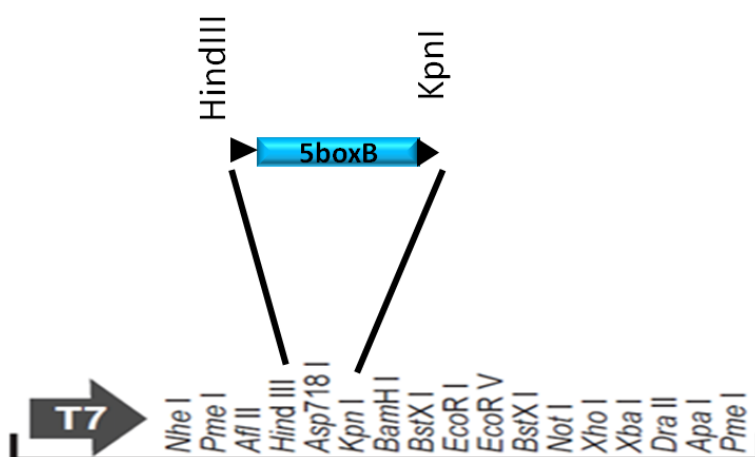


Figure 3.11: Schematic representation of pcDNA3-5boxB construct for *in vitro* RNA transcription

The sequence of 5boxB RNA is shown below:

TACGCCCTGAAAAAGGGCTGTACAGCCCTGAAAAAGGGCTCGA
GCCCTGAAAAAGGGCAATTGCCCTGAAAAAGGGCGTCGACGCCCTGAAAAAGGGCG

where the boxB sequence is highlighted in red.

To check that the transcribed RNA is a single pure band, it was run on a non-denaturing agarose gel. There was more than one band found in the transcribed RNA lane. On heating the product to 95 °C and quick cooling, again there were two bands found in the transcribed 5boxB RNA lane. To ascertain the purity of transcribed RNA, the RNA was reverse transcribed to obtain a cDNA product. The template PCR DNA, *in vitro* transcribed RNA and the cDNA were then run together on a non-denaturing gel as shown in figure 3.12.

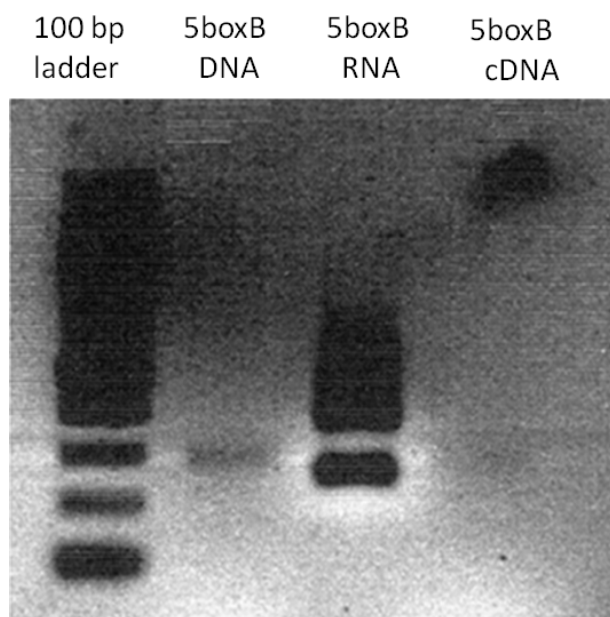


Figure 3.12: Gel picture showing the 5boxB template DNA used for *in vitro* transcription, the transcribed RNA and the cDNA synthesized from the transcribed RNA

The size of the cDNA band synthesized from the transcribed RNA was the same as for the initial DNA template used for RNA transcription, which indicated that the correct RNA is transcribed via *in vitro* transcription. The transcribed RNA showed more than one band when ran on an agarose gel, which as per Francisco J. Triana-Alonso *et al.* [60], might be RNA-coded *de novo* synthesis or self-coded 3'-end extension event occurring. This can happen if the UTP concentration in the buffer is high as then the T7 polymerase might accept the 3' end of the newly transcribed RNA which is free from secondary structure and start extending the 3' end of the RNA. This results in a secondary product which is half the double size of the RNA. Here, from the gel it is clear that the cDNA synthesized from the RNA gives the same size band as the template DNA. Therefore, the transcribed RNA is correct. But it is possible that some transcribed RNA molecules might have longer sequences than 5boxB fragment with additional nucleotides.

The concentration c of the *in vitro* transcribed RNA was calculated as shown in the formula below:

$$c = \frac{\gamma}{M};$$

where γ is the specific weight in nuclease free water and M is the molecular weight.

The molecular weight was calculated using the following formula (from www.ambion.com):

$$M = N_{nucleotides} \cdot 320.5 + 159;$$

where $N_{nucleotides}$ is the number of nucleotides.

To conduct the FRET experiments, first the donor proteins were added and the fluorescence emission spectra was recorded, next the acceptor was added and the emission spectra was recorded, finally the RNA was added and the fluorescence emission spectra was measured. The molar concentrations of the proteins and the RNA was kept in the same ratio(1:1:1) initially, later the concentration of RNA was increased in the cuvette to two fold(1:1:2) to observe if it affected in the emission spectra (figures A.1- A.7 appendix A).

Although there was no significant FRET change visible, the $\Delta R/R$ values were calculated for the different FRET pairs using the equation given in the methods section 2.2.6 on page 55. Tables 3.2 on the next page and 3.3 on page 78 show the obtained results from these calculations.

FRET Pair		$\Delta R/R$
EGFP λ -mKO2 λ #49	1XRNA	0.152
	2XRNA	0.097
EGFP λ -mKO2 λ #51	1XRNA	0.016
	2XRNA	0.067
EGFP λ -mKO2 λ #54	1XRNA	0.07
	2XRNA	0.38
EGFP λ -mKO2 λ #92	1XRNA	0.072
	2XRNA	0.056
EGFP λ -mKO2 λ #186	1XRNA	0.059
	2XRNA	0.0
EGFP λ -mKO3 λ	1XRNA	0.029
	2XRNA	0.029
EGFP λ - λ mKO3	1XRNA	0.015
	2XRNA	0.11

FRET Pair		$\Delta R/R$
λ EGFP-mKO2 λ #49	1XRNA	0.052
	2XRNA	0.02
λ EGFP-mKO2 λ #51	1XRNA	0.069
	2XRNA	0.039
λ EGFP-mKO2 λ #54	1XRNA	0.19
	2XRNA	0.058
λ EGFP-mKO2 λ #92	1XRNA	-
	2XRNA	0.053
λ EGFP-mKO2 λ #186	1XRNA	0.004
	2XRNA	0.021
λ EGFP-mKO3 λ	1XRNA	0.05
	2XRNA	0.039
λ EGFP- λ mKO3	1XRNA	-0.02
	2XRNA	0.011

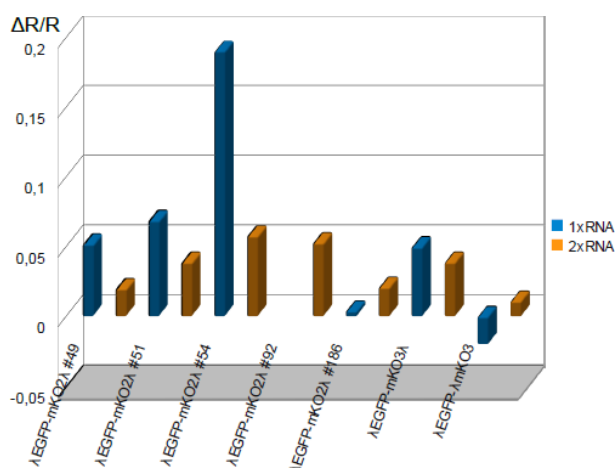
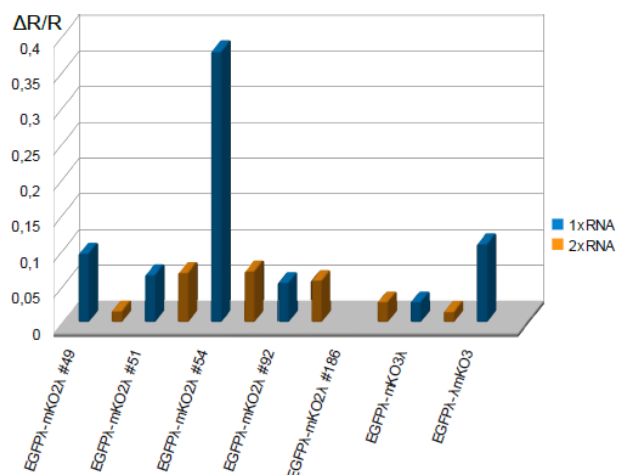


Table 3.2: The table shows the FRET ratio change, $\Delta R/R$, measured for the different λ_{N22} tagged donor and acceptor pairs on addition of 5boxB RNA in the cuvette. 1XRNA depicts equimolar concentration of RNA, donor and acceptor proteins in the solution. 2XRNA depicts when the concentration of RNA was two folds higher than the concentration of the donor and acceptor proteins in the solution. The $\Delta R/R$ values are also shown as bar graphs below the tables to show the FRET ratio change in the presence of RNA (1XRNA or 2XRNA) in comparison to zero RNA in the solution.

FRET Pair		$\Delta R/R$
mTFP1 λ -mKO2 λ #49	1XRNA	0.002
	2XRNA	0.118
mTFP1 λ -mKO2 λ #51	1XRNA	0.102
	2XRNA	0.168
mTFP1 λ -mKO2 λ #54	1XRNA	0.008
	2XRNA	0.064
mTFP1 λ -mKO2 λ #92	1XRNA	-0.009
	2XRNA	-0.12
mTFP1 λ -mKO2 λ #186	1XRNA	-0.019
	2XRNA	0.026
mTFP1 λ -mKO3 λ	1XRNA	0.01
	2XRNA	0.156
mTFP1 λ - λ mKO3	1XRNA	0.008
	2XRNA	0.076

FRET Pair		$\Delta R/R$
λ mTFP1-mKO2 λ #49	1XRNA	0.067
	2XRNA	0.069
λ mTFP1-mKO2 λ #51	1XRNA	0.039
	2XRNA	0.115
λ mTFP1-mKO2 λ #54	1XRNA	0.041
	2XRNA	0.095
λ mTFP1-mKO2 λ #92	1XRNA	-0.014
	2XRNA	-0.017
λ mTFP1-mKO2 λ #186	1XRNA	-0.009
	2XRNA	0.075
λ mTFP1-mKO3 λ	1XRNA	0.039
	2XRNA	0.096
λ mTFP1- λ mKO3	1XRNA	0.042
	2XRNA	0.057

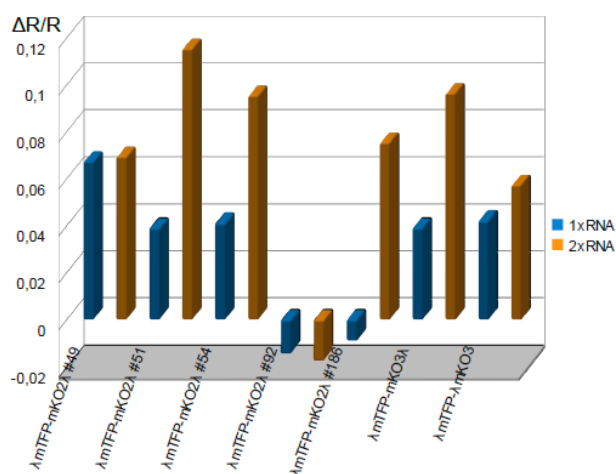
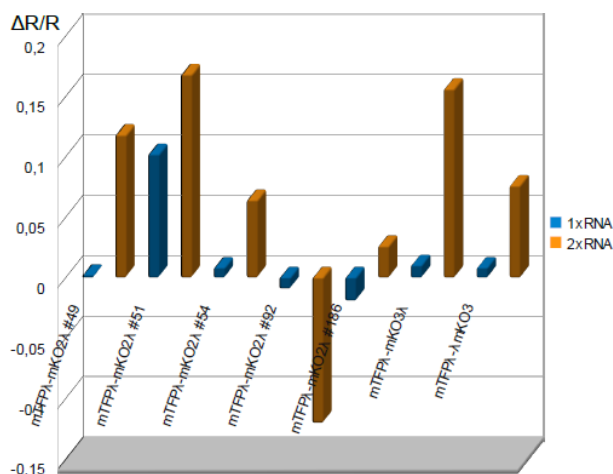


Table 3.3: The table shows the FRET ratio change, $\Delta R/R$, measured for the different λ_{N22} tagged donor and acceptor pairs on addition of 5boxB RNA in the cuvette. 1XRNA depicts equimolar concentration of RNA, donor and acceptor proteins in the solution. 2XRNA depicts when the concentration of RNA was two folds higher than the concentration of the donor and acceptor proteins in the solution. The $\Delta R/R$ values are also shown as bar graphs below the tables to show the FRET ratio change in the presence of RNA (1XRNA or 2XRNA) in comparison to zero RNA in the solution.

In parallel a small experiment was conducted to see if the currently available λ_{N22} and MS2 phage systems can be used to study RNA conformational change *in vivo*. The idea behind this experiment was to prove the principle of riboswitch action using FRET. RNA sequences used for the experiment were the λ_{N22} cognate binding site 5boxB RNA, and the MS2 phage binding sites (BS). On either side of thiM the RNA binding sites were tagged. The 5'UTR of the riboswitch was obtained from *E. coli* XL-blue competent cells in the lab via PCR. The cloning was done in pRSETB plasmid and then the entire construct containing the two specific RNA sequences: boxB and MS2 binding sites, with the thiM5'UTR in the middle was subcloned into pCDNA3 as shown in figure 3.13. the 5boxB

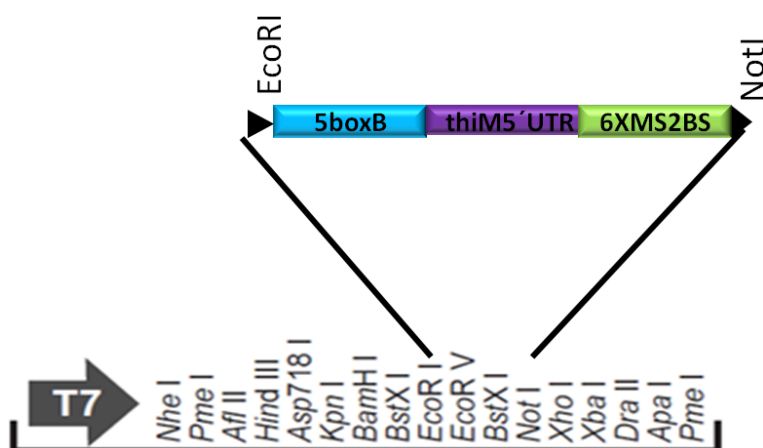


Figure 3.13: Schematic representation of 5boxB-thiM-MS2phage binding site construct inserted in pcDNA3

sequence was obtained via PCR using p5boxB-SRP RNA plasmid (obtained from Dr. Jan Ellenberg lab, EMBL, Heidelberg) as the template. pcDNA3-12XMS2BS plasmid (obtained from Dr. Robert Singer's lab, Albert Einstein College of Medicine, USA) was used a template to PCR out 6XMS2BS sequence.

The respective RNA binding proteins were tagged with the fluorescent proteins as shown in figure 3.14. They are the original plasmids obtained from Dr. Jan Ellenberg's lab and Dr. Robert Singer's lab.

The 5boxB-thiM-MS2BS construct was transfected in HeLa cells and then RNA was isolated from the transfected cells and semi-quantitative PCR was done to check the expression of the construct in the cells as shown in the gel picture 3.15.

After obtaining the expression of 5boxB-thiM-MS2 BS in the transfected HeLa cultures, next I tried to co-transfect HeLa cell culture with pcDNA3-5boxB-thiM-MS2 BS plasmid and either with λ_{N22} -



Figure 3.14: Schematic representation of RNA binding peptides tagged with fluorescent proteins. (a): λ_{N22} tagged with EGFP; (b): MS2-phage coat protein tagged with YFP.

EGFP or MS2 coat protein-YFP. The transfected cells were then imaged under a confocal microscope. The cells showed a pattern of expression and localization of fluorescent proteins (figure 3.16).

From the captured images it was evident that the λ_{N22} -EGFP and MS2 coat protein-YFP did not transport out of the nucleus of the HeLa cells, as it should since the 5boxB-thiM-MS2 BS construct has a poly-A tag to it and therefore the riboswitch construct must be transported out of the nucleus into the cytoplasm. Since there was no visible export of the fluorescently tagged RNA binding proteins out of the nucleus, it is an indication of the nls present on the RBPs not functioning efficiently in the HeLa cells which could lead to false results; plus the addition of TPP might not yield a fluorescent emission change as expected if the tagged-RBPs are not exported into the cytoplasm of the transfected cells. This led to the idea of developing an RNA binding and tagging system that is independent of the nls and can target the RNA in the cytoplasm and monitor its conformational change via a FRET readout.

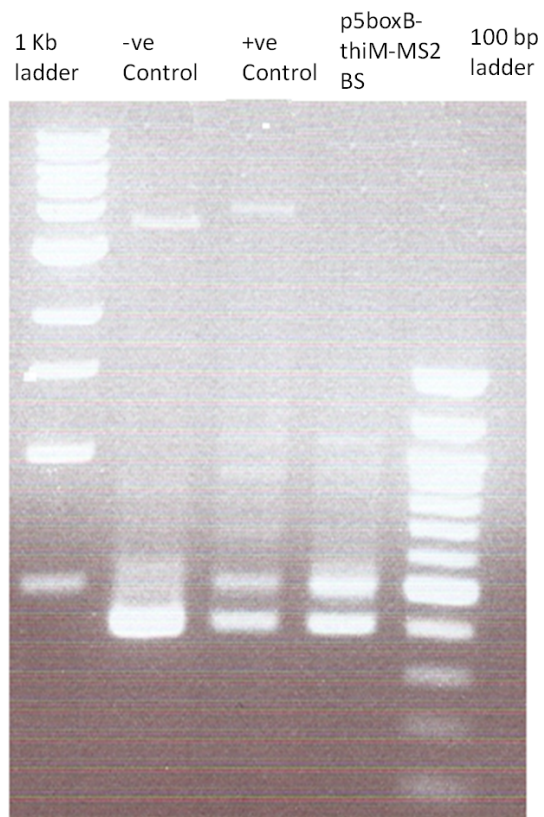


Figure 3.15: Results of the semi-quantitative PCR to check 5boxB-thiM-MS2BS expression in HeLa cell culture.

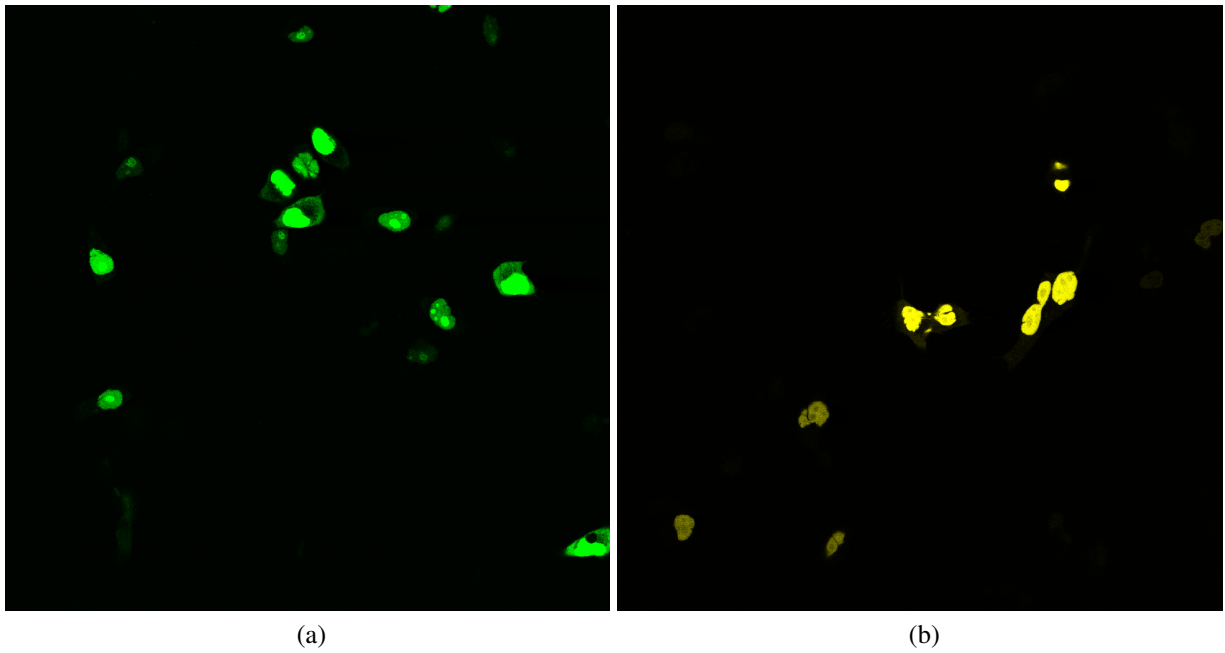


Figure 3.16: Confocal Images of HeLa cells co-transfected with 5boxB-thiM-MS2bs RNA and λ_{N22} -EGFP (a) or MS2 coat protein-YFP (b)

Chapter 4

Discussion

The aim of this thesis was to study aptamer induced FRET on binding of fluorescent tagged RBP *in vitro*, with a bigger picture of developing a method to label RNA in the cytoplasm via FRET readout and track their movement in the cell. Work has been done previously to study the spatial and temporal interaction between RNA and protein in the cytoplasm via FRET [61]. I wanted to work on RNA tagging *in vitro*, where FRET is the read out, and thus can be used to monitor the conformation change in the RNA on binding, e.g. riboswitches undergo a conformational change on binding of a ligand. I used the λ_{N22} system as the aptamer-RNA binding protein system.

As per our hypothesis, λ_{N22} tagged fluorescent proteins should bind the 5boxB RNA sequence in solution in the cuvette and once in close proximity on the aptamer, there should occur resonance energy transfer and a change in fluorescence emission spectra should be observed. This should indicate the binding of the λ_{N22} -fluorescent proteins on the RNA. Also, once the RNA is discharged or degraded the FRET should be reversed. A point to be considered here is that on binding of the peptide the aptamer might undergo a conformational change. Due to this the tethered fluorescent proteins might either come in favorable FÖRSTER radius range and orientation for a FRET change, or might be moved out of the FÖRSTER radius (depending on where they bind), or they might be in the FÖRSTER radius but their oscillation planes are oriented anti-parallel to each other. Therefore, the conformation the RNA adopts in solution would influence the resonance energy transfer between the fluorescent proteins.

The other bacteriophage system that is commonly used for *in vivo* RNA tagging is the MS2 phage (as mentioned in the introduction) and has been used successfully in quite a number of studies especially to study RNA trafficking in yeast. It is a system that was discovered prior to the λ_{N22} and has been

extensively modified for the purpose. Nevertheless the λ_{N22} was the system of choice due to the advantages it offered over the MS2 system and has been mentioned in the introduction also. The λ_{N22} is smaller in size than the MS2 coat protein. Since λ_{N22} binds as a monomer, it would offer fewer obstacles for the other fluorescent RBP to bind on the RNA than MS2 coat protein dimer. Also the MS2 coat protein binds as a dimer in anti-parallel orientation. Since not only distance, but orientation of the fluorescent proteins influence resonance energy transfer, MS2 coat protein was not an ideal choice.

Van Gilst *et al.* [62] reported that the N protein binds in its unfolded form, i.e. it is unfolded in solution, and this indicates that on binding its cognate boxB structural changes occur in N protein. It is estimated that 16–18 amino acids of the N-protein form an α -helix structure when N binds boxB RNA. Austin *et al.* [39] have shown that this α -helical structure binds within the major groove of the hairpin structure, as also shown in figure 1.8. These factors point to the flexible nature of λ_N and the conformational change it undergoes on binding the boxB RNA.

For the boxB RNA, Su *et al.* [38] proved that the boxB RNA also undergoes conformational change on binding of the λ_N , the loop conformation of boxB is stabilized. After that Xia *et al.* [63] showed that on binding of boxB RNA with the N protein there is not just a single structural change. They show that a continuous re-orientation of base stacking occurs between Tryptophan 18 of the N protein and A7, A8 and A10 bases of the RNA chain. Their findings indicated that in solution, the RNA-peptide conformations are inherently dynamic and a single static structure can't be assigned as a representative of the RNA-peptide complex.

All these findings indicated that there is no fixed structure of the λ_N that binds in a fixed groove of the boxB. In order to observe binding of the λ_{N22} peptides on the boxB RNA and also to observe a conformational change in the RNA on binding of peptide via FRET, there could not be a single functional orientation of the tagged fluorescent proteins, as it is not known how the tagged fluorescent proteins, will be oriented spatially once the λ_{N22} is bound to boxB sequence.

For achieving this orientation advantage, I wanted to generate mKO2- λ_{N22} variants where each different variant would offer a different distance and orientation when tethered to the RNA so as to avail the advantage of angular orientation for FRET efficiency when both the donor and acceptor are tethered to the RNA. Cloning of such mKO2- λ_{N22} variants required inserting the λ_{N22} peptide sequence in the middle of the mKO2 protein, and it was important that such insertions did not hinder the folding of mKO2 leading to the loss of fluorescence. Therefore it was necessary to identify tolerant insertion sites in mKO2.

One possible approach to achieve this was to introduce restriction enzyme sites in mKO2 via PCR and then screen the colonies that encode functional fluorescent proteins. But this can be a very time consuming and laborious process to check the whole sequence for tolerant sites via PCR. Another major disadvantage of this approach is that it might introduce undesired mutations in mKO2. The other approach was to use the random insertion behavior of a transposon and insert restriction enzyme sites in mKO2.

The commercially available transposon, EZ-Tn5, was used for this purpose as the mechanism of its action is already known, has been modified to achieve high transposition efficiency and has been successfully used in other labs [64]. Therefore, the EZ-Tn5 was used in the lab to insert NotI restriction enzyme sites in mKO2 by Anselm Geiger. This gave the flexibility to use such mKO2 constructs for insertion of different codons or protein tags. There were a few disadvantages with this approach, one was that the screening process for the mKO2 colonies after transposition reaction was extensive as each and every colony had to be screened to find out the site of insertion, some colonies were lost in this process. Another disadvantage was that only one restriction enzyme site was inserted in mKO2, due to which 70 % of the clones screened for λ_{N22} insertion had the sequence inserted in the reverse orientation. Due to the random behavior of EZ-Tn5, some insertions were in the central α -helical core of the mKO2 protein. Therefore the constructs had to be screened, the amino acid position of the insertion determined, and the position in the folded mKO2 protein checked using following programs:

<http://www.rcsb.org/pdb/home/home.do>

<http://www.pymol.org/>

Only those constructs were selected which would avail λ_{N22} for binding to the aptamer, i.e. inserted in the loop region or the β -barrel. Based on this, mKO2 variants with tolerant insertion sites, were chosen for this project. Figure 4.1 represents all the insertion tolerant sites obtained for mKO2 with this method and used in this thesis.

Cartoons with single insertion site as in the appendix figures B. I also wanted to have N- or C-terminus labeled acceptor proteins to complete the spectra of differently oriented λ_{N22} insertions. As previously observed in the lab, mKO2 is not tolerant to C-terminal tagging, therefore I used the mKO3 for N- terminus and C-terminus tagging with λ_{N22} .

The λ_{N22} -inserted mKO2 and mKO3 variants were characterized for their fluorescent properties like quantum yield and extinction coefficient. This was done in comparison to the mKO2 wild type so

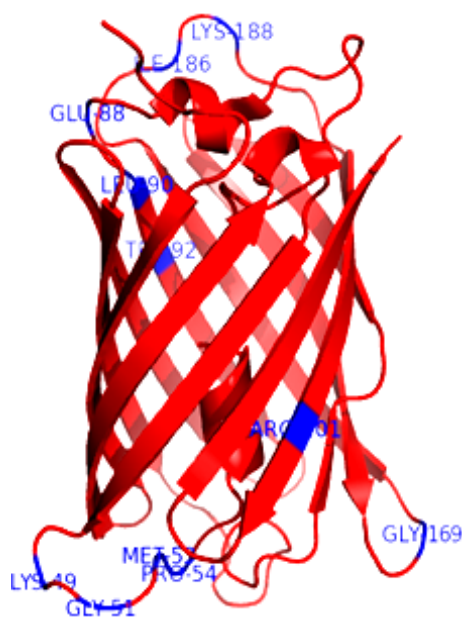


Figure 4.1: Various insertion sites tolerating in mKO2. See B for detailed figures of each construct.

as to determine their brightness in contrast to mKO2, since a high value of quantum yield, results in bright fluorescent protein. The fluorescent proteins were designed for use in FRET experiments, where the rate of energy transfer is influenced by the quantum yields of the donor and acceptor, and the fluorescent properties which are: absorption spectra, extinction coefficient and emission spectra. The table 3.1 as well as the graphs 3.6 and 3.7 in section 3.2 show the differences amongst the mKO2 and mKO3- λ_{N22} variants and with regards to the original mKO2 fluorescent protein. The mKO2- λ_{N22} variants #49, 51, 54, 92, 186, mKO3- λ_{N22} and λ_{N22} -mKO3 had high values for quantum yield (less than mKO2 (WT)), compared to the other variants #88 and 90. #49, 54, 186, mKO3- λ_{N22} and λ_{N22} -mKO3 had higher extinction coefficient at 549 nm mKO2 (WT). The extinction coefficient values of constructs #53, 169 and 188 were very low. Similar results were obtained for absorption spectra where #53, 88, 90, 169 and 188 fared pretty badly in comparison to the others. Based on these results the mKO2- λ variants #49, 51, 54, 92, 186, mKO3- λ and λ -mKO3 were selected for FRET experiments as from these properties it was apparent that these variants would form good acceptors for EGFP and mTFP1.

The donor proteins EGFP and mTFP1, were λ_{N22} tagged either at the N- or C-terminus. The donor mTFP1 has been used in the lab for FRET experiments with satisfactory results. The EGFP has also been used in the lab for previous experiments with satisfactory results. Therefore, the donor proteins

were considered good choice for FRET experiments.

Considering the above factors, it was reasoned that some of the mKO2 and mKO3 variants could yield a FRET ratio change when paired with either of the donors, in presence of the aptamer. The aptamer designed for the project had 5 boxB sites separated by a linker region, as shown in 3.4 on page 74. As Van Gilst *et al.* [62] have also shown that the boxB oligomer and λ_N form a complex with a stoichiometry 1:1, therefore on a 5boxB sequence at least 3 fluorescently tagged λ_N should bind assuming that the fluorescent protein might hinder another tagged λ_N molecule to bind the adjacent boxB loops. Rajan Lamichhane *et al.* have recently shown in their study [65] using steady state FRET (ssFRET) and time resolved FRET (trFRET) that the spaced length of at least 15 nucleotides is required for significant FRET read-out. If the spacer length between the RNA loops is 5 nucleotides or less, no FRET was visible. But in their experiment only 2 RNA loop regions linked by a spacer were used. In my experiment, 5boxB has a 4–6 nucleotides long spacer between the loop regions. But here as the number of loops is more, the small size of the spacer should not be a problem. Since the donor, acceptor and the RNA were present in 1:1:1 stoichiometry in the cuvette, hypothetically a donor and acceptor should bind on the same RNA sequence leading to resonance energy transfer.

As can be seen from the FRET results, there is seen a slight increase in mKO2 emission spectra, on addition of only mKO2 in the cuvette. This could not be due to excitation of mKO2 by the donor excitation wavelength, as care was taken to ensure that donor excitation wavelength which does not cause excitation of mKO2. This emission spectra observed on addition of λ_{N22} tagged fluorescent proteins could not be due to an interaction between λ_N - λ_N peptides, because mKO2 emission was observed even without λ_{N22} tagging on the fluorescent proteins. This can be seen from the graphs in figure A.17 and A.18 where mKO2 emission is measured for donor and acceptor pairs where either both or one of the FRET partners is not λ_{N22} tagged. This indicates an unspecific FRET ratio change occurring between the fluorescent proteins.

After this clarification, the $\Delta R/R$ values obtained for the FRET measurements (shown in the results section) on addition on RNA could be only due to a FRET change between the donor (λ_{N22} tagged EGFP/mTFP1) and the acceptor (λ_{N22} inserted mKO2/mKO3). There is an increase in $\Delta R/R$ values for some FRET pairs with 2 fold RNA. This increase in FRET ratio from 1-fold to 2-fold RNA concentration is not a trend observed for all FRET pairs. Even for the same mKO2 construct different results are seen. However, mKO3- λ_{N22} and λ_{N22} -mKO3 have exhibited high values of FRET ratio change with most donors, whereas, mKO2- λ_{N22} #92 exhibited negative FRET with λ_{N22} -mTFP1 and mTFP1- λ_{N22} . As a donor λ_{N22} -mTFP1 yielded the highest FRET ratio change with most of the

mKO2-and mKO3- λ_{N22} variants, followed by EGFP- λ_{N22} . λ_{N22} -EGFP and mTFP1- λ_{N22} yielded poor FRET ratio changes in comparison.

Since FRET is not only dependent on the distance but also on the favorable orientation dipoles between the donor and acceptor, it is possible these conditions were not satisfied for many FRET pairs. The observed difference in $\Delta R/R$ values with 1-fold and 2-fold RNA concentration also points to the same reason. With increase in the number of RNA molecules, any unbound donor and acceptor proteins present in the solution are tethered to the RNA, which might or might not be favorable conditions for FRET. The other theory that could be offered is that with increase in RNA molecules in the solution, a re-arrangement occurs amongst the molecules present in solution and some proteins bind to the newly available RNA. Due to this re-organization some arrangements offered favorable conditions for FRET while others did not. This could explain why some FRET pairs display an increase in FRET ratio change while others show a decrease, on increasing the RNA concentration.

Along with FRET ratio change there was also observed a decrease in emission intensity. This decrease in emission intensity is observed not only for the acceptor emission but also for the donor. As seen from the result graphs, there is a decrease in emission intensity on addition of equimolar concentration of RNA. On increasing the concentration of RNA in the cuvette to 2-fold, there is further drop in the emission intensity for almost all of the FRET pairs. Test was done to check if the emission intensity of the donor keeps on decreasing with increasing the RNA concentration in the solution. The FRET read out was taken with the same concentrations and under the same conditions as for the original experiment. The result of this experiment can be seen from figure 4.2. There is a decrease in emission intensity of the λ_{N22} tagged donors in the presence of equimolar concentration of RNA. However, there was no change observed in the absorption spectra of the donors on addition of RNA as is evident from the graphs in figure 4.3 on page 92.

This decrease in the emission intensity of the donor and the acceptor can be due to fluorescence quenching. Quenching is a phenomenon where the excited molecules relax to ground state via non-radiative pathways avoiding fluorescence emission (i.e. vibration, collision, intersystem crossing). There is also quenching via molecular oxygen and polar solvents such as water. This phenomenon of quenching was applied by Van Gilst *et al.* [62] to measure the binding between N protein and boxB. They observed that the N protein, which carried two Tryptophan residues, shows an appreciable overall decrease of fluorescence on binding with boxB. With saturation concentrations of RNA maximum quenching was observed. Going by this idea, in the current study, maximum quenching was probably observed on addition of equimolar concentration of RNA. Thus, the quenching might occur due to a

proximal nucleobase through an outer sphere electron transfer. The rate of quenching depends on the RNA sequence immediately next to the fluorophore as the quenching depends of the frequency of diffusional encounters of and the activation barrier for redox chemistry between the excited fluorophore and the base [66]. The role of RNA in decreasing the fluorescence emission of the donor could be the secondary structure it assumes in the buffer which might cause quenching. In the present study it is possible that the binding of the λ_{N22} tagged FPs to the boxB, while causing structural re-organization of boxB and the λ_{N22} , might have brought the FPs in proximity to certain bases that lead to quenching of fluorescence. Unfortunately, the result of RNA binding on only the acceptor emission intensity was not studied. To properly quantify for the FRET ratio change, it would be necessary to find out the percentage quenching due to RNA binding (also on increasing the RNA concentration). A useful experiment would also be to check the binding of the λ_{N22} tagged fluorescent proteins with single boxB RNA via electromobility shift assay.

With the small experiment to study the conformational change in RNA upon binding to a ligand *in vivo*, since no export of fluorescent proteins was observed in HeLa cells co-expressing RNA and RBP tagged with fluorescent protein, it could be assumed that either the RNA did not bind the RBP or there was no transport. As can be seen in the results section the RNA was expressed by the cells. Under such conditions addition of the ligand, Thiamine Pyrophosphate, would not yield a FRET change even if there is a conformational change in the RNA. This small experiment brought to light some of the problems associated with dependence on nuclear localization signal for tagging, transport of RNA and also to study conformational change in RNA. This also specified the importance of a method to monitor RNA tagging in the cytoplasm, via FRET change, and also for studying RNA dynamics.

In conclusion, an unspecific FRET ratio change, no related to aptamer binding, was observed between the λ_{N22} tagged EGFP/mTFP1 donor proteins and mKO2/mKO3- λ_{N22} variants. Apart from one variant, mKO2- λ_{N22} #92, most of the variants have shown FRET ratio change with the donors although it is not a significant FRET change in some cases. No clear trend could be observed for FRET, even for the same FRET pairs on increasing the RNA concentration. Another interesting observation was the quenching of emission intensity which was observed on binding of λ_{N22} tagged fluorescent proteins on the 5boxB RNA.

Outlook

This thesis shows an interesting aspect of λ_{N22} -boxB binding via FRET. There are a number of future experiments which should be conducted to answer some questions raised by the results obtained in this study.

Firstly, it is necessary to quantify the quenching of emission intensity of both the donor and acceptor proteins, separately and together, on binding of the RNA. The sequence and the structure of the in vitro transcribed RNA should be studied to help understanding the quenching of emission intensity. On the same note, the structure of the fluorescent protein tagged λ_{N22} , on binding of λ_{N22} -boxB, is important to understand if this quenching is due to proximity of the fluorescent protein with a nucleobase.

The donors EGFP/mTFP1 should also be generated with λ_{N22} inserted in different tolerant insertion sites using the EZ-TN5 system. This would provide more orientation flexibility for FRET and for the choice of a good donor-acceptor pair. But this experiment should be coupled with use of 2 boxB or 3 boxB RNA sequences also. In 2 boxB sequences, the length of the spacer between the loops could be increased to accommodate both the donor and acceptor on the same sequence. With 2 or 3 boxB sequences the number of binding sites on the RNA is reduced and this could give a better idea of distance and flexibility of the spacer affecting FRET.

A better modification to the above experiment would be to use two different bacteriophage systems, e. g. link MS2 phage binding site with boxB and label MS2 coat protein and λ_{N22} with either of the two FRET partners. This would decrease the chances of having both sites on the RNA occupied by either donor or acceptor protein, and would give a clear FRET readout. By varying the spacer distance between the two RNA loops and using differentially oriented fluorescent proteins (generated via EZ-Tn5 system) favorable FRET pairs can be designed which would be useful for RNA tagging and for studies involving conformational change of RNA.

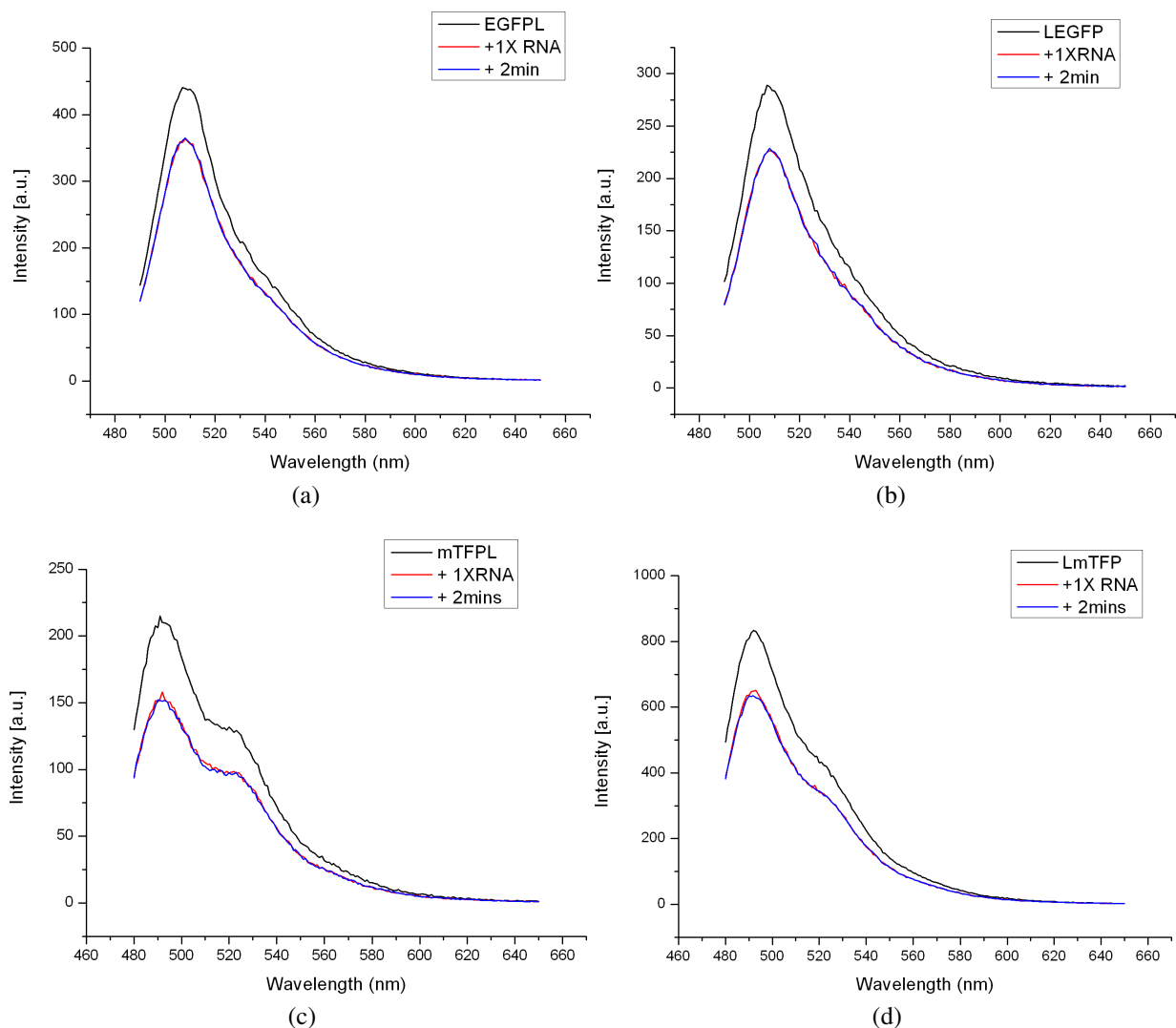


Figure 4.2: Fluorescence emission spectra of EGFP- λ_{N22} (a) and λ_{N22} -EGFP (b) with and without RNA. Excitation was at 465 nm and the emission spectra recorded from 480-650nm. Fluorescence emission spectra of mTFP1- λ_{N22} (c) and λ_{N22} -mTFP1 (d) with and without RNA. The excitation was at 460 nm and the emission spectra was taken from 470-650 nm. The black curve indicate the emission spectra of only the λ_{N22} tagged donor protein. Emission spectra of the donor on addition of equimolar concentration of 5boxB RNA is indicated by red curves, while the blue curves indicate the emission spectra for the second reading taken after 2 minutes.

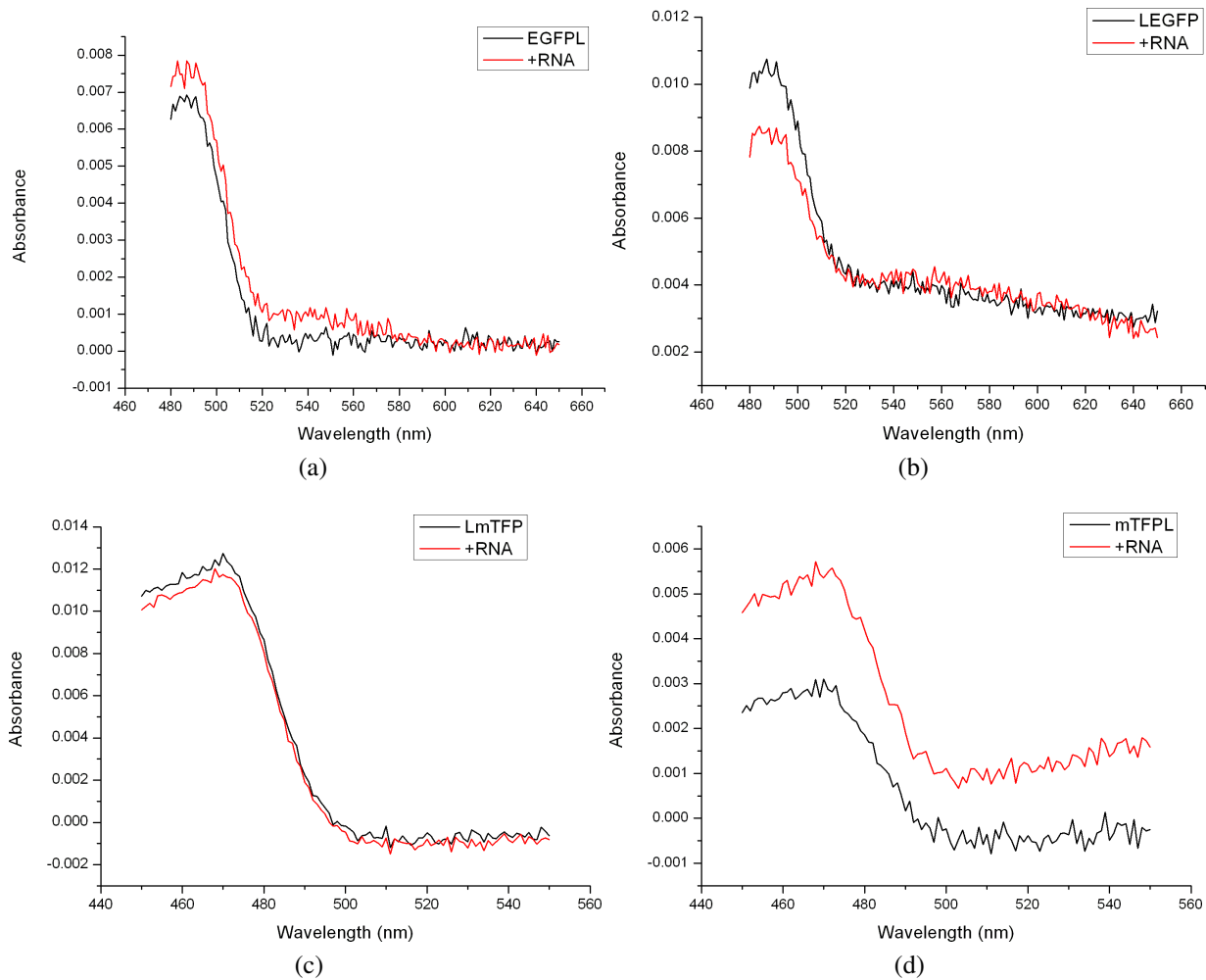


Figure 4.3: Graphs showing the absorption spectra of EGFP- λ_{N22} and λ_{N22} -EGFP with (a) and without RNA (b) and absorption spectra of λ_{N22} -mTFP1 and mTFP1- λ_{N22} with (c) and without RNA (d). The black curves indicate the absorption spectra of λ_{N22} tagged EGFP/mTFP1 and the red curves indicate the absorption spectra in the presence of equimolar concentration of 5boxB RNA.

Appendix A

Experiment Results

A.1 Result graphs

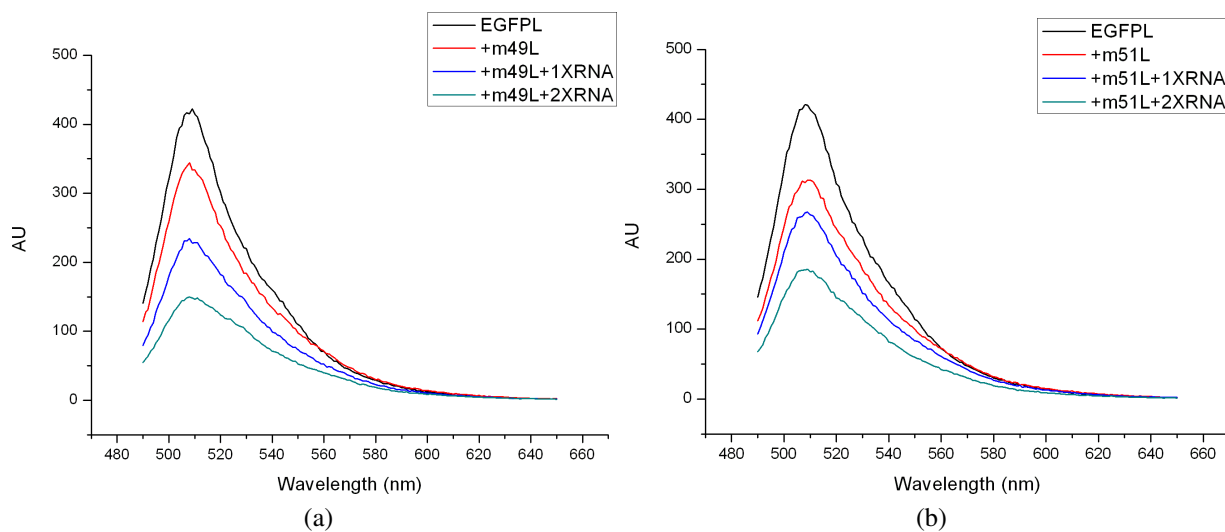


Figure A.1: Fluorescence emission spectra for FRET between EGFP- λ_{N22} and mKO2- λ_{N22} #49 (a) and #51 (b). The measurements were taken without RNA and with 1 and 2 fold molar ratio of RNA compared to the molar ratio of proteins in the cuvette. The excitation was at 465 nm and the emission spectra was taken from 480 nm – 650 nm. The black curves indicate the emission spectra of the λ_{N22} tagged donor proteins, the red curves indicate the emission spectra with λ_{N22} inserted acceptors, the blue curves for emission in the presence of equimolar concentration of 5boxB RNA and the green curves for the emission with two fold concentration of 5boxB RNA.

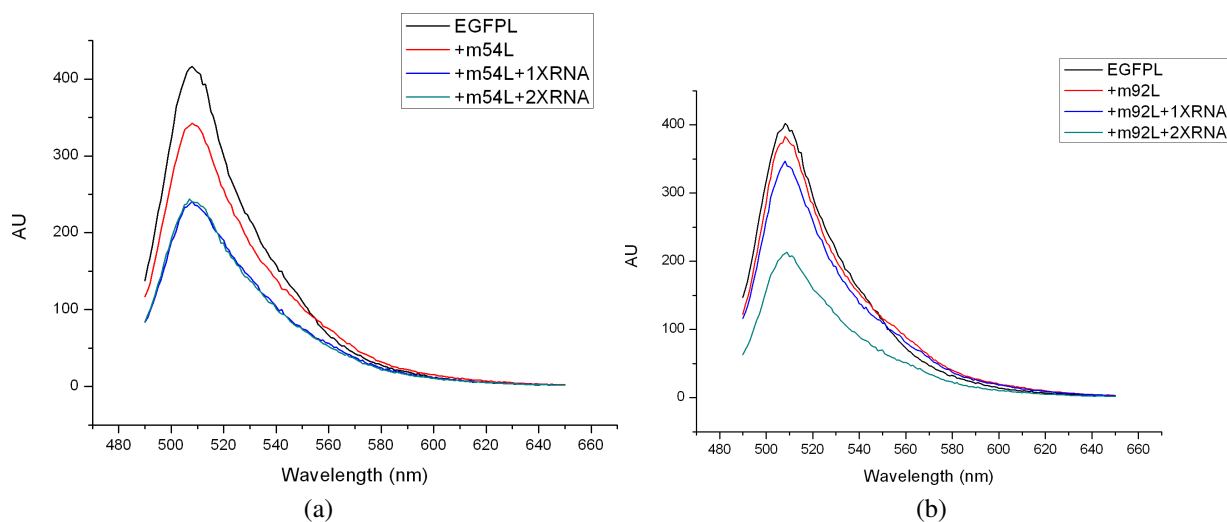


Figure A.2: Fluorescence emission spectra for FRET between EGFP- λ_{N22} and mKO2- λ_{N22} # 54 (a) and 92 (b). The measurements were taken without RNA and with 1 and 2 fold molar ratio of RNA compared to the molar ratio of proteins in the cuvette. The excitation was at 465 nm and the emission spectra was taken from 480 nm – 650 nm. The black curves indicate the emission spectra of the λ_{N22} tagged donor proteins, the red curves indicate the emission spectra with λ_{N22} inserted acceptors, the blue curves for emission in the presence of equimolar concentration of 5boxB RNA and the green curves for the emission with two fold concentration of 5boxB RNA.

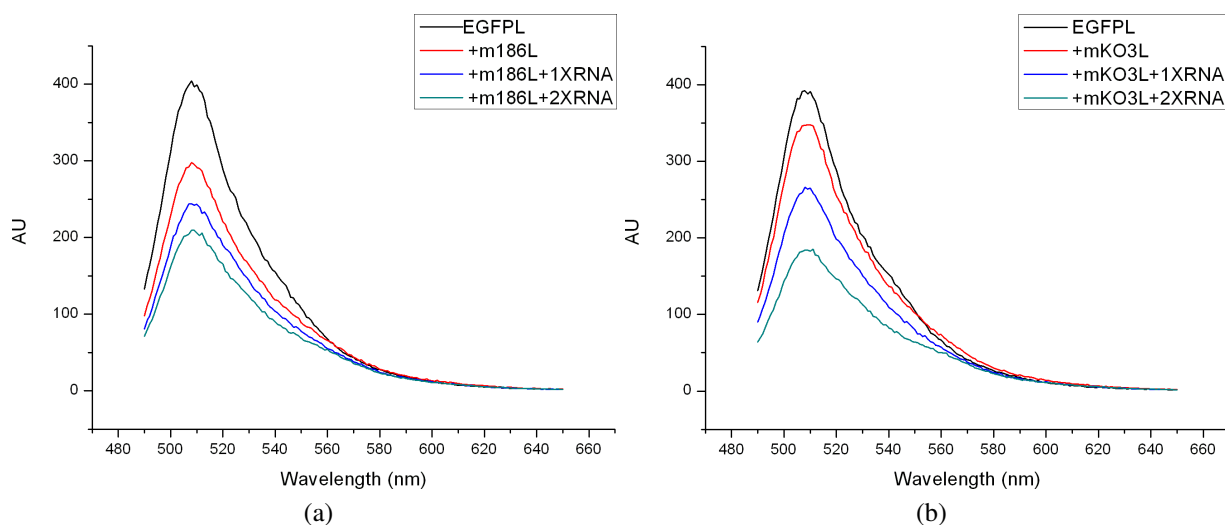


Figure A.3: Fluorescence emission spectra for FRET between EGFP- λ_{N22} and mKO2- λ_{N22} # 186 (a) and mKO3- λ_{N22} (b). The measurements were taken without RNA and with 1 and 2 fold molar ratio of RNA compared to the molar ratio of proteins in the cuvette. The excitation was at 465 nm and the emission spectra was taken from 480 nm – 650 nm. The black curves indicate the emission spectra of the λ_{N22} tagged donor proteins, the red curves indicate the emission spectra with λ_{N22} inserted acceptors, the blue curves for emission in the presence of equimolar concentration of 5boxB RNA and the green curves for the emission with two fold concentration of 5boxB RNA.

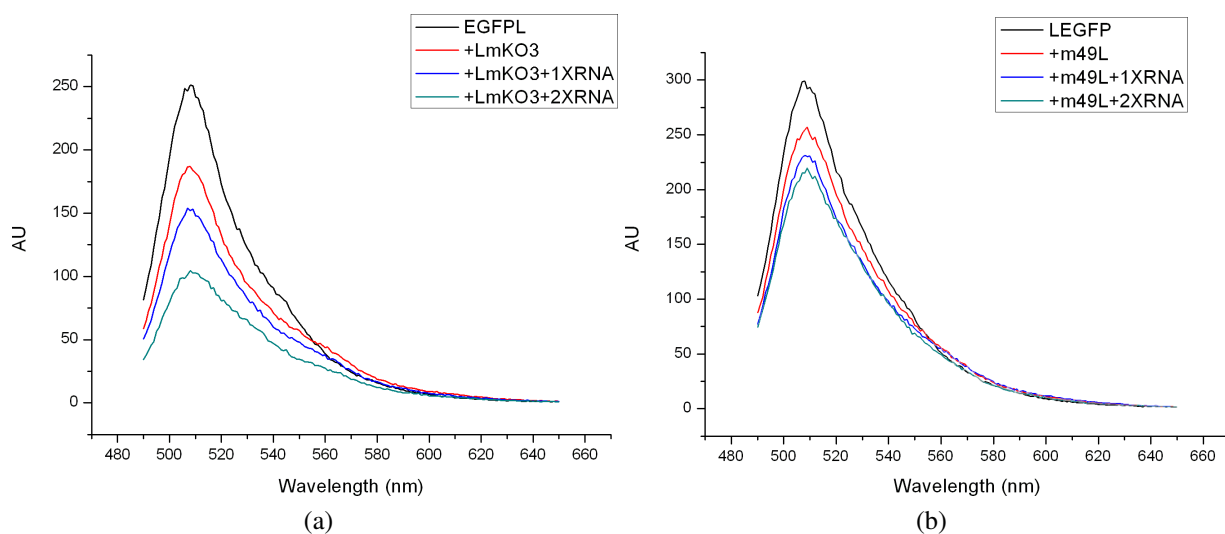


Figure A.4: Fluorescence emission spectra for FRET between EGFP- λ_{N22} and λ_{N22} -mKO3 (a) and between λ_{N22} -EGFP and mKO2- λ_{N22} # 49 (b). The measurements were taken without RNA and with 1 and 2 fold molar ratio of RNA compared to the molar ratio of proteins in the cuvette. The excitation was at 465 nm and the emission spectra was taken from 480 nm – 650 nm. The black curves indicate the emission spectra of the λ_{N22} tagged donor proteins, the red curves indicate the emission spectra with λ_{N22} inserted acceptors, the blue curves for emission in the presence of equimolar concentration of 5boxB RNA and the green curves for the emission with two fold concentration of 5boxB RNA.

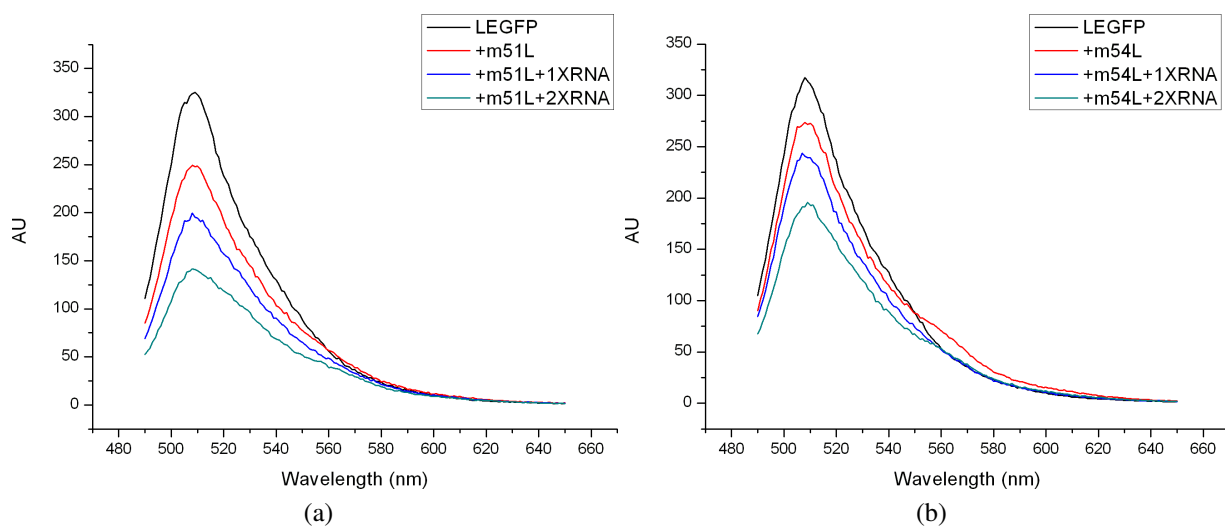


Figure A.5: Fluorescence emission spectra for FRET between λ_{N22} -EGFP and mKO2- λ_{N22} #51 (a) and #54 (b). The measurements were taken without RNA and with 1 and 2 fold molar ratio of RNA compared to the molar ratio of proteins in the cuvette. The excitation was at 465 nm and the emission spectra was taken from 480 nm – 650 nm. The black curves indicate the emission spectra of the λ_{N22} tagged donor proteins, the red curves indicate the emission spectra with λ_{N22} inserted acceptors, the blue curves for emission in the presence of equimolar concentration of 5boxB RNA and the green curves for the emission with two fold concentration of 5boxB RNA.

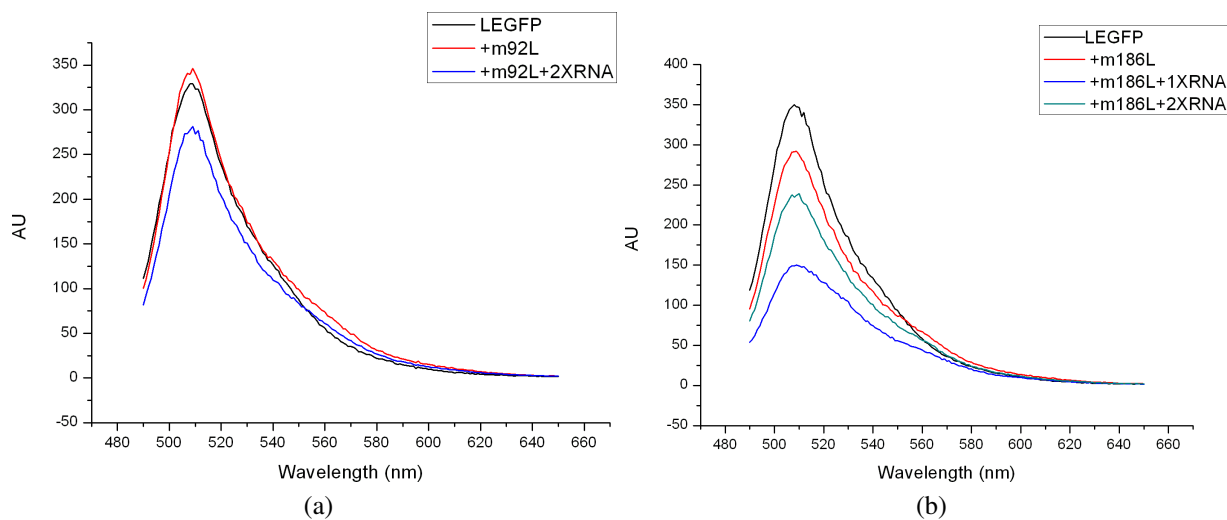


Figure A.6: Fluorescence emission spectra for FRET between λ_{N22} -EGFP and mKO2- λ_{N22} # 92 (a) and # 186 (b). The measurements were taken without RNA and with 1 and 2 fold molar ratio of RNA compared to the molar ratio of proteins in the cuvette. The excitation was at 465 nm and the emission spectra was taken from 480 nm – 650 nm. The black curves indicate the emission spectra of the λ_{N22} tagged donor proteins, the red curves indicate the emission spectra with λ_{N22} inserted acceptors, the blue curves for emission in the presence of equimolar concentration of 5boxB RNA and the green curves for the emission with two fold concentration of 5boxB RNA.

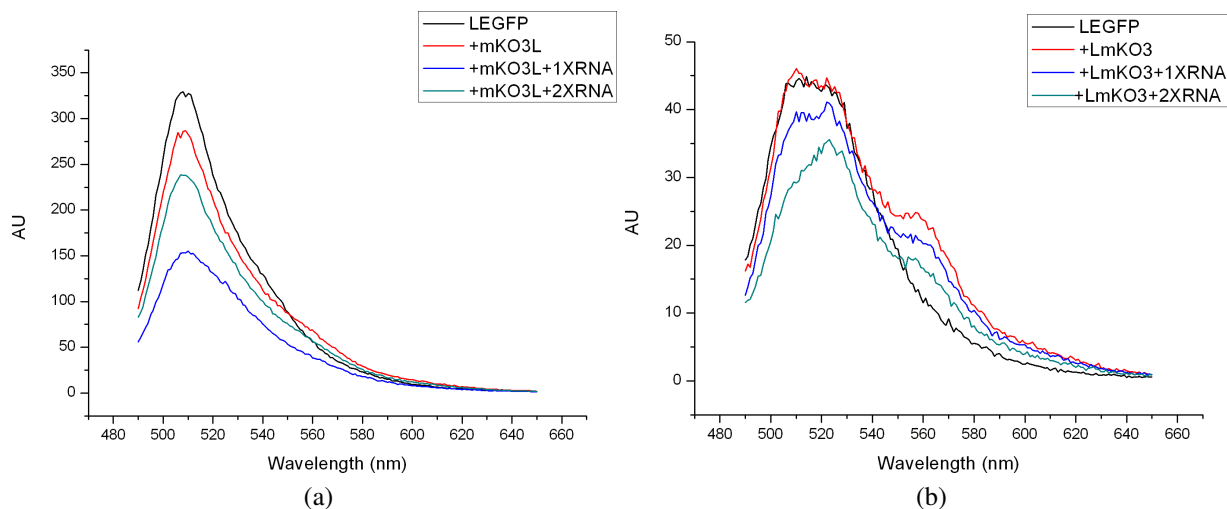


Figure A.7: Fluorescence emission spectra for FRET between λ_{N22} -EGFP and mKO3- λ_{N22} (a) and λ_{N22} -mKO3 (b). The measurements were taken without RNA and with 1 and 2 fold molar ratio of RNA compared to the molar ratio of proteins in the cuvette. The excitation was at 465 nm and the emission spectra was taken from 480 nm – 650 nm. The black curves indicate the emission spectra of the λ_{N22} tagged donor proteins, the red curves indicate the emission spectra with λ_{N22} inserted acceptors, the blue curves for emission in the presence of equimolar concentration of 5boxB RNA and the green curves for the emission with two fold concentration of 5boxB RNA.

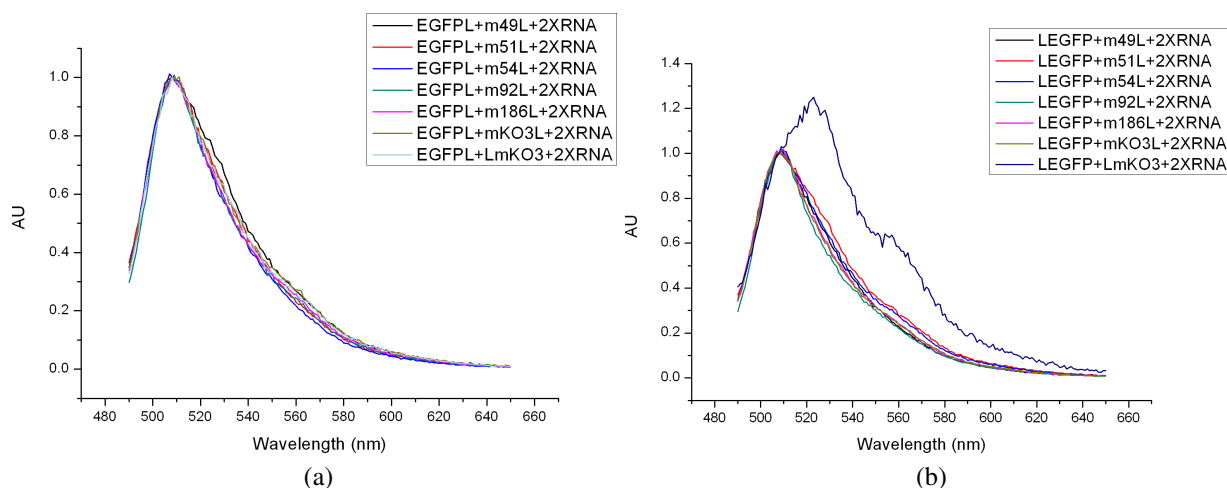


Figure A.8: Normalized fluorescence emission spectra for FRET of EGFP- λ_{N22} (a) and λ_{N22} -EGFP (b) with the various mKO2 and mKO3 variants. The spectra were normalized at 508 nm.

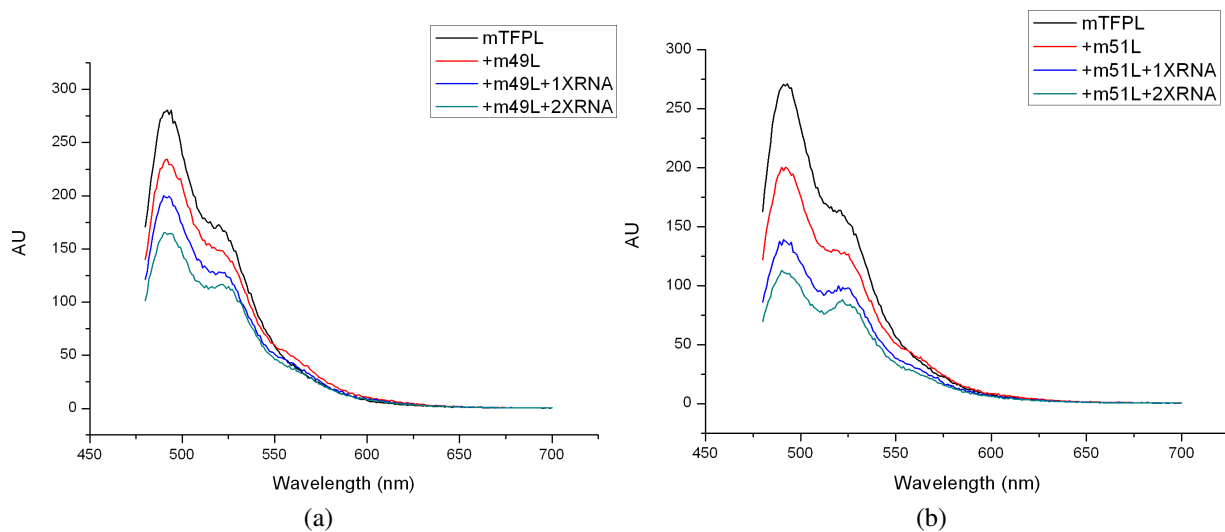


Figure A.9: Fluorescence emission spectra for FRET between mTFP1- λ_{N22} and mKO2- λ_{N22} # 49 (a) and # 51 (b). The measurements were taken without RNA and with 1 and 2 fold molar ratio of RNA compared to the molar ratio of proteins in the cuvette. The excitation was at 458 nm and the emission spectra was taken from 470 nm – 650 nm. The black curves indicate the emission spectra of the λ_{N22} tagged donor proteins, the red curves indicate the emission spectra with λ_{N22} inserted acceptors, the blue curves for emission in the presence of equimolar concentration of 5boxB RNA and the green curves for the emission with two fold concentration of 5boxB RNA.

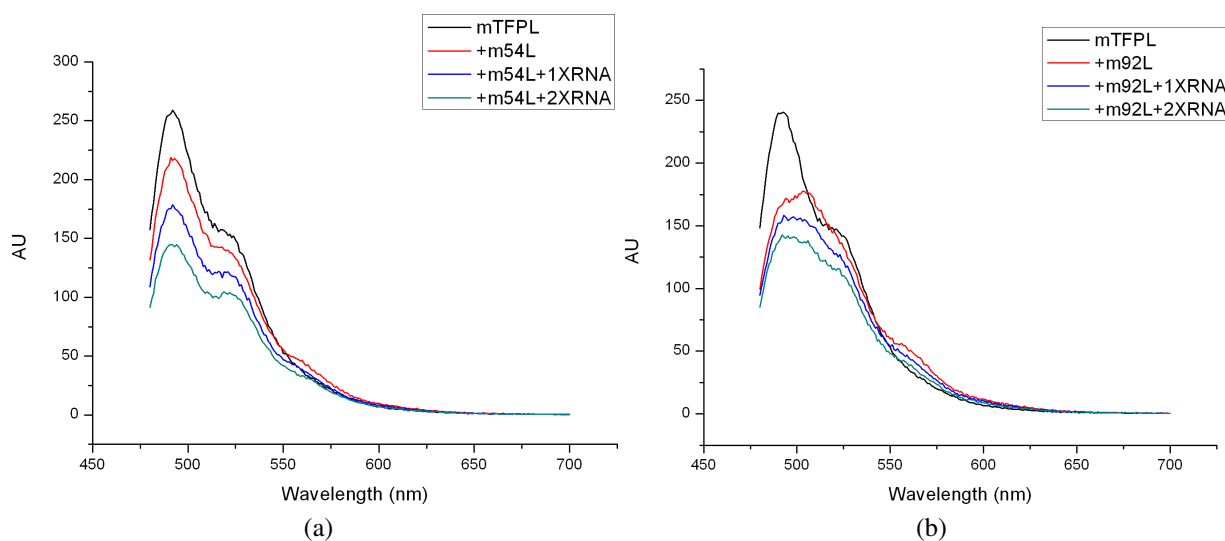


Figure A.10: Fluorescence emission spectra for FRET between mTFP1- λ_{N22} and mKO2- λ_{N22} # 54 (a) and # 92 (b). The measurements were taken without RNA and with 1 and 2 fold molar ratio of RNA compared to the molar ratio of proteins in the cuvette. The excitation was at 458 nm and the emission spectra was taken from 470 nm – 650 nm. The black curves indicate the emission spectra of the λ_{N22} tagged donor proteins, the red curves indicate the emission spectra with λ_{N22} inserted acceptors, the blue curves for emission in the presence of equimolar concentration of 5boxB RNA and the green curves for the emission with two fold concentration of 5boxB RNA.

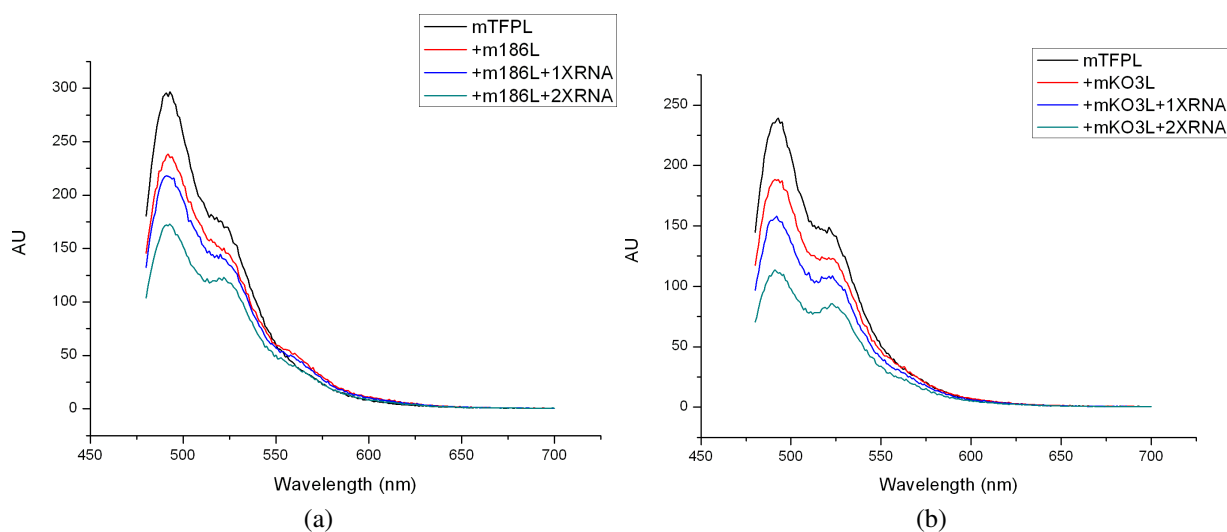


Figure A.11: Fluorescence emission spectra for FRET between mTFP1- λ_{N22} and mKO2- λ_{N22} # 186 (a) and mKO3- λ_{N22} (b). The measurements were taken without RNA and with 1 and 2 fold molar ratio of RNA compared to the molar ratio of proteins in the cuvette. The excitation was at 458 nm and the emission spectra was taken from 470 nm – 650 nm. The black curves indicate the emission spectra of the λ_{N22} tagged donor proteins, the red curves indicate the emission spectra with λ_{N22} inserted acceptors, the blue curves for emission in the presence of equimolar concentration of 5boxB RNA and the green curves for the emission with two fold concentration of 5boxB RNA.

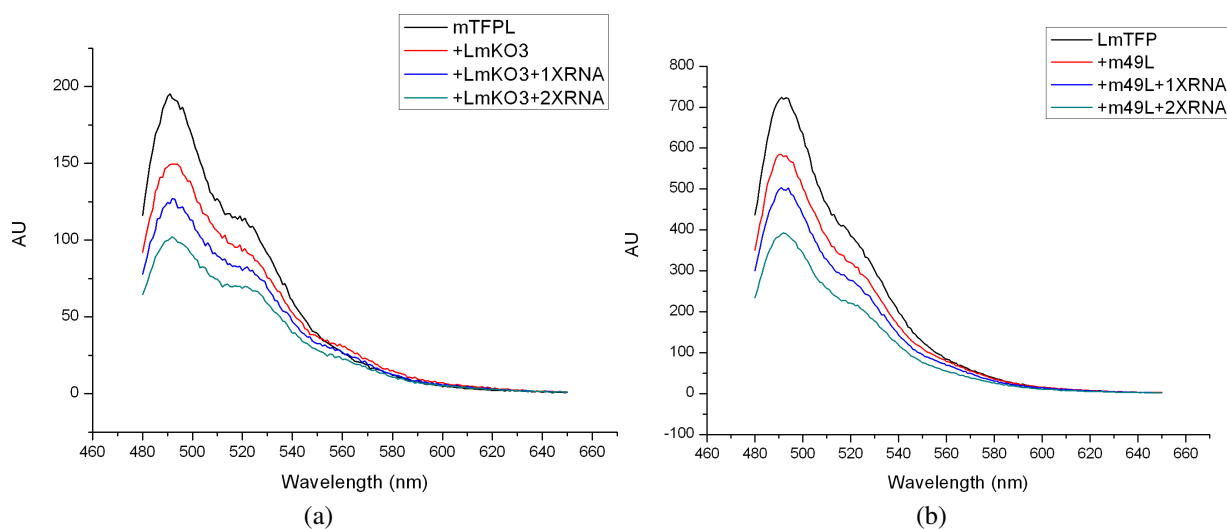


Figure A.12: Fluorescence emission spectra for FRET between mTFP1- λ_{N22} and λ_{N22} -mKO3 (a) and between λ_{N22} -mTFP1 and mKO2- λ_{N22} # 49 (b). The measurements were taken without RNA and with 1 and 2 fold molar ratio of RNA compared to the molar ratio of proteins in the cuvette. The excitation was at 458 nm and the emission spectra was taken from 470 nm – 650 nm. The black curves indicate the emission spectra of the λ_{N22} tagged donor proteins, the red curves indicate the emission spectra with λ_{N22} inserted acceptors, the blue curves for emission in the presence of equimolar concentration of 5boxB RNA and the green curves for the emission with two fold concentration of 5boxB RNA.

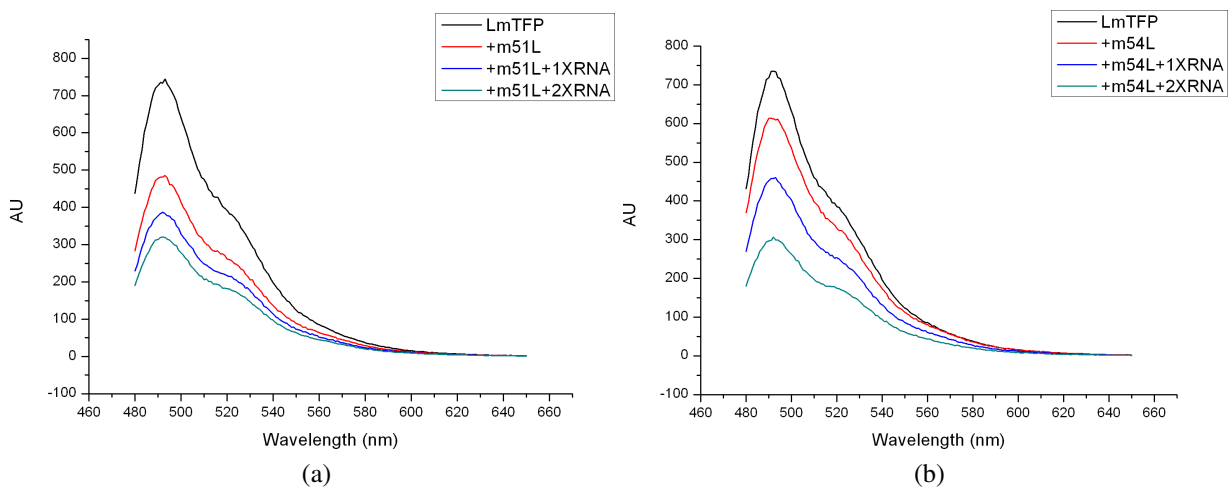


Figure A.13: Fluorescence emission spectra for FRET between λ_{N22} -mTFP1 and mKO2- λ_{N22} # 51 (a) and mKO2- λ_{N22} # 54 (b). The measurements were taken without RNA and with 1 and 2 fold molar ratio of RNA compared to the molar ratio of proteins in the cuvette. The excitation was at 458 nm and the emission spectra was taken from 470 nm – 650 nm. The black curves indicate the emission spectra of the λ_{N22} tagged donor proteins, the red curves indicate the emission spectra with λ_{N22} inserted acceptors, the blue curves for emission in the presence of equimolar concentration of 5boxB RNA and the green curves for the emission with two fold concentration of 5boxB RNA.

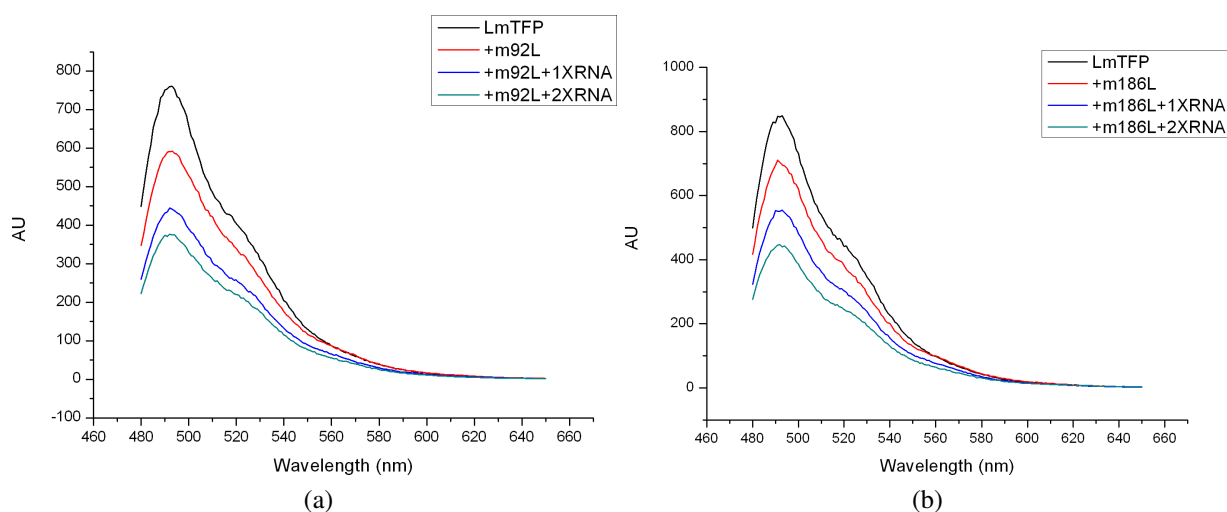


Figure A.14: Fluorescence emission spectra for FRET between λ_{N22} -mTFP1 and mKO2- λ_{N22} # 92 (a) and mKO2- λ_{N22} # 186 (b). The measurements were taken without RNA and with 1 and 2 fold molar ratio of RNA compared to the molar ratio of proteins in the cuvette. The excitation was at 458 nm and the emission spectra was taken from 470 nm – 650 nm. The black curves indicate the emission spectra of the λ_{N22} tagged donor proteins, the red curves indicate the emission spectra with λ_{N22} inserted acceptors, the blue curves for emission in the presence of equimolar concentration of 5boxB RNA and the green curves for the emission with two fold concentration of 5boxB RNA.

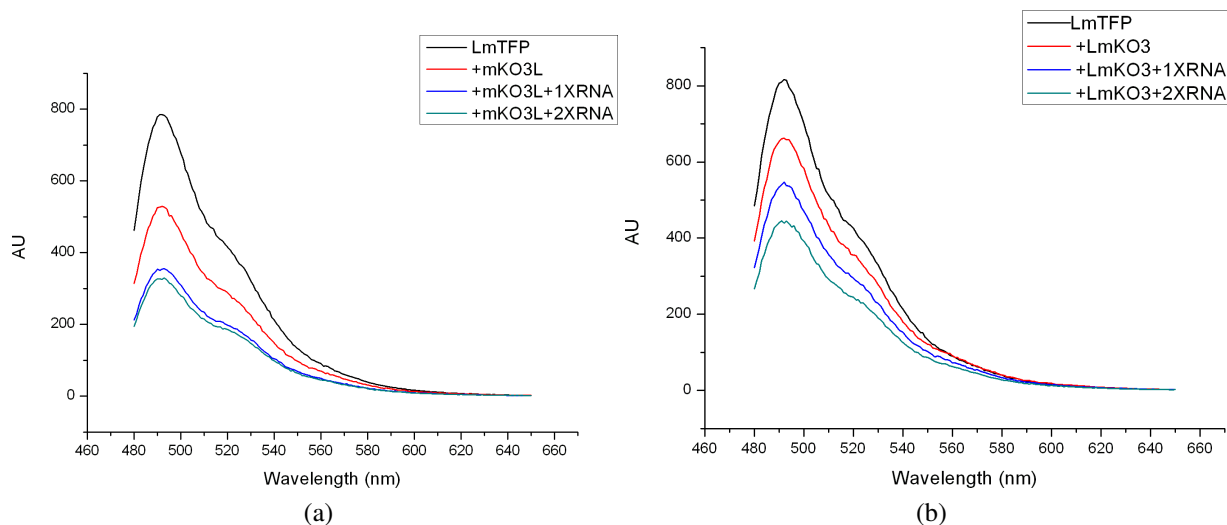


Figure A.15: Fluorescence emission spectra for FRET between λ_{N22} -mTFP1 and mKO3- λ_{N22} (a) and λ_{N22} -mKO3 (b). The measurements were taken without RNA and with 1 and 2 fold molar ratio of RNA compared to the molar ratio of proteins in the cuvette. The excitation was at 458 nm and the emission spectra was taken from 470 nm – 650 nm. The black curves indicate the emission spectra of the λ_{N22} tagged donor proteins, the red curves indicate the emission spectra with λ_{N22} inserted acceptors, the blue curves for emission in the presence of equimolar concentration of 5boxB RNA and the green curves for the emission with two fold concentration of 5boxB RNA.

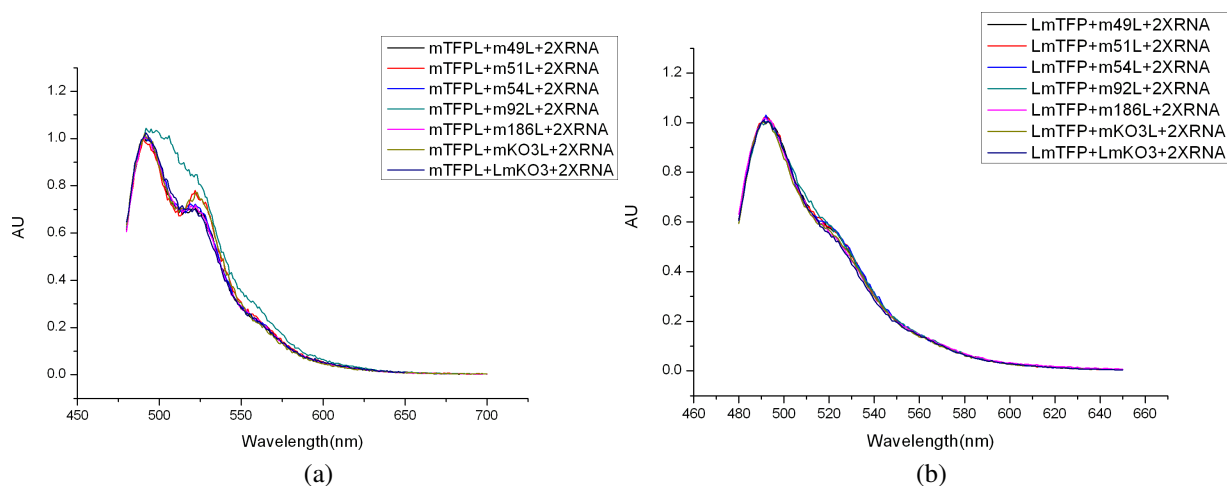


Figure A.16: Normalized fluorescence emission spectra for FRET of mTFP1- λ_{N22} (a) and λ_{N22} -mTFP1 (b) with the various mKO2 and mKO3 variants. The spectra were normalized at 490 nm.

A.2 Discussion graphs

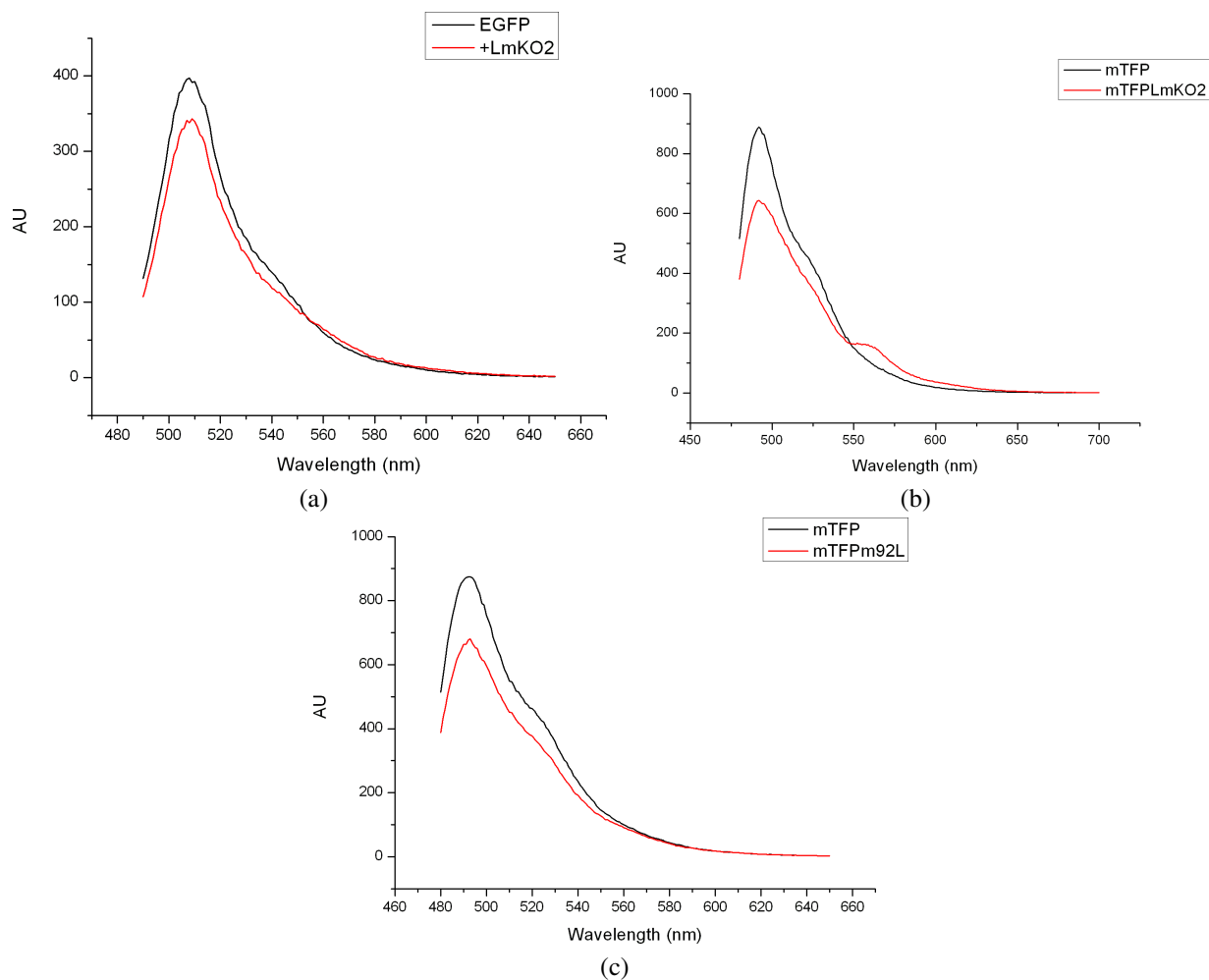


Figure A.17: Emission spectra measured for donor and acceptor pairs where either both or one of the FRET partners is not λ_{N22} tagged, in absence of RNA. Excitation was at 465 nm , where EGFP is the donor, and the emission spectra was taken from $480\text{ nm} - 650\text{ nm}$. Excitation was at 458 nm , where mTFP1 is the donor, and the emission spectra was taken from $470\text{ nm} - 650\text{ nm}$. The black curves indicate the emission spectra for the donor protein (with or without λ_{N22}) and the red curves indicate the emission spectra in the presence of the acceptor protein (with or without λ_{N22}).

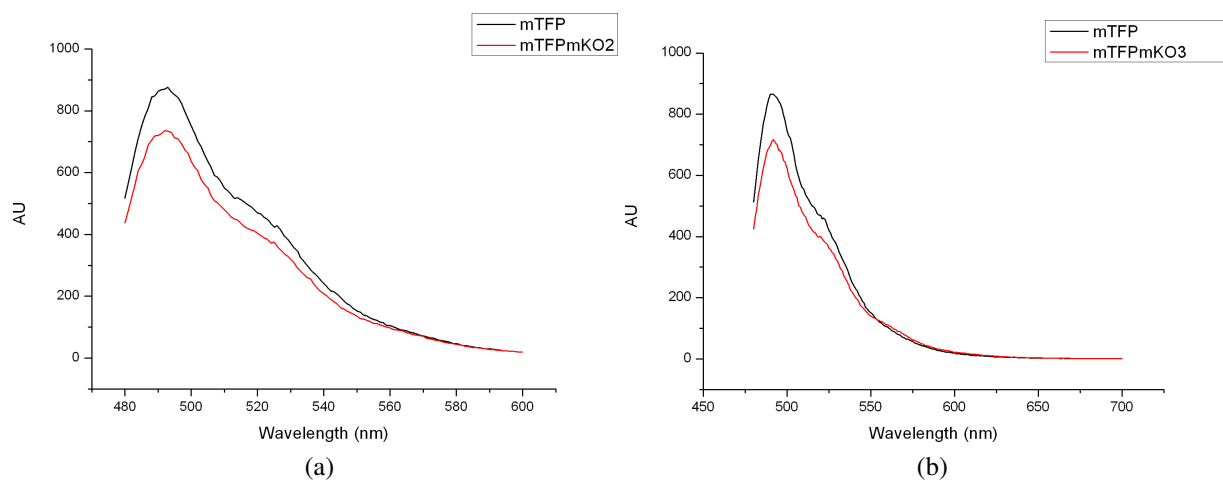


Figure A.18: Emission spectra measured for donor and acceptor pairs where either both or one of the FRET partners is not λ_{N22} tagged, in absence of RNA. Excitation was at 465 nm , where EGFP is the donor, and the emission spectra was taken from $480\text{ nm} - 650\text{ nm}$. Excitation was at 458 nm , where mTFP1 is the donor, and the emission spectra was taken from $470\text{ nm} - 650\text{ nm}$. The black curves indicate the emission spectra for the donor protein (with or without λ_{N22}) and the red curves indicate the emission spectra in the presence of the acceptor protein (with or without λ_{N22}).

Appendix B

Various tolerant insertion sites in mKO2

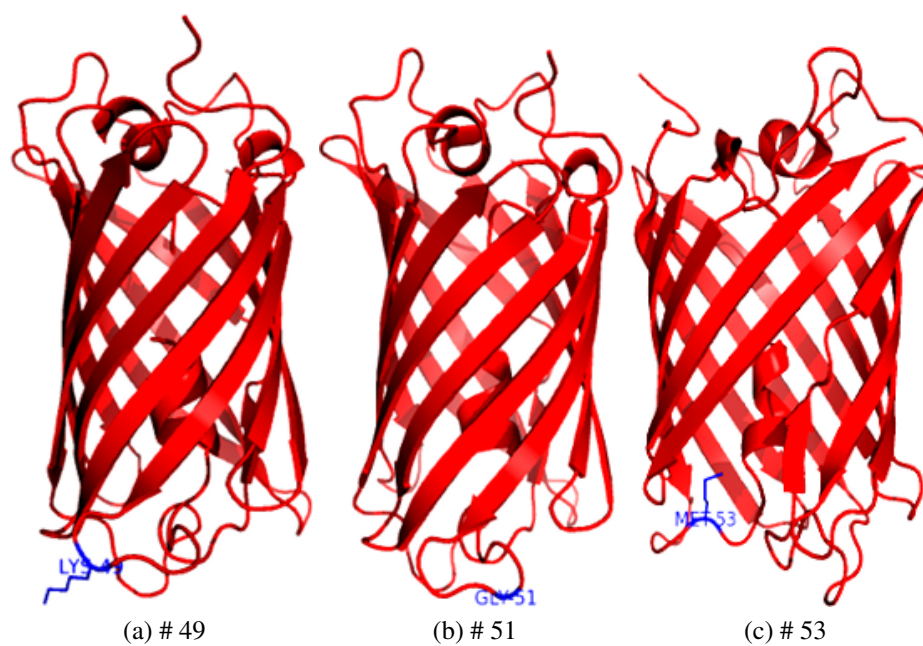


Figure B.1: Various tolerant insertion sites of mKO2 used in this thesis for λ_{N22} insertion.

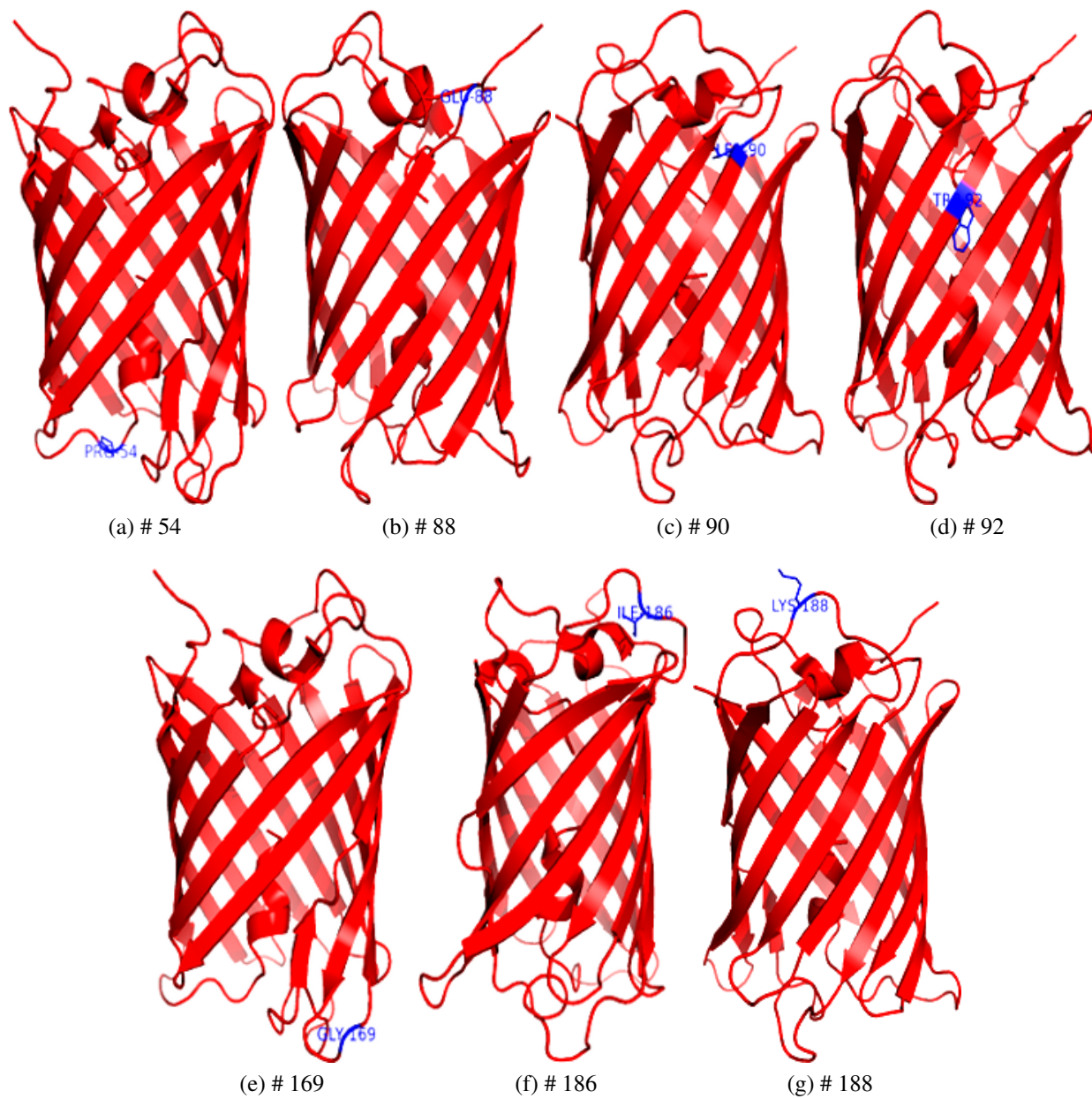


Figure B.2: Various tolerant insertion sites of mKO2 used in this thesis for λ_{N22} insertion (continuation).

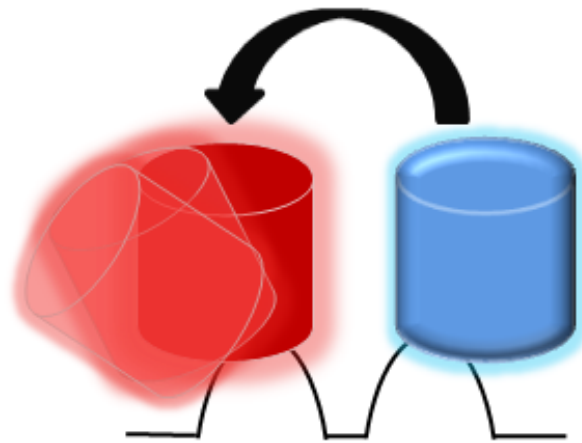


Figure B.3: Different docking orientation of mKO2- λ_{N22} variants on boxB loop. In black is depicted the boxB loop structure, blue is the λ_{N22} tagged donor protein, differentially oriented mKO2 fluorescent proteins are depicted in red.

List of Figures

1.1	thiM riboswitch structure model in the absence (left) and presence (right) of TPP. Nucleotides that form stem structures or loops in the TPP-bound state are color-coded. The nucleotides representing the SD region are depicted in green and the anti-SD region is colored in light orange [16].	14
1.2	Examples of asymmetrically localized mRNA, (A) <i>Drosophila</i> oocytes, (B) Egg of a <i>cindarian</i> , <i>Clytia</i> , (C) <i>Aplysia</i> sensory neuron, (D) <i>Drosophila</i> embryo, (E) Cultured mammalian fibroblasts, (F) <i>Xenopus</i> axonal growth cone. <i>Christine E.Holt et al. Science, Vol.326 #1212, 2009</i>	16
1.3	Schematic representation of different fluorogenic probes for detection of mRNAs. Donor (green), quencher (gray) and acceptor (yellow) dyes are attached to the probes and interact as indicated. <i>Sanjay Tyagi, Nature Methods, Vol.6 #5, May 2009</i>	20
1.4	Malachite green binds to mRNA and makes it fluorescent. (a) Chemical Structure of Malachite Green, it is non fluorescent because of the phenyl rings that rotate like a propeller and dissipate the energy that the dye absorbs from light. (b) Schematic representation of an mRNA with aptamer motifs bound to Malachite green in the UTR. <i>Sanjay Tyagi, Nature Methods, Vol.6 #5, May 2009</i>	21

- 1.5 mRNA imaging with GFP tagged RBPs. (a) Schematic representation of MS2 phage coat protein-GFP based tagging. A number of MS2 coat proteins bind to cognate RNA sequence which is introduced in the 3'UTR of the target mRNA. Since each MS2 coat protein carries a GFP tag, it makes the mRNA more fluorescent than the surrounding. (b) Fluorescence image of a fibroblast expressing MS2 coat protein-GFP and an mRNA containing a RAB13 UTR, and 24 copies of MS2 phage hairpin. *Sanjay Tyagi, Nature Methods, Vol.6 #5, May 2009* 22
- 1.6 Alignment of arginine-rich N sequences in phages λ (Franklin 1985b; Chattopadhyay *et al.* 1995b (a) Consensus boxB hairpin in phage λ showing specific pattern of base-pairing and base-flipping (purines 7 and 9) (b). Three sites of peptide-base contact (Su *et al.* 1997) are as indicated. The open box indicates a sheared GA base pair; the black box highlights the position of contact with Ala-3 in the major groove. The RNase footprint of the N protein (Chattopadhyay *et al.* 1995a) is shown at left; the proposed allosteric surface involved in binding to the core antitermination complex is shown at right. (R) The proposed interaction of the flipped base (R9) with NusA in an antitermination complex is indicated. *Su L et al. Genes Dev. 1997; 11:2214-2226* 24
- 1.7 (A) The N protein binds to an RNA enhancer element in the nascent message (nut site; asterisk indicates boxB RNA hairpin) and to host factors and RNAP to direct formation of a processive antitermination complex. (B) Closing base pair (U5 and A11) and purine-rich pentaloop (bases 6–10; underlined) of 15-basenutL boxB(5'-GCCUGAAGAAGGGC-3'), with numbering scheme as shown. Red-outlined box (Trp-18) and nucleoside position (7) indicate site of indole–adenine stacking; blue nucleosides (7–10) exhibit a specific pattern of base-pairing (A10), -stacking (asterisk), and flipping (G9). Black rectangles indicate stacking between closing base pair (UA) and GA sheared base pair. Bidirectional arrows indicate NOEs between purines; base 9 is “flipped out.” Peptide–RNA contacts (such as A7–Trp-18) were identified by isotope-filtered NMR experiments designed to resolve NOEs between ¹³C- or ¹⁵N-attached protons in a labeled peptide and ¹²C- or ¹⁴N-attached protons in the unlabeled RNA . *Su L et al. Genes Dev. 1997; 11:2214-2226* 25

1.8	Structural model of λ_{N22} - λ boxB. The second base in λ boxB (in Grey) loop stacks with Trp18 of λ_{N22} (in red) in the cognate complexes. <i>Ryan J. Austin, et al. JACS, 124, 10966-10967, 2002</i>	26
1.9	Schematic representation of the GFP-based tagging with λ_{N22} . (a) Expression plasmids encoding RNA fused to 4XboxB (left), and the RNA reporter protein, a fusion of 4X λ_{N22} , 3XmEGFP and M9 nuclear localization sequence (NLS). Arrow shows binding of λ_{N22} peptide to the RNA hairpin. (b,c) Test plasmid, RNA product and cartoon representation of expected sub-cellular localization of mRNA and encoded protein for an mRNA exported from the nucleus and localized to the cell leading edge (b) and targeted to the ER (c). Expression driven by pCMV promoter. <i>Daigel & Ellenberg, Nature Methods, Vol.4, No.8, 2007</i>	27
1.10	Typical applications of FÖRSTER resonance energy transfer (FRET) with fused fluorescent proteins. <i>D</i> and <i>A</i> refer to the donor and acceptor, respectively <i>Kees Jalink, Netherlands Cancer Institute (NKI-AVL)</i>	31
1.11	Spectral overlap of donor emission and acceptor absorption: emitted photons from the donor are within the wavelength range of the acceptor. Nevertheless, the energy from donor to acceptor is transferred radiationless. <i>Author: Maurel Damien</i>	32
1.12	Green Fluorescent Protein drawn in cartoon style with fluorophore highlighted as ball-and-stick	35
1.13	A San Diego beach scene drawn with an eight color palette of bacterial colonies expressing fluorescent proteins derived from GFP and the red-fluorescent coral protein dsRed. The colors include BFP, mTFP1, Emerald, Citrine, mOrange, mApple, mCherry and mGrape. <i>Artwork by Nathan Shaner, photography by Paul Steinbach, created in the lab of Roger Tsien in 2006</i>	36
1.14	Excitation and emission spectra of mTFP and mKO2 <i>Yuansheng Sun and Cynthia F. Booker and Sangeeta Kumari and Richard N. Day and Mike Davidson and Ammasi Periasamy, Characterization of an orange acceptor fluorescent protein for sensitized spectral fluorescence resonance energy transfer microscopy using a white-light laser, Journal of Biomedical Optics (2009), S. 054009</i>	38

2.1	NotI Digestion and Religation of the EZ-Tn5<NotI/KAN-3> Transposon <i>EZ-Tn5TM In-Frame Linker Insertion Kit, EPICENTRE</i>	45
3.1	pRSETB Vector map	66
3.2	Amino acid positions in mKO2 where the NotI site is inserted via EZ-Tn5 transposon element is inserted	66
3.3	Schematic representation of λ_{N22} insertion in mKO2 containing transposon intro- duced NotI site	67
3.4	Schematic representation of mKO3 tagged at (a) N-terminus and (b) C-terminus with λ_{N22} 67	67
3.5	SDS PAGE run for purified λ_{N22} variants	68
3.6	Absorption spectra of the mKO2- λ_{N22} variants in comparison to mKO2 (WT)	69
3.7	Fluorescence emission spectra of various mKO2- λ_{N22} (a) and mKO3- λ_{N22} (b) vari- ants in comparison to mKO2 (WT)	70
3.8	Schematic representation of mTFP1 tagged at (a) N-terminus and (b) C-terminus with λ_{N22}	72
3.9	Schematic representation of EGFP tagged at (a) C-terminus and (b) N-terminus with λ_{N22}	73
3.10	SDS PAGE for purified proteins	73
3.11	Schematic representation of pcDNA3-5boxB construct for <i>in vitro</i> RNA transcription	74
3.12	Gel picture showing the 5boxB template DNA used for <i>in vitro</i> transcription, the transcribed RNA and the cDNA synthesized from the transcribed RNA	75
3.13	Schematic representation of 5boxB-thiM-MS2phage binding site construct inserted in pcDNA3	79
3.14	Schematic representation of RNA binding peptides tagged with fluorescent proteins. (a): λ_{N22} tagged with EGFP; (b): MS2-phage coat protein tagged with YFP.	80
3.15	Results of the semi-quantitative PCR to check 5boxB-thiM-MS2BS expression in HeLa cell culture.	81
3.16	Confocal Images of HeLa cells co-transfected with 5boxB-thiM-MS2bs RNA and λ_{N22} -EGFP (a) or MS2 coat protein-YFP (b)	82
4.1	Various insertion sites tolerating in mKO2. See B for detailed figures of each construct.	86

4.2	Fluorescence emission spectra of EGFP- λ_{N22} (a) and λ_{N22} -EGFP (b) with and without RNA. Excitation was at 465 nm and the emission spectra recorded from 480-650nm. Fluorescence emission spectra of mTFP1- λ_{N22} (c) and λ_{N22} -mTFP1 (d) with and without RNA. The excitation was at 460 nm and the emission spectra was taken from 470-650 nm. The black curve indicate the emission spectra of only the λ_{N22} tagged donor protein. Emission spectra of the donor on addition of equimolar concentration of 5boxB RNA is indicated by red curves, while the blue curves indicate the emission spectra for the second reading taken after 2 minutes.	91
4.3	Graphs showing the absorption spectra of EGFP- λ_{N22} and λ_{N22} -EGFP with (a) and without RNA (b) and absorption spectra of λ_{N22} -mTFP1 and mTFP1- λ_{N22} with (c) and without RNA (d). The black curves indicate the absorption spectra of λ_{N22} tagged EGFP/mTFP1 and the red curves indicate the absorption spectra in the presence of equimolar concentration of 5boxB RNA.	92
A.1	Fluorescence emission spectra for FRET between EGFP- λ_{N22} and mKO2- λ_{N22} #49 (a) and #51 (b). The measurements were taken without RNA and with 1 and 2 fold molar ratio of RNA compared to the molar ratio of proteins in the cuvette. The excitation was at 465 nm and the emission spectra was taken from 480 nm – 650 nm. The black curves indicate the emission spectra of the λ_{N22} tagged donor proteins, the red curves indicate the emission spectra with λ_{N22} inserted acceptors, the blue curves for emission in the presence of equimolar concentration of 5boxB RNA and the green curves for the emission with two fold concentration of 5boxB RNA.	93
A.2	Fluorescence emission spectra for FRET between EGFP- λ_{N22} and mKO2- λ_{N22} # 54 (a) and 92 (b). The measurements were taken without RNA and with 1 and 2 fold molar ratio of RNA compared to the molar ratio of proteins in the cuvette. The excitation was at 465 nm and the emission spectra was taken from 480 nm – 650 nm. The black curves indicate the emission spectra of the λ_{N22} tagged donor proteins, the red curves indicate the emission spectra with λ_{N22} inserted acceptors, the blue curves for emission in the presence of equimolar concentration of 5boxB RNA and the green curves for the emission with two fold concentration of 5boxB RNA.	94

A.3 Fluorescence emission spectra for FRET between EGFP- λ_{N22} and mKO2- λ_{N22} # 186 (a) and mKO3- λ_{N22} (b). The measurements were taken without RNA and with 1 and 2 fold molar ratio of RNA compared to the molar ratio of proteins in the cuvette. The excitation was at 465 nm and the emission spectra was taken from 480 nm – 650 nm. The black curves indicate the emission spectra of the λ_{N22} tagged donor proteins, the red curves indicate the emission spectra with λ_{N22} inserted acceptors, the blue curves for emission in the presence of equimolar concentration of 5boxB RNA and the green curves for the emission with two fold concentration of 5boxB RNA. 95

A.4 Fluorescence emission spectra for FRET between EGFP- λ_{N22} and λ_{N22} -mKO3 (a) and between λ_{N22} -EGFP and mKO2- λ_{N22} # 49 (b). The measurements were taken without RNA and with 1 and 2 fold molar ratio of RNA compared to the molar ratio of proteins in the cuvette. The excitation was at 465 nm and the emission spectra was taken from 480 nm – 650 nm. The black curves indicate the emission spectra of the λ_{N22} tagged donor proteins, the red curves indicate the emission spectra with λ_{N22} inserted acceptors, the blue curves for emission in the presence of equimolar concentration of 5boxB RNA and the green curves for the emission with two fold concentration of 5boxB RNA. 96

A.5 Fluorescence emission spectra for FRET between λ_{N22} -EGFP and mKO2- λ_{N22} #51 (a) and #54 (b). The measurements were taken without RNA and with 1 and 2 fold molar ratio of RNA compared to the molar ratio of proteins in the cuvette. The excitation was at 465 nm and the emission spectra was taken from 480 nm – 650 nm. The black curves indicate the emission spectra of the λ_{N22} tagged donor proteins, the red curves indicate the emission spectra with λ_{N22} inserted acceptors, the blue curves for emission in the presence of equimolar concentration of 5boxB RNA and the green curves for the emission with two fold concentration of 5boxB RNA. 97

- A.6 Fluorescence emission spectra for FRET between λ_{N22} -EGFP and mKO2- λ_{N22} # 92 (a) and # 186 (b). The measurements were taken without RNA and with 1 and 2 fold molar ratio of RNA compared to the molar ratio of proteins in the cuvette. The excitation was at 465 nm and the emission spectra was taken from 480 nm – 650 nm. The black curves indicate the emission spectra of the λ_{N22} tagged donor proteins, the red curves indicate the emission spectra with λ_{N22} inserted acceptors, the blue curves for emission in the presence of equimolar concentration of 5boxB RNA and the green curves for the emission with two fold concentration of 5boxB RNA. 98
- A.7 Fluorescence emission spectra for FRET between λ_{N22} -EGFP and mKO3- λ_{N22} (a) and λ_{N22} -mKO3 (b). The measurements were taken without RNA and with 1 and 2 fold molar ratio of RNA compared to the molar ratio of proteins in the cuvette. The excitation was at 465 nm and the emission spectra was taken from 480 nm – 650 nm. The black curves indicate the emission spectra of the λ_{N22} tagged donor proteins, the red curves indicate the emission spectra with λ_{N22} inserted acceptors, the blue curves for emission in the presence of equimolar concentration of 5boxB RNA and the green curves for the emission with two fold concentration of 5boxB RNA. 99
- A.8 Normalized fluorescence emission spectra for FRET of EGFP- λ_{N22} (a) and λ_{N22} -EGFP (b) with the various mKO2 and mKO3 variants. The spectra were normalized at 508 nm. 99
- A.9 Fluorescence emission spectra for FRET between mTFP1- λ_{N22} and mKO2- λ_{N22} # 49 (a) and # 51 (b). The measurements were taken without RNA and with 1 and 2 fold molar ratio of RNA compared to the molar ratio of proteins in the cuvette. The excitation was at 458 nm and the emission spectra was taken from 470 nm – 650 nm. The black curves indicate the emission spectra of the λ_{N22} tagged donor proteins, the red curves indicate the emission spectra with λ_{N22} inserted acceptors, the blue curves for emission in the presence of equimolar concentration of 5boxB RNA and the green curves for the emission with two fold concentration of 5boxB RNA. 100

A.10 Fluorescence emission spectra for FRET between mTFP1- λ_{N22} and mKO2- λ_{N22} # 54 (a) and # 92 (b). The measurements were taken without RNA and with 1 and 2 fold molar ratio of RNA compared to the molar ratio of proteins in the cuvette. The excitation was at 458 nm and the emission spectra was taken from 470 nm – 650 nm. The black curves indicate the emission spectra of the λ_{N22} tagged donor proteins, the red curves indicate the emission spectra with λ_{N22} inserted acceptors, the blue curves for emission in the presence of equimolar concentration of 5boxB RNA and the green curves for the emission with two fold concentration of 5boxB RNA. 101

A.11 Fluorescence emission spectra for FRET between mTFP1- λ_{N22} and mKO2- λ_{N22} # 186 (a) and mKO3- λ_{N22} (b). The measurements were taken without RNA and with 1 and 2 fold molar ratio of RNA compared to the molar ratio of proteins in the cuvette. The excitation was at 458 nm and the emission spectra was taken from 470 nm – 650 nm. The black curves indicate the emission spectra of the λ_{N22} tagged donor proteins, the red curves indicate the emission spectra with λ_{N22} inserted acceptors, the blue curves for emission in the presence of equimolar concentration of 5boxB RNA and the green curves for the emission with two fold concentration of 5boxB RNA. 102

A.12 Fluorescence emission spectra for FRET between mTFP1- λ_{N22} and λ_{N22} -mKO3 (a) and between λ_{N22} -mTFP1 and mKO2- λ_{N22} # 49 (b). The measurements were taken without RNA and with 1 and 2 fold molar ratio of RNA compared to the molar ratio of proteins in the cuvette. The excitation was at 458 nm and the emission spectra was taken from 470 nm – 650 nm. The black curves indicate the emission spectra of the λ_{N22} tagged donor proteins, the red curves indicate the emission spectra with λ_{N22} inserted acceptors, the blue curves for emission in the presence of equimolar concentration of 5boxB RNA and the green curves for the emission with two fold concentration of 5boxB RNA. 103

- A.13 Fluorescence emission spectra for FRET between λ_{N22} -mTFP1 and mKO2- λ_{N22} # 51 (a) and mKO2- λ_{N22} # 54 (b). The measurements were taken without RNA and with 1 and 2 fold molar ratio of RNA compared to the molar ratio of proteins in the cuvette. The excitation was at 458 nm and the emission spectra was taken from 470 nm – 650 nm. The black curves indicate the emission spectra of the λ_{N22} tagged donor proteins, the red curves indicate the emission spectra with λ_{N22} inserted acceptors, the blue curves for emission in the presence of equimolar concentration of 5boxB RNA and the green curves for the emission with two fold concentration of 5boxB RNA. 104
- A.14 Fluorescence emission spectra for FRET between λ_{N22} -mTFP1 and mKO2- λ_{N22} # 92 (a) and mKO2- λ_{N22} # 186 (b). The measurements were taken without RNA and with 1 and 2 fold molar ratio of RNA compared to the molar ratio of proteins in the cuvette. The excitation was at 458 nm and the emission spectra was taken from 470 nm – 650 nm. The black curves indicate the emission spectra of the λ_{N22} tagged donor proteins, the red curves indicate the emission spectra with λ_{N22} inserted acceptors, the blue curves for emission in the presence of equimolar concentration of 5boxB RNA and the green curves for the emission with two fold concentration of 5boxB RNA. 105
- A.15 Fluorescence emission spectra for FRET between λ_{N22} -mTFP1 and mKO3- λ_{N22} (a) and λ_{N22} -mKO3 (b). The measurements were taken without RNA and with 1 and 2 fold molar ratio of RNA compared to the molar ratio of proteins in the cuvette. The excitation was at 458 nm and the emission spectra was taken from 470 nm – 650 nm. The black curves indicate the emission spectra of the λ_{N22} tagged donor proteins, the red curves indicate the emission spectra with λ_{N22} inserted acceptors, the blue curves for emission in the presence of equimolar concentration of 5boxB RNA and the green curves for the emission with two fold concentration of 5boxB RNA. 106
- A.16 Normalized fluorescence emission spectra for FRET of mTFP1- λ_{N22} (a) and λ_{N22} -mTFP1 (b) with the various mKO2 and mKO3 variants. The spectra were normalized at 490 nm. 106

A.17	Emission spectra measured for donor and acceptor pairs where either both or one of the FRET partners is not λ_{N22} tagged, in absence of RNA. Excitation was at 465 nm, where EGFP is the donor, and the emission spectra was taken from 480 nm – 650 nm. Excitation was at 458 nm, where mTFP1 is the donor, and the emission spectra was taken from 470 nm – 650 nm. The black curves indicate the emission spectra for the donor protein (with or without λ_{N22}) and the red curves indicate the emission spectra in the presence of the acceptor protein (with or without λ_{N22}).	108
A.18	Emission spectra measured for donor and acceptor pairs where either both or one of the FRET partners is not λ_{N22} tagged, in absence of RNA. Excitation was at 465 nm, where EGFP is the donor, and the emission spectra was taken from 480 nm – 650 nm. Excitation was at 458 nm, where mTFP1 is the donor, and the emission spectra was taken from 470 nm – 650 nm. The black curves indicate the emission spectra for the donor protein (with or without λ_{N22}) and the red curves indicate the emission spectra in the presence of the acceptor protein (with or without λ_{N22}).	109
B.1	Various tolerant insertion sites of mKO2 used in this thesis for λ_{N22} insertion.	111
B.2	Various tolerant insertion sites of mKO2 used in this thesis for λ_{N22} insertion (continuation).	112
B.3	Different docking orientation of mKO2- λ_{N22} variants on boxB loop. In black is depicted the boxB loop structure, blue is the λ_{N22} tagged donor protein, differentially oriented mKO2 fluorescent proteins are depicted in red.	113

Bibliography

- [1] Raj, A. and vanOudenaarden, A. (2008) *Cell* **135(2)**, 216 – 226.
- [2] Frith, M. C., Pheasant, M., and Mattick, J. S. (2005) *Eur J Hum Genet* **13(8)**, 894–7.
- [3] Riddihough, G. (2005) *Science* **309(5740)**, 1507–.
- [4] Lee, R. C., Feinbaum, R. L., and Ambros, V. (1993) *Cell* **75(5)**, 843 – 854.
- [5] Lim, L. P., Lau, N. C., Garrett-Engle, P., Grimson, A., Schelter, J. M., Castle, J., Bartel, D. P., Linsley, P. S., and Johnson, J. M. (2005) *Nature* **433(7027)**, 769–73.
- [6] Valadkhan, S. (2005) *Current Opinion in Chemical Biology* **9(6)**, 603 – 608 Biopolymers / Model systems.
- [7] Malone, C. D. and Hannon, G. J. (2009) *Cell* **136(4)**, 656 – 668.
- [8] Albert, Hopkin, J. Essential Cell Biology, Third edition, , .
- [9] Collins, L. J. and Penny, D. (2009) *Trends in Genetics* **25(3)**, 120 – 128.
- [10] Jurica, M. S. and Moore, M. J. (2003) *Mol Cell* **12(1)**, 5–14.
- [11] Waters, L. S. and Storz, G. (2009) *Cell* **136(4)**, 615–28.
- [12] Croft, M. T., Moulin, M., Webb, M. E., and Smith, A. G. (2007) *Proc Natl Acad Sci U S A* **104(52)**, 20770–5.
- [13] Sudarsan, N., Barrick, J. E., and Breaker, R. R. (2003) *RNA* **9(6)**, 644–7.
- [14] Edwards, T. E. and Ferre-D’Amare, A. R. (2006) *Structure* **14(9)**, 1459–68.

- [15] Miranda-Rios, J. (2007) *Structure* **15(3)**, 259–65.
- [16] Rentmeister, A., Mayer, G., Kuhn, N., and Famulok, M. (2007) *Nucleic Acids Res* **35(11)**, 3713–22.
- [17] Lange, S., Katayama, Y., Schmid, M., Burkacky, O., Brauchle, C., Lamb, D. C., and Jansen, R. P. (2008) *Traffic* **9(8)**, 1256–67.
- [18] Lecuyer, E., Yoshida, H., Parthasarathy, N., Alm, C., Babak, T., Cerovina, T., Hughes, T. R., Tomancak, P., and Krause, H. M. (2007) *Cell* **131(1)**, 174–87.
- [19] Jeffery, W. R., Tomlinson, C. R., and Brodeur, R. D. (1983) *Dev Biol* **99(2)**, 408–17.
- [20] Holt, C. E. and Bullock, S. L. (2009) *Science* **326(5957)**, 1212–6.
- [21] Zarnack, K. and Feldbrugge, M. (2007) *Mol Genet Genomics* **278(4)**, 347–59.
- [22] Bertrand, E., Chartrand, P., Schaefer, M., Shenoy, S. M., Singer, R. H., and Long, R. M. (1998) *Mol Cell* **2(4)**, 437–45.
- [23] Zipor, G., Haim-Vilmovsky, L., Gelin-Licht, R., Gadir, N., Brocard, C., and Gerst, J. E. (2009) *Proc Natl Acad Sci U S A* **106(47)**, 19848–53.
- [24] Okita, T. W. and Choi, S. B. (2002) *Curr Opin Plant Biol* **5(6)**, 553–9.
- [25] Leung, K. M., vanHorck, F. P., Lin, A. C., Allison, R., Standart, N., and Holt, C. E. (2006) *Nat Neurosci* **9(10)**, 1247–56.
- [26] Guzowski, J. F., Lyford, G. L., Stevenson, G. D., Houston, F. P., McGaugh, J. L., Worley, P. F., and Barnes, C. A. (2000) *J Neurosci* **20(11)**, 3993–4001.
- [27] Bagni, C. and Greenough, W. T. (2005) *Nat Rev Neurosci* **6(5)**, 376–87.
- [28] Steward, O., Wallace, C. S., Lyford, G. L., and Worley, P. F. (1998) *Neuron* **21(4)**, 741–51.
- [29] Shepherd, J. D., Rumbaugh, G., Wu, J., Chowdhury, S., Plath, N., Kuhl, D., Huganir, R. L., and Worley, P. F. (2006) *Neuron* **52(3)**, 475–84.
- [30] Byrne, M. C., Whitley, M. Z., and Follettie, M. T. (2001) *Curr Protoc Neurosci* **Chapter 4**, Unit 4.26.

- [31] Cooper, T. A., Wan, L., and Dreyfuss, G. (2009) *Cell* **136(4)**, 777–93.
- [32] Guzowski, J. F. and Worley, P. F. (2001) *Curr Protoc Neurosci* **Chapter 1**, Unit 1.8.
- [33] K. A. A. a. N. B. L. Irina V. Novikova (2010) *Biosensors*, , .
- [34] Tyagi, S. (2009) *Nat Methods* **6(5)**, 331–8.
- [35] Keryer-Bibens, C., Barreau, C., and Osborne, H. B. (2008) *Biol Cell* **100(2)**, 125–38.
- [36] Chattopadhyay, S., Garcia-Mena, J., DeVito, J., Wolska, K., and Das, A. (1995) *Proc Natl Acad Sci U S A* **92(9)**, 4061–5.
- [37] Tan, R. and Frankel, A. D. (1995) *Proc Natl Acad Sci U S A* **92(12)**, 5282–6.
- [38] Su, L., Radek, J. T., Labeots, L. A., Hallenga, K., Hermanto, P., Chen, H., Nakagawa, S., Zhao, M., Kates, S., and Weiss, M. A. (1997) *Genes Dev* **11(17)**, 2214–26.
- [39] Austin, R. J., Xia, T., Ren, J., Takahashi, T. T., and Roberts, R. W. (2002) *J Am Chem Soc* **124(37)**, 10966–7.
- [40] Liu, J., Rivas, F. V., Wohlschlegel, J., Yates, 3rd, J. R., Parker, R., and Hannon, G. J. (2005) *Nat Cell Biol* **7(12)**, 1261–6.
- [41] Vasudevan, S. and Steitz, J. A. (2007) *Cell* **128(6)**, 1105–18.
- [42] Daigle, N. and Ellenberg, J. (2007) *Nat Methods* **4(8)**, 633–6.
- [43] Minshall, N., Allison, R., Marnef, A., Wilczynska, A., and Standart, N. (2010) *Methods* **51(1)**, 165–9.
- [44] Chudakov, D. M., Lukyanov, S., and Lukyanov, K. A. (2005) *Trends Biotechnol* **23(12)**, 605–13.
- [45] SHIMOMURA, O., JOHNSON, F. H., and SAIGA, Y. (1962) *J Cell Comp Physiol* **59**, 223–39.
- [46] Prasher, D. C., Eckenrode, V. K., Ward, W. W., Prendergast, F. G., and Cormier, M. J. (1992) *Gene* **111(2)**, 229–33.
- [47] Chalfie, M., Tu, Y., Euskirchen, G., Ward, W. W., and Prasher, D. C. (1994) *Science* **263(5148)**, 802–5.

- [48] Ormo, M., Cubitt, A. B., Kallio, K., Gross, L. A., Tsien, R. Y., and Remington, S. J. (1996) *Science* **273(5280)**, 1392–5.
- [49] Yang, F., Moss, L. G., and Phillips, Jr, G. N. (1996) *Nat Biotechnol* **14(10)**, 1246–51.
- [50] Tsien, R. Y. (1998) *Annu Rev Biochem* **67**, 509–44.
- [51] Ward, W., Prentice, H., Roth, A., Cody, C., and Reeves, S.
- [52] Thastrup O, Tullin S, K. P. L. US patent Technical report (1995).
- [53] Nagai, T., Yamada, S., Tominaga, T., Ichikawa, M., and Miyawaki, A. (2004) *Proc Natl Acad Sci U S A* **101(29)**, 10554–9.
- [54] Sakaue-Sawano, A., Kurokawa, H., Morimura, T., Hanyu, A., Hama, H., Osawa, H., Kashiwagi, S., Fukami, K., Miyata, T., Miyoshi, H., Imamura, T., Ogawa, M., Masai, H., and Miyawaki, A. (2008) *Cell* **132(3)**, 487 – 498.
- [55] Sun, Y., Booker, C. F., Kumari, S., Day, R. N., Davidson, M., and Periasamy, A. (2009) *Journal of Biomedical Optics* **14(5)**, 054009.
- [56] Ai, H. W., Henderson, J. N., Remington, S. J., and Campbell, R. E. (2006) *Biochem J* **400(3)**, 531–40.
- [57] Li, Y., Sierra, A., Ai, H., and Campbell, R.
- [58] Betzig, E., Patterson, G. H., Sougrat, R., Lindwasser, O. W., Olenych, S., Bonifacino, J. S., Davidson, M. W., Lippincott-Schwartz, J., and Hess, H. F. (2006) *Science* **313(5793)**, 1642–5.
- [59] Rust, Michael, J., Bates, Mark, and Zhuang, Xiaowei.
- [60] Triana-Alonso, F. J., Dabrowski, M., Wadzack, J., and Nierhaus, K. H. (1995) *J Biol Chem* **270(11)**, 6298–307.
- [61] Huranova, M., Jablonski, J. A., Benda, A., Hof, M., Stanek, D., and Caputi, M. (2009) *RNA* **15(11)**, 2063–71.
- [62] Van Gilst, M. R., Rees, W. A., Das, A., and vonHippel, P. H. (1997) *Biochemistry* **36(6)**, 1514–24.

- [63] Xia, T., Becker, H. C., Wan, C., Frankel, A., Roberts, R. W., and Zewail, A. H. (2003) *Proc Natl Acad Sci U S A* **100(14)**, 8119–23.
- [64] Sheridan, D. L., Berlot, C. H., Robert, A., Inglis, F. M., Jakobsdottir, K. B., Howe, J. R., and Hughes, T. E. (2002) *BMC Neurosci* **3**, 7.
- [65] Lamichhane, R., Daubner, G. M., Thomas-Crusells, J., Auweter, S. D., Manatschal, C., Austin, K. S., Valniuk, O., Allain, F. H., and Rueda, D. (2010) *Proc Natl Acad Sci U S A* **107(9)**, 4105–10.
- [66] Walter, N. G. (2001) *Methods* **25(1)**, 19–30.

Acknowledgments

I am grateful to my supervisors Dr. Oliver Griesbeck and Prof. Dr. Axel Borst for supervising and accompanying this PhD project, for the generous support and scientific freedom, and to have offered me the opportunity to work in a motivating and stimulating atmosphere. A special thanks to my parents and my brother, for their unconditional support, encouragement and their faith in me. I thank for always being there for me and for making it possible for me to pass through some really hard times.

I am grateful to the ‘Griesbecks’, for helping me out with the experiments and for constructive discussion for the thesis. I specially thank Gayane, Anselm, Martina, Stephan and Thomas for always being ready to help. Thanks to Anja and Birgit for help with the buffers, cells, plates and the other basic needs of the lab. Thanks to Jonny for his inputs on work. I would like to thank the former lab member, Marco, for sharing his experience and wisdom. A special thanks to all the members of the Borst group for a lively atmosphere in the department for coffee-break talks and for cake sessions. Special thanks to Sarah Nicola, Bettina, Friedrich, Jing and Wolfgang for motivational talks, for constant support, restriction enzymes and encouragement and especially for keeping the atmosphere light during some stressful times. A special thanks to Dr. Shashikant Acharaya, for guiding me and always eager to listen to problems and come up with solutions, or empathy. Thanks to my friend Jasbeer, for theoretical teasing out of the experiments. Thanks to Harsha for always worrying about me. A big thanks to people from Tübingen, Dennis, Petra, Christian, Rebecca, for being such great friends and making me feel at home in a new country.

Curriculum Vitae

Personal information

Name Amrita Anup Kuthiala
Date of birth 15.04.1980

Current position

2007 – present **PhD Position**
In-vitro Studies on Aptamer-Induced FRET Between λ_{N22}
Tagged Fluorescent Protein Variants
*Max Planck Institute for Neurobiology, Martinsried (near Mu-
nich), Germany*
Supervisor: Dr. Oliver Griesbeck
www.neuro.mpg.de

Professional experience

10/2005 – **Visiting Scientist**
08/2007
Kinetics of Arc mRNA expression induction on neuronal stim-
ulation, transport to the activated synapses and its translation
into Arc protein
Hertie Institute for Clinical Brain Research, Tübingen, Germany
Supervisor: Dr. Michael Calhoun
www.hih-tuebingen.de

10/2003 – **Junior Research Fellow**
08/2005
Effects of anxiety on synaptic plasticity of neurons in the amyg-
dala and effects of anti-anxiety drug Gabapentine
National Centre for Biological Sciences, Bangalore, India
Supervisor: Dr.Sumantra Chatarjee
www.ncbs.res.in

06/2002 – **Master Thesis**
02/2003
Isolation of cellulose degrading co-cultures and isolating cel-
lulose degrading micro-organism from artificially enriched soils
for biofuels production
Maharaja Sayajirao University, Vadodara, India
Supervisor: Dr. Shashikant Acharaya
www.msubaroda.ac.in

Education

- 2001 – 2003 **Master in Biochemistry**
(Biochemistry, Molecular Biology, Microbiology, Ecology)
Maharaja Sayajirao University, Vadodara, India
- 1998 – 2001 **Bachelor in Botany**
(Botany, Zoology, Chemistry)
Maharaja Sayajirao University, Vadodara, India
- 1996 – 1998 **Higher Secondary School**
Don Bosco High School, Vadodara, India

Versicherung

Ehrenwörtliche Versicherung

Ich versichere hiermit ehrenwörtlich, dass ich die Dissertation mit dem Titel "*In-vitro* Studies on Aptamer-Induced FRET Between λ_{N22} Tagged Fluorescent Protein Variants" selbständig und ohne unerlaubte Beihilfe angefertigt habe. Ich habe mich dabei keiner anderen als der von mir ausdrücklich bezeichneten Hilfen und Quellen bedient.

Erklärung

Hiermit erkläre ich, dass ich mich nicht anderweitig einer Doktorprüfung ohne Erfolg unterzogen habe. Die Dissertation wurde in ihrer jetzigen oder ähnlichen Form bei keiner anderen Hochschule eingereicht und hat noch keinen sonstigen Prüfungszwecken gedient.

München, im September 2010

.....
Amrita Kuthiala